THE UNIVERSITY OF CHICAGO

LYMPHATIC TRANSPORT OF EXTRACELLULAR VESICLES IN CANCER METASTASIS

A DISSERTATION SUBMITTED TO

THE FACULTY OF THE PRITZKER SCHOOL OF MOLECULAR ENGINEERING

IN CANDIDACY FOR THE DEGREE OF

DOCTOR OF PHILOSOPHY

BY

LEA MAILLAT

CHICAGO, ILLINOIS

MARCH 2021

To my best life and science partner, my husband Lambert Potin.

This thesis brought us together, and our partnership drove most of the ideas, excitement and hard work behind it. I will forever be grateful to you for your unconditional love and support throughout this journey.

TABLE OF CONTENTS

LIST OF FIGURES

LIST OF TABLES

ACKNOWLEDGEMENTS

This thesis and my development as a scientist are the result of the exceptional mentorship I have received and of exciting collaborations I have been involved in during my Ph.D.

I would like to thank my advisor, Dr. Melody Swartz. Since the first time we met, you gave me confidence in my abilities, encouraged me to aim big and provided me with invaluable support in my training. Thank you for inspiring me and for sharing your creativity and passion for science with me.

I would like to thank the members of my candidacy and thesis committees, Dr. Marsha Rosner, Dr. Jeffrey Hubbell, Dr. Juan de Pablo and Dr. Lev Becker. Your expertise was invaluable in the development of my thesis, and you taught me to think about problems from various angles.

I am extremely thankful to all the Swartz and Hubbell lab members who contributed to my scientific development and who made the lab feel like a family. I am particularly grateful to Alexandre de Titta, Marco Pisano, Renata Mezyk-Kopec, Witek Kilarski, Katharina Maisel and Maria Broggi for mentoring me and teaching me to design, perform and analyze experiments, manage my projects and communicate science effectively. I also would like to thank Peyman Hosseinchi, Nick Mitrousis, Priscilla Briquez, Trevin Kurtanich, Rachel Gleyzer, Maria Stella Sasso, Jorge Emiliano Medellin, Shann Yu, Elyse Watkins, Rachel Weathered and Luis Alonzo for our great collaborations and friendship. I am also grateful to all my friends outside of the lab who contributed to making my past 6 years in Chicago a life-changing experience.

Living far away from home has been the hardest part of my Ph.D., and so I am incredibly grateful to my family and friends who visited me in Chicago, and to those who are always there for me in Switzerland. Among them, I would like to thank my parents, Anne and Stéphane Maillat, for their many trips to visit me in Chicago, their support of my scientific endeavors and their love. Finally, I would like to thank my husband Lambert Potin. You have been by my side in every step of this journey, and you have made me a better and stronger person.

ABSTRACT

Cancer metastasis, the spread of tumor cells from a primary site to secondary sites in the body, is the most common cause of cancer mortality. Prior to metastasis, primary tumor-derived factors are transported to secondary sites to suppress host immunity and to form an environment that supports metastatic tumor growth, called a pre-metastatic niche. Among these factors, extracellular vesicles (EVs) have been reported to play crucial roles. In the first part of this work, I investigate the routes of EV transport from primary tumors to secondary sites, and the consequences of modulating EV transport on premetastatic niche formation and metastasis. In the second part of this work, I analyzed EVs in another disease context, namely lipedema, with the goal of identifying disease-specific biomarkers.

In Chapter 1, I introduce the fields of lymphatic biology and EVs. I describe the mechanisms of lymphatic drainage and the roles of lymphatic vessels in health and disease development. Then, I describe the production, properties and functions of EVs.

In Chapter 2, I adapt methods to study EVs *in vitro* and *in vivo*. Such methods include producing, purifying and fluorescently labeling EVs. Additionally, I optimize the measurement of EV contents in various biological milieus.

In Chapter 3, I investigate the roles of lymphatic vessels in the distribution of EVs from the healthy skin and melanoma tumors to draining lymph nodes and distant sites. For this, I perform EV biodistribution studies in wild type mice and in a transgenic mouse model which lacks dermal lymphatics.

In Chapter 4, I investigate the consequences of tumor lymphangiogenesis on EV transport and on pre-metastatic niche formation. I analyze these mechanisms in two different

mouse tumor models which were transduced to stably overexpress the main lymphangiogenic growth factor VEGFC.

In Chapter 5, I characterize the fluid part of lipoaspirate samples as a source of adipose tissue-specific factors. In these samples, I analyze adipokines and EVs in lipedema patients compared with control patients.

In Chapter 6, I discuss the consequences of this thesis in the field of cancer metastasis and biomarker development. Finally, I suggest future work that will address remaining questions following upon this thesis.

CHAPTER 1

INTRODUCTION

1.1. The lymphatic system

The lymphatic system consists of a network of conduits throughout the body that has the main function of regulating tissue fluid homeostasis and absorption of dietary fats. It runs in parallel to the blood venous system in returning fluids to the blood circulation [1–4]. In healthy individuals, the lymphatic system drains and returns 1-2 liters of interstitial fluid, which contain 40-60 grams of proteins, to the blood circulation per day [5]. Additionally, it plays a crucial role in immunity by providing a conduit for immune cells and antigens to lymph nodes. Lymphatic vessels are necessary to human life, and lymphatic dysfunction may be associated with pathological conditions such as chronic edema, immune deficiency, obesity and atherosclerosis [6–10]. The growth of new lymphatic vessels is associated with a number of conditions such as inflammation, wound healing and cancer, and plays important roles in disease development [5,11].

Structure of the lymphatic system

The lymphatic system is made of five main types of conduits: initial vessels (or capillaries), collecting vessels, lymph nodes, trunks and ducts. The fluid that forms within lymphatic vessels is called lymph. The lymph contains fluids, cells, and solutes collected from the tissue interstitium, the space between capillaries and cells. Lymph flows unidirectionally through the collecting vessels, into and out of the lymph nodes, through trucks and ducts. Finally, the lymph flows from the ducts to the blood circulation [1,12].

Initial lymphatic vessels are responsible for the formation of lymph. They are blind-ended structures with wide lumen (10-60 μm) made of a single layer of lymphatic endothelial

cells (LEC; **Figure 1.1**). They are surrounded by a thin or no basement membrane and are directly connected to the extracellular matrix [1].

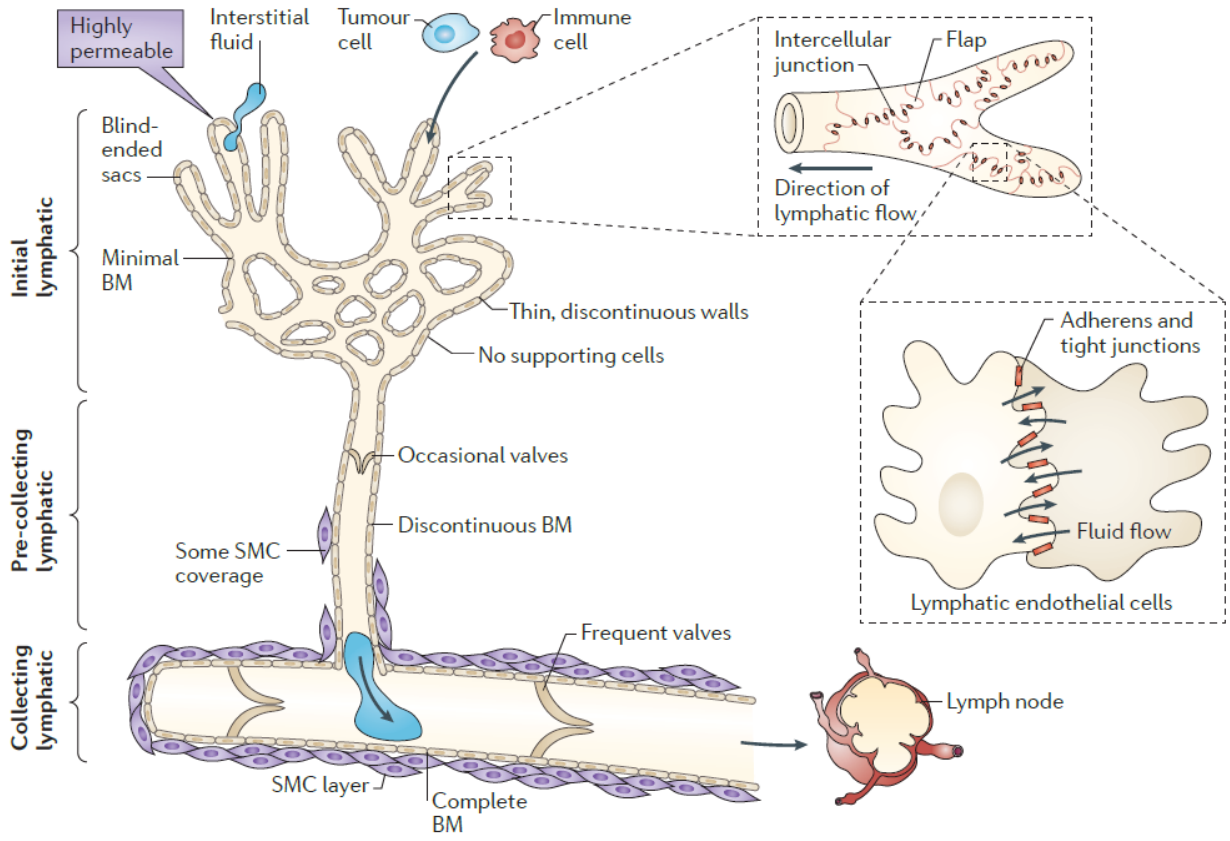

Figure 1.1. Structure of the lymphatic vasculature. BM: basement membrane, SMC: smooth muscle cell. From Stacker et al. [13].

To maintain unidirectional flow, initial lymphatics are thought to possess a unique valve system based on tethering elastic fibers (anchoring filaments), which has been suggested to facilitate fluid convection into the vessel lumen [13]. The lymph is transported unidirectionally towards the central circulation, and its flow rate within capillaries is affected by two mechanisms: lymph formation and lymph propulsion from capillaries to collecting vessels [1]. Initial lymphatic vessels converge into collecting vessels, which are larger (50-

200 μm) and surrounded by smooth muscle cells with an intrinsic pumping activity. Collecting vessels are arranged into segments, which are separated by one-way valves and contract sequentially. In addition to vessel pumping activity, passive factors such as movement of the peripheral tissue may also contribute to lymph flow [1].

Fluid and solute transport

The interstitium consists of the extracellular matrix (ECM) which is primarily composed of collagen fibers and glycosaminoglycans, and of interstitial fluid [14,15]. To maintain fluid homeostasis in the interstitium, the flux of plasma exiting blood capillaries is balanced by a flux of interstitial fluid entering lymphatic capillaries. This is enabled by a pressure gradient that drives interstitial fluid flow towards initial lymphatics. Additional factors such as tissue movement and external forces may contribute to fluid flow through the interstitium as well [1,15]. Interstitial fluid is thought to be primarily taken up into initial lymphatics via hydraulic pressure gradients across the vessel wall. A microvalve system was described in which, upon strain on the extracellular matrix and the anchoring filaments of initial lymphatic vessels, vessels open and form a short, small negative pressure that draws fluids in while preventing backflow [16].

Because of the directionality of interstitial flow towards lymphatics, macromolecules and particles released in the interstitium are driven by virtue of convection towards lymphatic vessels, making them their main transport route to the systemic circulation. As such, the lymphatic system is the major route of albumin and other macromolecule and particulate transport from the interstitium to the systemic circulation [15,17].

Traditionally, lymphatic vessels were thought to solely contribute to the passive drainage of molecules and cells. However, recent evidence suggests that LECs can greatly modulate solute transport based on different contexts. LEC permeability can be increased by inflammatory cues such as TNF-α, IL-1β, IL-6 and IFN-γ through cytoskeleton and cellular junction reorganization [18,19]. Interstitial flow was also shown to regulate fluid and solute transport across LECs [20,21]. LEC permeability may also be reduced by microenvironment cues, which could prevent viral dissemination and diet-induced obesity [22,23]. Recent evidence suggests that fluids and solutes are also transported across LECs via vesicular pathways, and that as a result LECs actively regulate translymphatic transport by modulating both paracellular and transcellular transport pathways [20,21]. Together, these pieces of information indicate that lymph formation is not a passive process and that lymph formation is strongly controlled by LECs and their local environment.

Immune cell trafficking and regulation of immune responses

Lymphatic vessels play a crucial role in immunity and tolerance, as they represent the main channels to transport self- and foreign antigens as well as immune cells from peripheral organs to lymph nodes. As such, in mice lacking dermal lymphatics immune responses to skin vaccination are largely impaired [8].

LECs attract and facilitate migration of immune cells into lymphatic vessels via the expression of a variety of chemokines and adhesion molecules. For example, LECs express high levels of the chemokine CCL21 and generate a chemokine density gradient in the interstitial space toward which $CCR7^+$ dendritic cells and T cells can migrate. LECs can upregulate their expression of selected chemokines upon inflammatory conditions as well, such as CCL2, CCL5 and CXCL10 which may contribute to recruiting additional immune cell

types. LECs express multiple adhesion molecules which facilitate cell entry into lymphatics and lymph nodes such as ICAM-1, VCAM-1 and E-Selectin [24,25]. Increased transendothelial flow, typical of inflammatory conditions, was found to increase LEC expression of CCL21 and ICAM-1 to enable a greater immune cell trafficking to lymph nodes [20].

In addition to their transport and cell recruitment functions, LECs can directly modulate adaptive immune responses by interacting with T cells through expression of immunosuppressive molecules PDL1, TGFβ, IDO and survival factor IL-7, as well as presentation of antigens on MHCI and MHCII molecules [26–29]. Furthermore, while most antigen-presenting cells such as dendritic cells (DCs) carry antigen for just a few days, it was recently found that LECs in the lymph node can store antigens that they take up from the lymph for weeks after vaccination [30].

Molecular regulation of lymphangiogenesis

The lymphatic system is made of endothelial cells and originates from embryonic veins. Embryonic lymphatic vessel network formation involves blood endothelial cells acquiring LEC gene expression profile and separating from the blood vasculature [31]. The prospero-related homebox-1 (PROX1) transcription factor is expressed by the first LECs and is essential for lymphatic development. *Prox1*-knockout mouse embryos lack lymphatic vessels and die at mid-gestation [32]. PROX1 reprograms endothelial cells by upregulating lymphatic-specific genes and suppressing selected blood-specific genes [33,34]. In addition to inducing a LEC phenotype, PROX1 activity is required to maintain LEC identity during embryonic, postnatal and adult stages [35].

The vascular endothelial growth factor C (VEGFC) signals through the VEGF receptor 3 (VEGFR3) and promotes sprouting, proliferation and survival of PROX1-positive LECs. *Vegfc*-knockout mice lack lymphatic vessels and die before birth, and *Vegfc*-heterozygous mice develop lymphedema [6]. Additionally, expression of a soluble VEGFR3 receptor in mouse skin to locally inhibit VEGFC signaling results in a lack of dermal lymphatics and consequently lymphedema [7].

VEGFD is another growth factor signaling through VEGFR3 and stimulating lymphangiogenesis in tissues and tumors, but which is dispensable for lymphatic development [36]. Neuropilin-2 (NRP2) is expressed by LECs and interacts with VEGFR3 to bind VEGFC and VEGFD and enhance lymphangiogenesis [37]. Additional growth factors which may have direct or indirect lymphangiogenic activity include VEGF, fibroblast growth factor (FGF), hepatocyte growth factor (HGF), PDGF, insulin-like growth factor-1 (IGF1) and IGF2 [38].

Lymphatic network maturation and functional differentiation is regulated by a complex gene programming involving the forkhead box transcription factor 2, the mucin-type sialoglycoprotein podoplanin (PDPN) and the ligands ephrin-B2 and angiopoietin-2 [31]. LYVE1 is expressed by lymphatic vessels since early in development and is widely used as a LEC marker [39]. LYVE1 is also expressed by subsets of macrophages and liver, spleen and lymph node sinusoidal endothelial cells [40]. Later in development, LEC progenitors start expressing additional specification markers, including podoplanin (PDPN or GP38). PDPN is a mucin-type O-glycoprotein expressed by LECs and lymph node fibroblastic reticular cells (FRC). *Pdpn*-knockout mice die early after birth with severe lymphedema due to abnormal lymphatic network formation [41].

Roles of lymphatics in disease

The lymphatic system plays important roles in a wide variety of pathological conditions. Lymphatic dysfunction often results in lymphedema, a progressive and lasting condition for which no cure exists. Lymphedema is characterized by an accumulation of fluids and solutes in tissues, which leads to swelling as well as inflammation and fibrosis [42]. Primary lymphedema is caused by defects in lymphatic vascular development or function and is largely attributed to inherited genetic mutations. It is rare and affects about 1/100,000 children [42]. Secondary lymphedema is caused by obstruction and/or disruption of the lymphatic vascular system. The most common cause of secondary lymphedema worldwide is lymphatic filariasis infection, affecting between 140 and 200 million people worldwide, mainly in developing countries [43]. In the western world, secondary lymphedema results mainly from surgical and radiation therapies for cancer treatment and affects about 1/1,000 Americans, commonly breast cancer survivors [42,44].

Metastasis is the primary cause of mortality due to cancer. Many solid cancers first metastasize to the tumor-draining lymph node before reaching distant organs [13]. Cancer cells are thought to reach the tumor-draining lymph node by entering local lymphatic vessels, which connect them physically to the tumor-draining lymph node. Moreover, tumor expression of VEGFC, as well as induction of lymphangiogenesis in or around the tumor, strongly correlate with metastasis in a number of cancer types [13,45,46].

Intestinal lymphatic vessels named lacteals control dietary lipid absorption [23]. Additionally, in peripheral tissues, lymphatic vessels return lipoproteins to the blood circulation, a process known as reverse cholesterol transport [10,47]. As such, lymphatic

functionality contributes to control the body weight and impacts the pathogenesis of obesity [9,23,48,49].

Lymphatic function is also altered in cardiovascular diseases [50]. After myocardial infarction, cardiac lymphatics undergo expansion, and increasing lymphangiogenesis further by VEGFC treatment results in improved cardiac function in mouse [51]. Stimulation of lymphangiogenesis reduces myocardial edema and fibrosis by increasing fluid and immune cell clearance [52,53]. As lymphatic vessels are important in lipid and immune cell transport from arterial walls, insufficient lymphangiogenesis can contribute to atherosclerosis plaque development [10,54].

Meningeal lymphatic vessels play important roles in regulating the central nervous system, and may be involved in neurological disorder development, such as Alzheimer and multiple sclerosis [55,56].

Lastly, because of its central role in immunity, the lymphatic vasculature is strongly involved in immune disorders and inflammation [57]. Lymphangiogenesis often occurs as a result of inflammation, and lymphatic vessel function is strongly involved in pathologies resulting from bacterial and viral infection [22], autoimmunity and allergy [58].

The roles that lymphatics play in a wide range of diseases, although still poorly understood, have been largely attributed to their transport and immune-modulatory functions. The multitude of pathologies lymphatics are involved is reflected by the diversity of materials they can transport for molecular and cellular communication. Interestingly, in the last few years, researchers in intercellular communication and biomarker discovery identified another component as a key player in their respective fields: extracellular vesicles

(EVs). Over the last decade, EVs have been shown to play crucial roles in shaping disease pathogenesis, by acting as a carrier of biomolecules for intercellular communication. It remains to be determined whether lymphatics regulate transport and effects of EVs on disease progression.

1.2. EVs and their roles in health and disease

EVs carry diverse cargos of biomolecules for intercellular communication, both within a tissue and at distant sites. Due to their efficient transport and transfer of molecular messengers, EVs are involved in various biological processes in health and disease. Additionally, they are increasingly investigated as source of disease biomarkers, as their contents reflect their cell of origin and can be detected in various biofluids.

EV biogenesis and characteristics

The best characterized type of EVs are called exosomes. Exosomes are small EVs 30-200 nm in size derived from endocytic compartments of most cell types and present in most body fluids [59,60]. They are formed upon reverse budding of the membrane of late endosomes, which generates multivesicular bodies. The intraluminal vesicles – or exosomes – are released upon fusion of the multivesicular body with the plasma membrane (Figure 1.2). In addition to their lipid bilayer membrane, proteins, RNA and DNA have been reported to get selectively encapsulated into exosomes [60,61].

Other types of EVs, called microvesicles or ectosomes, can be formed by outward budding of the plasma membrane and enclose such biomolecules as well. While microvesicles are typically larger than exosomes (200 nm – 1 μm), EVs of same size and density as exosomes were shown to originate from the plasma membrane as well and cannot be

separated from exosomes efficiently using current purification methods [60]. Therefore, although this thesis is primarily focused on exosomes, we will use the term EV for scientific rigor as suggested by the Society of Extracellular Vesicles [62].

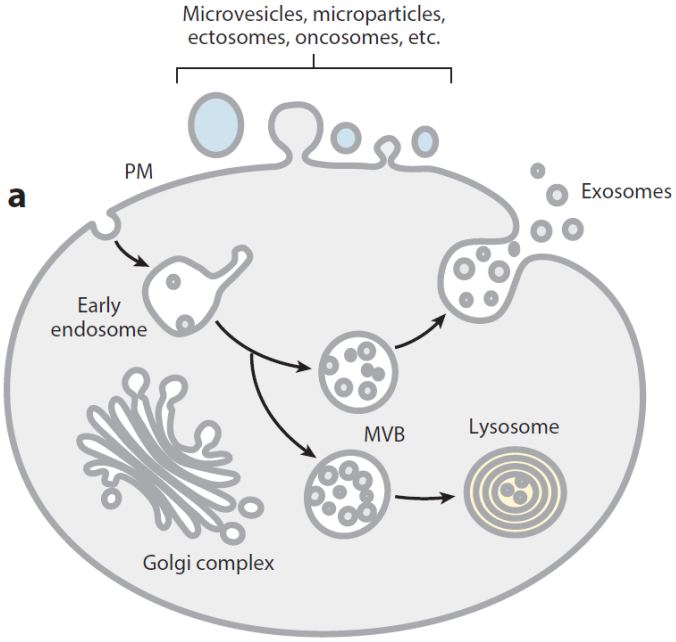

Figure 1.2. Formation of extracellular vesicles. PM: plasma membrane, MVB: multivesicular body. From Colombo et al. [59].

Non-EV particles, such as cell-secreted nanoparticles of ~30-50 nm diameter named exomeres, as well as different types of lipoprotein particles, may be co-purified with EVs and contain proteins, lipids and nucleic acids [63–65]. Therefore, the selection of purification techniques is crucial and depends on the biological source of EVs and required purity.

EV contents and physical properties

EVs contribute to local and systemic cell-cell communication due to their cargos rich in signal transduction biomolecules. EV cargos include proteins involved in vesicle trafficking, cytoskeleton organization, antigen presentation [66,67], adhesion and protection from lysis

by the complement, as well as enzymes and other cytosolic proteins, lipids and nucleic acids [59,61,68]. Among nucleic acids, micro-RNAs (miRNA) are particularly enriched and contribute to gene expression remodeling in target cells. Recent evidence suggests that EVs play important roles both in normal physiological processes and in pathogenic processes.

Roles of EVs in disease

EVs produced by cells of the tumor microenvironment play important roles in regulating tumorigenesis and contribute to many original and emerging hallmark features of cancer development described by Hanahan and Weinberg [69,70]. Cancer cell EVs can act in an autocrine manner to promote their proliferation and invasiveness, and induce tumor angiogenesis [71,72]. Additionally, breast cancer cells can acquire EVs from cancer-associated fibroblasts to sustain their proliferation, chemotherapy resistance and invasiveness [73-75]. Tumor EVs can induce tumor-promoting inflammation and avoid immune destruction within the tumor microenvironment by recruiting and reprogramming immune and stromal cells [76-79]. EVs can also induce such changes at distant sites and as such contribute to the formation of a pro-metastatic environment, called the premetastatic niche.

Increasing evidence suggests that EVs play important roles in a variety of metabolic diseases. In obesity, miRNAs transferred by EVs induce adipose inflammation and insulin resistance [80,81]. Adipose tissue-derived EVs can also travel to the liver and be involved in metabolism modulation, inflammation and fibrosis, and contribute to the development of nonalcoholic fatty liver disease such as nonalcoholic steatohepatitis (NASH) [82].

Although EVs are known to play important roles both locally and at a distance, it is still unclear how EVs are transported and what affects their distribution.

Use of EVs as disease biomarkers

EVs secreted by cells in pathologic tissues have been shown to reflect disease status and to carry proteins and micro-RNAs (miRNA) that could be used as biomarkers of disease stage, prognosis and treatment response [83–86]. EVs can be isolated from liquid biopsies, typically from the blood. However, as the blood carries EVs sampled from the whole body, pathological EV subsets are often difficult to detect. Therefore, a better understanding of EV distribution routes and kinetics is required to guide liquid biopsy sampling for EV biomarker detection.

1.3. References

[1] M.A. Swartz, The physiology of the lymphatic system, Adv. Drug Deliv. Rev. 50 (2001) 3–20. https://doi.org/https://doi.org/10.1016/S0169-409X(01)00150-8.

[2] J.E. Moore, C.D. Bertram, Lymphatic System Flows, Annu. Rev. Fluid Mech. 50 (2018) 459–482. https://doi.org/10.1146/annurev-fluid-122316-045259.

[3] T. V Petrova, G.Y. Koh, Biological functions of lymphatic vessels, Science (80-.). 369 (2020) 4063. https://doi.org/10.1126/science.aax4063.

[4] G. Oliver, J. Kipnis, G.J. Randolph, N.L. Harvey, Leading Edge The Lymphatic Vasculature in the 21 st Century: Novel Functional Roles in Homeostasis and Disease, Cell. 182 (2020) 270–296. https://doi.org/10.1016/j.cell.2020.06.039.

[5] T. Tammela, K. Alitalo, Lymphangiogenesis: Molecular Mechanisms and Future Promise, Cell. 140 (2010) 460–476. https://doi.org/10.1016/j.cell.2010.01.045.

[6] M.J. Karkkainen, P. Haiko, K. Sainio, J. Partanen, J. Taipale, T. V. Petrova, M. Jeltsch, D.G. Jackson, M. Talikka, H. Rauvala, C. Betsholtz, K. Alitalo, Vascular endothelial growth factor C is required for sprouting of the first lymphatic vessels from embryonic veins, Nat. Immunol. 5 (2004) 74–80. https://doi.org/10.1038/ni1013.

[7] T. Mäkinen, L. Jussila, T. Veikkola, T. Karpanen, M.I. Kettunen, K.J. Pulkkanen, R. Kauppinen, D.G. Jackson, H. Kubo, S. Nishikawa, S. Ylä-Herttuala, K. Alitalo, Inhibition of lymphangiogenesis with resulting lymphedema in transgenic mice expressing soluble VEGF receptor-3., Nat. Med. 7 (2001) 199–205. https://doi.org/10.1038/84651.

[8] S.N. Thomas, J.M. Rutkowski, M. Pasquier, E.L. Kuan, K. Alitalo, G.J. Randolph, M.A. Swartz, Impaired humoral immunity and tolerance in K14-VEGFR-3-Ig mice that lack dermal lymphatic drainage., J. Immunol. 189 (2012) 2181–90. https://doi.org/10.4049/jimmunol.1103545.

[9] N.L. Harvey, R.S. Srinivasan, M.E. Dillard, N.C. Johnson, M.H. Witte, K. Boyd, M.W. Sleeman, G. Oliver, Lymphatic vascular defects promoted by Prox1 haploinsufficiency cause adult-onset obesity, Nat. Genet. 37 (2005) 1072–1081. https://doi.org/10.1038/ng1642.

[10] C. Martel, W. Li, B. Fulp, A.M. Platt, E.L. Gautier, M. Westerterp, R. Bittman, A.R. Tall, S.H. Chen, M.J. Thomas, D. Kreisel, M.A. Swartz, M.G. Sorci-Thomas, G.J. Randolph, Lymphatic vasculature mediates macrophage reverse cholesterol transport in mice, J. Clin. Invest. 123 (2013) 1571–1579. https://doi.org/10.1172/JCI63685.

[11] K. Alitalo, The lymphatic vasculature in disease, Nat. Med. 17 (2011) 1371–1380. https://doi.org/10.1038/nm.2545.

[12] G.J. Randolph, V. Angeli, M.A. Swartz, Dendritic-cell trafficking to lymph nodes through lymphatic vessels, Nat. Rev. Immunol. 5 (2005) 617–28. https://doi.org/10.1038/nri1670.

[13] S.A. Stacker, S.P. Williams, T. Karnezis, R. Shayan, S.B. Fox, M.G. Achen, Lymphangiogenesis and lymphatic vessel remodelling in cancer, Nat. Rev. Cancer. 14 (2014) 159–72. https://doi.org/10.1038/nrc3677.

[14] K. Aukland, R.K. Reed, Interstitial-lymphatic mechanisms in the control of extracellular fluid volume, Physiol. Rev. 73 (1993) 1–78. https://doi.org/10.1152/physrev.1993.73.1.1.

[15] H. Wiig, M.A. Swartz, Interstitial fluid and lymph formation and transport: physiological regulation and roles in inflammation and cancer., Physiol. Rev. 92 (2012) 1005–60. https://doi.org/10.1152/physrev.00037.2011.

[16] J. Trzewik, S.K. Mallipattu, G.M. Artmann, F.A. Delano, G.W. Schmid-Schönbein, Evidence for a second valve system in lymphatics: Endothelial microvalves, FASEB J. 15 (2001) 1711–1717. https://doi.org/10.1096/fj.01-0067com.

[17] R.M. Patterson, C.L. Ballard, K. Wasserman, H.S. Mayerson, Lymphatic permeability to albumin, 1958. www.physiology.org/journal/ajplegacy (accessed January 8, 2020).

[18] Y. Kawai, M. Kaidoh, Y. Yokoyama, T. Ohhashi, Pivotal Roles of Lymphatic Endothelial Cell Layers in the Permeability to Hydrophilic Substances through Collecting Lymph Vessel Walls: Effects of Inflammatory Cytokines, Lymphat. Res. Biol. 12 (2014) 124–135. https://doi.org/10.1089/lrb.2014.0002.

[19] W.E. Cromer, S.D. Zawieja, B. Tharakan, E.W. Childs, M.K. Newell, D.C. Zawieja, The effects of inflammatory cytokines on lymphatic endothelial barrier function, Angiogenesis. 17 (2014) 395–406. https://doi.org/10.1007/s10456-013-9393-2.

[20] D.O. Miteva, J.M. Rutkowski, J.B. Dixon, W. Kilarski, J.D. Shields, M.A. Swartz,

Transmural flow modulates cell and fluid transport functions of lymphatic endothelium., Circ. Res. 106 (2010) 920–31. https://doi.org/10.1161/CIRCRESAHA.109.207274.

[21] V. Triacca, E. Güç, W.W. Kilarski, M. Pisano, M.A. Swartz, Transcellular Pathways in Lymphatic Endothelial Cells Regulate Changes in Solute Transport by Fluid Stress, Circ. Res. 120 (2017) 1440–1452. https://doi.org/10.1161/CIRCRESAHA.116.309828.

[22] C.P. Loo, N.A. Nelson, R.S. Lane, J.L. Booth, S.C. Loprinzi Hardin, A. Thomas, M.K. Slifka, J.C. Nolz, A.W. Lund, Lymphatic Vessels Balance Viral Dissemination and Immune Activation following Cutaneous Viral Infection, Cell Rep. 20 (2017) 3176–3187. https://doi.org/10.1016/j.celrep.2017.09.006.

[23] F. Zhang, G. Zarkada, J. Han, J. Li, A. Dubrac, R. Ola, G. Genet, K. Boyé, P. Michon, S.E. Künzel, J.P. Camporez, A.K. Singh, G.H. Fong, M. Simons, P. Tso, C. Fernández-Hernando, G.I. Shulman, W.C. Sessa, A. Eichmann, Lacteal junction zippering protects against diet-induced obesity, Science (80-.). 361 (2018) 599–603. https://doi.org/10.1126/science.aap9331.

[24] C.M. Card, S.S. Yu, M.A. Swartz, Emerging roles of lymphatic endothelium in regulating adaptive immunity, J. Clin. Invest. 124 (2014) 943–952. https://doi.org/10.1172/JCI73316.

[25] J. Millán, L. Hewlett, M. Glyn, D. Toomre, P. Clark, A.J. Ridley, Lymphocyte transcellular migration occurs through recruitment of endothelial ICAM-1 to caveola- and F-actin-rich domains, Nat. Cell Biol. 8 (2006) 113–123. https://doi.org/10.1038/ncb1356.

[26] J. Dubrot, F. V. Duraes, L. Potin, F. Capotosti, D. Brighouse, T. Suter, S. LeibundGut-Landmann, N. Garbi, W. Reith, M.A. Swartz, S. Hugues, Lymph node stromal cells acquire peptide-MHCII complexes from dendritic cells and induce antigen-specific CD4+ T cell tolerance., J. Exp. Med. 211 (2014) 1153–1166. https://doi.org/10.1084/jem.20132000.

[27] S. Hirosue, E. Vokali, V.R. Raghavan, M. Rincon-restrepo, A.W. Lund, P. Corthésy-Henrioud, F. Capotosti, C. Halin Winter, S. Hugues, M.A. Swartz, Steady-State Antigen Scavenging, Cross-Presentation, and CD8+ T Cell Priming: A New Role for Lymphatic Endothelial Cells., J. Immunol. 192 (2014) 5002–11. https://doi.org/10.4049/jimmunol.1302492.

[28] L.C. Dieterich, K. Ikenberg, T. Cetintas, K. Kapaklikaya, C. Hutmacher, M. Detmar, Tumor-associated lymphatic vessels upregulate PDL1 to inhibit T-cell activation, Front. Immunol. 8 (2017) 66. https://doi.org/10.3389/fimmu.2017.00066.

[29] D. Malhotra, A.L. Fletcher, J. Astarita, V. Lukacs-Kornek, P. Tayalia, S.F. Gonzalez, K.G. Elpek, S.K. Chang, K. Knoblich, M.E. Hemler, M.B. Brenner, M.C. Carroll, D.J. Mooney, S.J. Turley, Transcriptional profiling of stroma from inflamed and resting lymph nodes defines immunological hallmarks., Nat. Immunol. 13 (2012) 499–510. https://doi.org/10.1038/ni.2262.

[30] B.A. Tamburini, M.A. Burchill, R.M. Kedl, Antigen capture and archiving by lymphatic

endothelial cells following vaccination or viral infection, Nat. Commun. 5 (2014) 1–13. https://doi.org/10.1038/ncomms4989.

[31] R.H. Adams, K. Alitalo, Molecular regulation of angiogenesis and lymphangiogenesis, Nat. Rev. Mol. Cell Biol. 8 (2007) 464–478. https://doi.org/10.1038/nrm2183.

[32] J.T. Wigle, G. Oliver, Prox1 function is required for the development of the murine lymphatic system, Cell. 98 (1999) 769–778. https://doi.org/10.1016/S0092-8674(00)81511-1.

[33] Y.-K. Hong, N. Harvey, Y.-H. Noh, V. Schacht, S. Hirakawa, M. Detmar, G. Oliver, Prox1 is a master control gene in the program specifying lymphatic endothelial cell fate, Dev. Dyn. 225 (2002) 351–357. https://doi.org/10.1002/dvdy.10163.

[34] T. V. Petrova, T. Mäkinen, T.P. Mäkelä, J. Saarela, I. Virtanen, R.E. Ferrell, D.N. Finegold, D. Kerjaschki, S. Ylä-Herttuala, K. Alitalo, Lymphatic endothelial reprogramming of vascular endothelial cells by the Prox-1 homeobox transcription factor, EMBO J. 21 (2002) 4593–4599. https://doi.org/10.1093/emboj.

[35] N.C. Johnson, M.E. Dillard, P. Baluk, D.M. McDonald, N.L. Harvey, S.L. Frase, G. Oliver, Lymphatic endothelial cell identity is reversible and its maintenance requires Prox1 activity, Genes Dev. 22 (2008) 3282–3291. https://doi.org/10.1101/gad.1727208.

[36] M.E. Baldwin, M.M. Halford, S. Roufail, R.A. Williams, M.L. Hibbs, D. Grail, H. Kubo, S.A. Stacker, M.G. Achen, Vascular Endothelial Growth Factor D Is Dispensable for Development of the Lymphatic System, Mol. Cell. Biol. 25 (2005) 2441–2449. https://doi.org/10.1128/mcb.25.6.2441-2449.2005.

[37] L. Yuan, D. Moyon, L. Pardanaud, C. Bréant, M.J. Karkkainen, K. Alitalo, A. Eichmann, Abnormal lymphatic vessel development in neuropilin 2 mutant mice | Development, Development. 129 (2002) 4797–4806. https://dev.biologists.org/content/129/20/4797 (accessed March 27, 2020).

[38] K. Alitalo, T. Tammela, T. V. Petrova, Lymphangiogenesis in development and human disease, Nature. 438 (2005) 946–953. https://doi.org/10.1038/nature04480.

[39] S. Banerji, J. Ni, S.X. Wang, S. Clasper, J. Su, R. Tammi, M. Jones, D.G. Jackson, LYVE-1, a new homologue of the CD44 glycoprotein, is a lymph-specific receptor for hyaluronan, J. Cell Biol. 144 (1999) 789–801. https://doi.org/10.1083/jcb.144.4.789.

[40] N. Escobedo, G. Oliver, Lymphangiogenesis: Origin, Specification, and Cell Fate Determination, Annu. Rev. Cell Dev. Biol. 32 (2016) 677–691. https://doi.org/10.1146/annurev-cellbio-111315-124944.

[41] V. Schacht, M.I. Ramirez, Y. Hong, S. Hirakawa, D. Feng, N. Harvey, M. Williams, A.M. Dvorak, H.F. Dvorak, G. Oliver, M. Detmar, T1α/podoplanin deficiency disrupts normal lymphatic vasculature formation and causes lymphedema, EMBO J. 22 (2003) 3546–3556. https://doi.org/10.1093/emboj.

[42] A.K. Greene, Epidemiology and morbidity of lymphedema, in: Lymphedema Present. Diagnosis, Treat., Springer International Publishing, 2015: pp. 33–44.

https://doi.org/10.1007/978-3-319-14493-1_4.

[43] S. Babu, T.B. Nutman, Immunopathogenesis of lymphatic filarial disease, Semin. Immunopathol. 34 (2012) 847–861. https://doi.org/10.1007/s00281-012-0346-4.

[44] J.N. Cormier, R.L. Askew, K.S. Mungovan, Y. Xing, M.I. Ross, J.M. Armer, Lymphedema beyond breast cancer, Cancer. 116 (2010) 5138–5149. https://doi.org/10.1002/cncr.25458.

[45] M. Skobe, T. Hawighorst, D.G. Jackson, R. Prevo, L. Janes, P. Velasco, L. Riccardi, K. Alitalo, K. Claffey, M. Detmar, C. Biology, M.G. Hospital, J.R. Hospital, Induction of tumor lymphangiogenesis by VEGF-C promotes breast cancer metastasis., Nat. Med. 7 (2001) 192–8. https://doi.org/10.1038/84643.

[46] G. Acs, G. Paragh, Z. Rakosy, C. Laronga, P.J. Zhang, The extent of retraction clefts correlates with lymphatic vessel density and VEGF-C expression and predicts nodal metastasis and poor prognosis in early-stage breast carcinoma, Mod. Pathol. 25 (2011) 163–177. https://doi.org/10.1038/modpathol.2011.138.

[47] M.N. Duong, K. Uno, V. Nankivell, C. Bursill, S.J. Nicholls, Induction of obesity impairs reverse cholesterol transport in ob/ob mice, PLoS One. 13 (2018). https://doi.org/10.1371/journal.pone.0202102.

[48] N. Escobedo, G. Oliver, The Lymphatic Vasculature: Its Role in Adipose Metabolism and Obesity, Cell Metab. 26 (2017) 598–609. https://doi.org/10.1016/j.cmet.2017.07.020.

[49] A. Chakraborty, S. Barajas, G.M. Lammoglia, A.J. Reyna, T.S. Morley, J.A. Johnson, P.E. Scherer, J.M. Rutkowski, Vascular Endothelial Growth Factor–D (VEGF-D) Overexpression and Lymphatic Expansion in Murine Adipose Tissue Improves Metabolism in Obesity, Am. J. Pathol. 189 (2019) 924–939. https://doi.org/10.1016/j.ajpath.2018.12.008.

[50] R.R. Bradham, E.F. Parker, The Cardiac Lymphatics, Ann. Thorac. Surg. 15 (1973) 526–528. https://doi.org/10.1016/S0003-4975(10)65339-8.

[51] L. Klotz, S. Norman, J.M. Vieira, M. Masters, M. Rohling, K.N. Dubé, S. Bollini, F. Matsuzaki, C.A. Carr, P.R. Riley, Cardiac lymphatics are heterogeneous in origin and respond to injury, Nature. 522 (2015) 62–67. https://doi.org/10.1038/nature14483.

[52] O. Henri, C. Pouehe, M. Houssari, L. Galas, L. Nicol, F. Edwards-Lévy, J.P. Henry, A. Dumesnil, I. Boukhalfa, S. Banquet, D. Schapman, C. Thuillez, V. Richard, P. Mulder, E. Brakenhielm, Selective Stimulation of Cardiac Lymphangiogenesis Reduces Myocardial Edema and Fibrosis Leading to Improved Cardiac Function Following Myocardial Infarction, Circulation. 133 (2016) 1484–1497. https://doi.org/10.1161/CIRCULATIONAHA.115.020143.

[53] J.M. Vieira, S. Norman, C.V. Del Campo, T.J. Cahill, D.N. Barnette, M. Gunadasa-Rohling, L.A. Johnson, D.R. Greaves, C.A. Carr, D.G. Jackson, P.R. Riley, The cardiac lymphatic system stimulates resolution of inflammation following myocardial infarction, J. Clin. Invest. 128 (2018) 3402–3412. https://doi.org/10.1172/JCI97192.

[54] H.Y. Lim, C.H. Thiam, K.P. Yeo, R. Bisoendial, C.S. Hii, K.C.Y. McGrath, K.W. Tan, A. Heather, J.S.J. Alexander, V. Angeli, Lymphatic vessels are essential for the removal of cholesterol from peripheral tissues by SR-BI-Mediated transport of HDL, Cell Metab. 17 (2013) 671–684. https://doi.org/10.1016/j.cmet.2013.04.002.

[55] S. Da Mesquita, A. Louveau, A. Vaccari, I. Smirnov, R.C. Cornelison, K.M. Kingsmore, C. Contarino, S. Onengut-Gumuscu, E. Farber, D. Raper, K.E. Viar, R.D. Powell, W. Baker, N. Dabhi, R. Bai, R. Cao, S. Hu, S.S. Rich, J.M. Munson, M.B. Lopes, C.C. Overall, S.T. Acton, J. Kipnis, Functional aspects of meningeal lymphatics in ageing and Alzheimer's disease, Nature. 560 (2018) 185–191. https://doi.org/10.1038/s41586-018-0368-8.

[56] A. Louveau, J. Herz, M.N. Alme, A.F. Salvador, M.Q. Dong, K.E. Viar, S.G. Herod, J. Knopp, J.C. Setliff, A.L. Lupi, S. Da Mesquita, E.L. Frost, A. Gaultier, T.H. Harris, R. Cao, S. Hu, J.R. Lukens, I. Smirnov, C.C. Overall, G. Oliver, J. Kipnis, CNS lymphatic drainage and neuroinflammation are regulated by meningeal lymphatic vasculature, Nat. Neurosci. 21 (2018) 1380–1391. https://doi.org/10.1038/s41593-018-0227-9.

[57] K. Maisel, M.S. Sasso, L. Potin, M.A. Swartz, Exploiting lymphatic vessels for immunomodulation: Rationale, opportunities, and challenges, Adv. Drug Deliv. Rev. 114 (2017) 43–59. https://doi.org/10.1016/j.addr.2017.07.005.

[58] K. Shin, R.P. Kataru, H.J. Park, B.-I. Kwon, T.W. Kim, Y.K. Hong, S.-H. Lee, TH2 cells and their cytokines regulate formation and function of lymphatic vessels, Nat. Commun. 6 (2015) 6196. https://doi.org/10.1038/ncomms7196.

[59] M. Colombo, G. Raposo, C. Théry, Biogenesis, Secretion, and Intercellular Interactions of Exosomes and Other Extracellular Vesicles, Annu. Rev. Cell Dev. Biol. 30 (2014) 255–289. https://doi.org/10.1146/annurev-cellbio-101512-122326.

[60] M. Mathieu, L. Martin-Jaular, G. Lavieu, C. Théry, Specificities of secretion and uptake of exosomes and other extracellular vesicles for cell-to-cell communication, Nat. Cell Biol. 21 (2019) 9–17. https://doi.org/10.1038/s41556-018-0250-9.

[61] H. Valadi, K. Ekström, A. Bossios, M. Sjöstrand, J.J. Lee, J.O. Lötvall, Exosome-mediated transfer of mRNAs and microRNAs is a novel mechanism of genetic exchange between cells, Nat. Cell Biol. 9 (2007) 654–659. https://doi.org/10.1038/ncb1596.

[62] C. Théry, K.W. Witwer, E. Aikawa, M.J. Alcaraz, J.D. Anderson, e t Al., Minimal information for studies of extracellular vesicles 2018 (MISEV2018): a position statement of the International Society for Extracellular Vesicles and update of the MISEV2014 guidelines, J. Extracell. Vesicles. 7 (2018). https://doi.org/10.1080/20013078.2018.1535750.

[63] H. Zhang, D. Freitas, H.S. Kim, K. Fabijanic, Z. Li, H. Chen, M.T. Mark, H. Molina, A.B. Martin, L. Bojmar, J. Fang, S. Rampersaud, A. Hoshino, I. Matei, C.M. Kenific, M. Nakajima, A.P. Mutvei, P. Sansone, W. Buehring, H. Wang, J.P. Jimenez, L. Cohen-gould, N. Paknejad, M. Brendel, K. Manova-todorova, J.R. Cubillos-ruiz, G. Galletti, P. Giannakakou, A.M. Cuervo, Identification of distinct nanoparticles and subsets of extracellular vesicles by asymmetric flow field-flow fractionation, Nat. Cell Biol. 20 (2018). https://doi.org/10.1038/s41556-018-0040-4.

[64] Q. Zhang, J.N. Higginbotham, D.K. Jeppesen, Y.P. Yang, W. Li, E.T. McKinley, R. Graves-Deal, J. Ping, C.M. Britain, K.A. Dorsett, C.L. Hartman, D.A. Ford, R.M. Allen, K.C. Vickers, Q. Liu, J.L. Franklin, S.L. Bellis, R.J. Coffey, Transfer of Functional Cargo in Exomeres, Cell Rep. 27 (2019) 940-954.e6. https://doi.org/10.1016/j.celrep.2019.01.009.

[65] K.C. Vickers, B.T. Palmisano, B.M. Shoucri, R.D. Shamburek, A.T. Remaley, MicroRNAs are transported in plasma and delivered to recipient cells by high-density lipoproteins, Nat. Cell Biol. 13 (2011) 423–435. https://doi.org/10.1038/ncb2210.

[66] G. Raposo, H.W. Nijman, W. Stoorvogel, R. Leijendekker, C. V. Harding, C.J.M. Melief, H.J. Geuze, B lymphocytes secrete antigen-presenting vesicles, J. Exp. Med. 183 (1996) 1161–1172. https://doi.org/10.1084/jem.183.3.1161.

[67] J. Wolfers, A. Lozier, G. Raposo, A. Regnault, C. Théry, C. Masurier, C. Flament, S. Pouzieux, F. Faure, T. Tursz, E. Angevin, S. Amigorena, L. Zitvogel, Tumor-derived exosomes are a source of shared tumor rejection antigens for CTL cross-priming, Nat. Med. 7 (2001) 297–303. https://doi.org/10.1038/85438.

[68] P.D. Robbins, A.E. Morelli, Regulation of immune responses by extracellular vesicles., Nat. Rev. Immunol. 14 (2014) 195–208. https://doi.org/10.1038/nri3622.

[69] D. Hanahan, R.A. Weinberg, The hallmarks of cancer, Cell. 100 (2000) 57–70. https://doi.org/10.1016/S0092-8674(00)81683-9.

[70] D. Hanahan, R.A. Weinberg, Hallmarks of cancer: the next generation., Cell. 144 (2011) 646–74. https://doi.org/10.1016/j.cell.2011.02.013.

[71] J. Skog, T. Würdinger, S. van Rijn, D.H. Meijer, L. Gainche, W.T. Curry, B.S. Carter, A.M. Krichevsky, X.O. Breakefield, S. Van Rijn, D.H. Meijer, L. Gainche, M. Sena-esteves, W.T. Curry, B.S. Carter, A.M. Krichevsky, X.O. Breakefield, Glioblastoma microvesicles transport RNA and proteins that promote tumour growth and provide diagnostic biomarkers, Nat. Cell Biol. 10 (2008) 1470–1476. https://doi.org/10.1038/ncb1800.

[72] P. Kucharzewska, H.C. Christianson, J.E. Welch, K.J. Svensson, E. Fredlund, M. Ringnér, M. Mörgelin, E. Bourseau-Guilmain, J. Bengzon, M. Belting, Exosomes reflect the hypoxic status of glioma cells and mediate hypoxia-dependent activation of vascular cells during tumor development., Proc. Natl. Acad. Sci. U. S. A. 110 (2013) 7312–7. https://doi.org/10.1073/pnas.1220998110.

[73] M.C. Boelens, T.J. Wu, B.Y. Nabet, B. Xu, Y. Qiu, T. Yoon, D.J. Azzam, C. Twyman-Saint Victor, B.Z. Wiemann, H. Ishwaran, P.J. Ter Brugge, J. Jonkers, J. Slingerland, A.J. Minn, Exosome transfer from stromal to breast cancer cells regulates therapy resistance pathways., Cell. 159 (2014) 499–513. https://doi.org/10.1016/j.cell.2014.09.051.

[74] V. Luga, L. Zhang, A.M. Viloria-Petit, A. a Ogunjimi, M.R. Inanlou, E. Chiu, M. Buchanan, A.N. Hosein, M. Basik, J.L. Wrana, Exosomes mediate stromal mobilization of autocrine Wnt-PCP signaling in breast cancer cell migration., Cell. 151 (2012) 1542–56. https://doi.org/10.1016/j.cell.2012.11.024.

[75] K.E. Richards, A.E. Zeleniak, M.L. Fishel, J. Wu, L.E. Littlepage, R. Hill, Cancer-associated

fibroblast exosomes regulate survival and proliferation of pancreatic cancer cells, Oncogene. 36 (2017) 1770–1778. https://doi.org/10.1038/onc.2016.353.

[76] J. Webber, R. Steadman, M.D. Mason, Z. Tabi, A. Clayton, Cancer exosomes trigger fibroblast to myofibroblast differentiation, Cancer Res. 70 (2010) 9621–9630. https://doi.org/10.1158/0008-5472.CAN-10-1722.

[77] H. Peinado, H. Zhang, I.R. Matei, B. Costa-Silva, A. Hoshino, G. Rodrigues, B. Psaila, R.N. Kaplan, J.F. Bromberg, Y. Kang, M.J. Bissell, T.R. Cox, A.J. Giaccia, J.T. Erler, S. Hiratsuka, C.M. Ghajar, D. Lyden, Pre-metastatic niches: Organ-specific homes for metastases, Nat. Rev. Cancer. 17 (2017) 302–317. https://doi.org/10.1038/nrc.2017.6.

[78] B. Costa-Silva, N.M. Aiello, A.J. Ocean, S. Singh, H. Zhang, B.K. Thakur, A. Becker, A. Hoshino, M.T. Mark, H. Molina, J. Xiang, T. Zhang, T.-M. Theilen, G. García-Santos, C. Williams, Y. Ararso, Y. Huang, G. Rodrigues, T.-L. Shen, K.J. Labori, I.M.B. Lothe, E.H. Kure, J. Hernandez, A. Doussot, S.H. Ebbesen, P.M. Grandgenett, M.A. Hollingsworth, M. Jain, K. Mallya, S.K. Batra, W.R. Jarnagin, R.E. Schwartz, I. Matei, H. Peinado, B.Z. Stanger, J. Bromberg, D. Lyden, Pancreatic cancer exosomes initiate pre-metastatic niche formation in the liver, Nat. Cell Biol. 17 (2015) 816–826. https://doi.org/10.1038/ncb3169.

[79] D. Daassi, K.M. Mahoney, G.J. Freeman, The importance of exosomal PDL1 in tumour immune evasion., Nat. Rev. Immunol. (2020). https://doi.org/10.1038/s41577-019-0264-y.

[80] Z. Bin Deng, A. Poliakov, R.W. Hardy, R. Clements, C. Liu, Y. Liu, J. Wang, X. Xiang, S. Zhang, X. Zhuang, S. V Shah, D. Sun, S. Michalek, W.E. Grizzle, T. Garvey, J. Mobley, H.G. Zhang, Adipose Tissue Exosome-Like Vesicles Mediate Activation of Macrophage-Induced Insulin Resistance, Diabetes. 58 (2009) 2498–2505. https://doi.org/10.2337/db09-0216.

[81] C. Castaño, S. Kalko, A. Novials, M. Párrizas, Obesity-associated exosomal miRNAs modulate glucose and lipid metabolism in mice., Proc. Natl. Acad. Sci. U. S. A. 115 (2018) 12158–12163. https://doi.org/10.1073/pnas.1808855115.

[82] I. Huang-doran, C. Zhang, A. Vidal-puig, Extracellular Vesicles : Novel Mediators of Cell Communication In Metabolic Disease, Trends Endocrinol. Metab. 28 (2017) 3–18. https://doi.org/10.1016/j.tem.2016.10.003.

[83] H. Peinado, M. Alec, S. Lavotshkin, I. Matei, B. Costa-silva, G. Moreno-bueno, M. Hergueta-redondo, C. Williams, G. García-santos, C.M. Ghajar, A. Nitadori-hoshino, C. Hoffman, K. Badal, B.A. Garcia, M.K. Callahan, J. Yuan, V.R. Martins, J. Skog, R.N. Kaplan, M.S. Brady, J.D. Wolchok, P.B. Chapman, Y. Kang, Melanoma exosomes educate bone marrow progenitor cells toward a pro-metastatic phenotype through MET, Nat. Med. 18 (2012) 883–891. https://doi.org/10.1038/nm.2753.

[84] A. Hoshino, B. Costa-Silva, T.-L. Shen, G. Rodrigues, A. Hashimoto, M. Tesic Mark, H. Molina, S. Kohsaka, A. Di Giannatale, S. Ceder, S. Singh, C. Williams, N. Soplop, K. Uryu, L. Pharmer, T. King, L. Bojmar, A.E. Davies, Y. Ararso, T. Zhang, H. Zhang, J. Hernandez, J.M. Weiss, V.D. Dumont-Cole, K. Kramer, L.H. Wexler, A. Narendran, G.K. Schwartz, J.H.

Healey, P. Sandstrom, K. Jørgen Labori, E.H. Kure, P.M. Grandgenett, M.A. Hollingsworth, M. de Sousa, S. Kaur, M. Jain, K. Mallya, S.K. Batra, W.R. Jarnagin, M.S. Brady, O. Fodstad, V. Muller, K. Pantel, A.J. Minn, M.J. Bissell, B.A. Garcia, Y. Kang, V.K. Rajasekhar, C.M. Ghajar, I. Matei, H. Peinado, J. Bromberg, D. Lyden, Tumour exosome integrins determine organotropic metastasis, Nature. 527 (2015) 329–335. https://doi.org/10.1038/nature15756.

[85] Y. Chen, J.J. Buyel, M.J.W. Hanssen, F. Siegel, R. Pan, J. Naumann, M. Schell, A. Van Der Lans, C. Schlein, H. Froehlich, J. Heeren, K.A. Virtanen, W. Van Marken Lichtenbelt, A. Pfeifer, Exosomal microRNA miR-92a concentration in serum reflects human brown fat activity, Nat. Commun. 7 (2016) 1–9. https://doi.org/10.1038/ncomms11420.

[86] P. Vallabhajosyula, L. Korutla, A. Habertheuer, M. Yu, S. Rostami, C.X. Yuan, S. Reddy, C. Liu, V. Korutla, B. Koeberlein, J. Trofe-Clark, M.R. Rickels, A. Naji, Tissue-specific exosome biomarkers for noninvasively monitoring immunologic rejection of transplanted tissue, J. Clin. Invest. 127 (2017) 1375–1391. https://doi.org/10.1172/JCI87993.

CHAPTER 2

OPTIMIZATION OF METHODS TO STUDY

EXTRACELLULAR VESICLES

2.1. Introduction

State-of-the-art techniques to produce and purify extracellular vesicles (EVs)

Extracellular vesicles (EVs), including exosomes, are produced by most mammalian cell types in homeostasis conditions. Their production can be modulated in response to internal and external stress stimuli and, as such, production and composition of EVs *in vitro* varies across cell types and cell culture conditions [1].

Traditionally, EVs have been purified from cell culture supernatants and from biological fluids based on their physical properties, specifically size and density. The gold standard purification method involves clearing fluids from cells and large debris by centrifugation, followed by pelleting EVs by ultracentrifugation [2]. However, this method has several limitations. First, the yield of EVs is low, often with less than 10% recovery of EVs. Additionally, non-EV particles of similar properties may be co-purified. For example, high-density lipoproteins (HDL), in high abundance in the blood and in other body fluids, have a similar density to exosomes [3,4]. After ultracentrifugation, it is possible to further purify EVs based on their precise density by density gradient ultracentrifugation [5]. However, this step generates a high loss of EVs and as such is typically only used for selected EV characterization studies.

In recent years, size-exclusion chromatography (SEC) has emerged as an alternative EV purification method. Here, cell culture supernatants are typically concentrated using centrifugal filters, after which the concentrate is applied to a size-exclusion column with a pore size of 40-70 nm, to exclude small particles and proteins (<70 nm) from EVs (>40 nm or >70 nm depending on the column used). This method effectively separates exosomes from

HDL and may enable better yields than ultracentrifugation [6]. However, used by itself, low density particles larger than the column pore size, such as LDL, VLDL and chilomicrons may be co-purified [3]. Recently, a new purification method, namely asymmetric flow fractionation, enables highly accurate size-based separation and can be used after pre-enrichment of EVs by ultracentrifugation and appears useful to separate distinct EV subsets [7,8].

Affinity-based purification appears to achieve high purity by selectively enriching EVs using EV-specific markers, such as tetraspanins CD63, CD81 and CD9. Multiple studies reported using beads conjugated to anti-tetraspanin antibody for subsequent analysis by flow cytometry or mass spectrometry [5,9,10]. However, current methods are very low yield and have limited downstream applications due to the capture of EVs on antibody-functionalized surfaces.

Lastly, new technologies have been developed to attempt to address the limitations of the previously mentioned methods. For example, EV precipitation agents, such as ExoQuick™ (System Biosciences) or Total Exosome Isolation Reagent™ (Invitrogen) kits may be used to purify exosomes from small samples, at the cost of lower purity [11].

EV characterization

The International Society for Extracellular Vesicles has established guidelines to characterize EV preparations [4,12]. They include size measurement and shape visualization of single vesicles through two independent methods, such as TEM and nanoparticle tracking analysis (NTA). Additionally, the presence of at least two EV-positive markers including a transmembrane and a cytosolic protein, and absence of at least one negative protein markers

must be shown on bulk EV preparations. Additionally, calculations of particle to protein ratio may give an indication of particle purity.

Despite the exponential growth of the field of extracellular vesicle research, quantification of EVs has remained challenging and there is currently no benchmark method to quantify EVs [4]. The most widely used methods include total protein quantification and particle concentration quantification via NTA. Additional quantification methods may include RNA and lipid quantification.

EV labeling

EVs contain multiple components which are suitable for labeling. Lipid dyes have been widely used due to their easy use and brightness. Among them, PKH dyes (Sigma) and Di dyes (Invitrogen) are commonly used [13,14]. Other labeling approaches involve chemical conjugation of EV surface proteins via amine reaction using dyes such as Carboxyfluorescein succinimidyl ester (CFSE), Alexa Fluor protein labeling kits (Invitrogen) or Cellbrite Fix™ (Biotium)[15,16]. Lastly, cell lines can be genetically modified to produce labeled EVs. For example, fusion of a protein enriched in EVs (such as CD63, CD81 or CD9) with a fluorescent protein (such as GFP or mCherry) may be recombinantly expressed, such as it gets incorporated into EVs prior to release [17,18].

In this chapter, we aimed to validate and optimize methods to produce, characterize and label EVs using B16F10 tumor cells as a model system.

2.2. Materials and methods

Materials

Chemicals were purchased from Sigma-Aldrich, cell culture reagents were purchased from Gibco, flow cytometry antibodies were purchased from Biolegend, unless otherwise stated.

Cell lines

B16-F10 melanoma cells (American Type Culture Collection) were maintained in high-glucose DMEM with L-glutamate supplemented with 10% heat-inactivated FBS. For EV production, media were supplemented with 2-5% exosome-depleted FBS. All cell lines were routinely tested negative for mycoplasma contamination.

EV purification by size-exclusion

EVs were purified from 2- to 3-day cell–conditioned medium by concentration and size-exclusion separation. Briefly, cells and debris were cleared from supernatant by serial centrifugations 5 min at 300 g, 15 min at 2,000 g, and 20 min at 12,000 g. Then, the supernatant was concentrated to 500 µl using Amicon Ultra-15 Centrifugal Filter Units, and EVs were separated from free proteins using qEVoriginal Size Exclusion Columns (Izon).

EV purification by ultracentrifugation

EVs were purified from 2- to 3-day cell–conditioned medium. Cells and debris were cleared from supernatant by serial centrifugations 5 min at 300 g, 15 min at 2,000 g, and 20 min at 12,000 g. Supernatants were then centrifuged 1h30 at 110,000 g, pellets were resuspended in PBS, centrifuged again 1h30 at 110,000 g and resuspended in PBS. EV concentration was quantified by NTA and protein contents were quantified by BCA assay (Thermo).

EV fluorescent labeling

EV membranes were labeled with PKH26 (Sigma-Aldrich), DiD or DiL (Invitrogen), and EV surface proteins were labeled with the Alexa Fluor 647 Protein Labeling Kit (Invitrogen) or Cellbrite (Biotium) according to the manufacturer's protocols and purified from unbound dye using a qEVoriginal Size Exclusion Column or ultracentrifugation for 1h30 at 110,000 g.

Nanoparticle tracking analysis

NTA measurements were performed with a NanoSight NS300 (Malvern Instruments Ltd, Malvern, UK), equipped with a Low Volume Flow Cell Gasket and a 488 nm Blue Laser Module. The samples were injected manually with 1 ml tuberculin syringes (Excel) until the solution reached the tip of the nozzle, and then infused at constant flow rate using a syringe pump. The samples were measured for 60 s with manual shutter and gain adjustments. Three measurements per sample were performed. The software used for capturing and analyzing the data was the NTA 3.2 Dev Build 3.2.16.

Western blot

EVs or cell lysates were mixed with Laemmli SDS sample buffer (Alfa Aesar), incubated 10 min at 95°C, and cooled to 4°C. Electrophoresis was performed on Mini-PROTEAN TGX Gels (Bio-Rad). Proteins were transferred to a polyvinylide difluoride membrane (Bio-Rad). After overnight blocking at 4°C in Tris-buffered saline (TBS) 5% milk, primary antibodies in TBS 1–5% milk were applied for 1 h at room temperature, and secondary, HRP-conjugated, antibodies were applied in TBS 1–5% milk for 1 h at RT. The following antibodies were used: anti-CD9(1:500; C9993; Sigma-Aldrich), anti-CD63 (1:200; SC-15363; Santa Cruz Biotechnology), anti-CD81 (1:1,000; SAB 3500454; Sigma-Aldrich), and TSG101 (1:1,000; T5701; Sigma-Aldrich).

Statistical analysis

Data were processed using Microsoft Excel v.16.0. Data were represented and statistics were computed using Prism v.8 (GraphPad). Numerical data are shown as mean ± SEM unless otherwise stated. Asterisks show groups statistically different and represent p values of specific statistical tests described in figure legends.

2.3. Results

Cell culture conditions affect EV production in vitro

In order to produce exosomes *in vitro*, we first analyzed the release of particles from B16F10 tumor cells under standard culture conditions, with various levels of fetal bovine serum (FBS) and cell density over 48 hr by NTA. In all conditions, high densities of particles were detected in cell-conditioned medium, with particle size modes of 105-120 nm as previously reported for B16F10 EVs by others [17] (**Figure 2.1** A-B). Increasing serum level lead to increased particle densities, which may be due to increased cell growth as this difference is not observed upon normalization to cell metabolic activity (**Figure 2.1** C-D). Interestingly, particle production did not increase proportionally with cell numbers, as doubling cell numbers from 50,000 cells to 100,000 cells per well led to a mild increase in particle density.

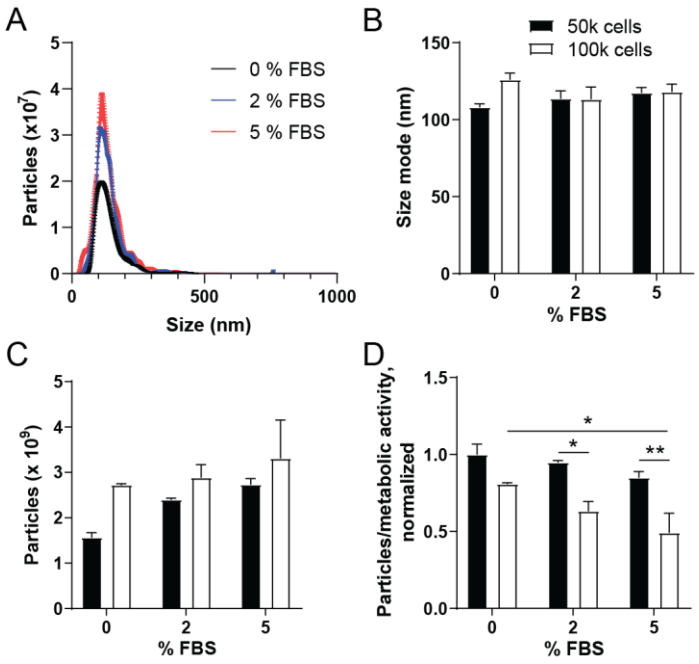

Figure 2.1. Nanoparticle tracking analysis in tumor cell-conditioned medium. (A-D) Analysis of particles released by B16F10 cells *in vitro* over 48 h in medium supplemented with indicated levels of exosome-depleted fetal bovine serum (FBS). Size distribution of particles released by 50,000 cells (A), particle size mode (B), particle concentration (C), and particle concentration normalized to cell metabolic activity measured by Alamar blue assay at experimental endpoint (D). n=3. Bars represent mean ± SEM, *p<0.05, **p<0.01 using 2-way ANOVA.

EV purification methods result in different EV yields

We tested two methods to isolate EVs from cell-conditioned medium, namely the ultracentrifugation and size-exclusion methods (**Figure 2.2**). In both methods, cell-conditioned medium is cleared from cells and debris by serial centrifugation steps (300 g, 2000 g, 12,000 g). Then, EVs are pelleted by ultracentrifugation, washed in PBS, pelleted again by ultracentrifugation and resuspended in PBS. Alternatively, supernatant is concentrated using centrifugal filters, and then applied to size-exclusion columns with pore size of 70 nm. The first fractions are collected which contain EVs larger than 70 nm.

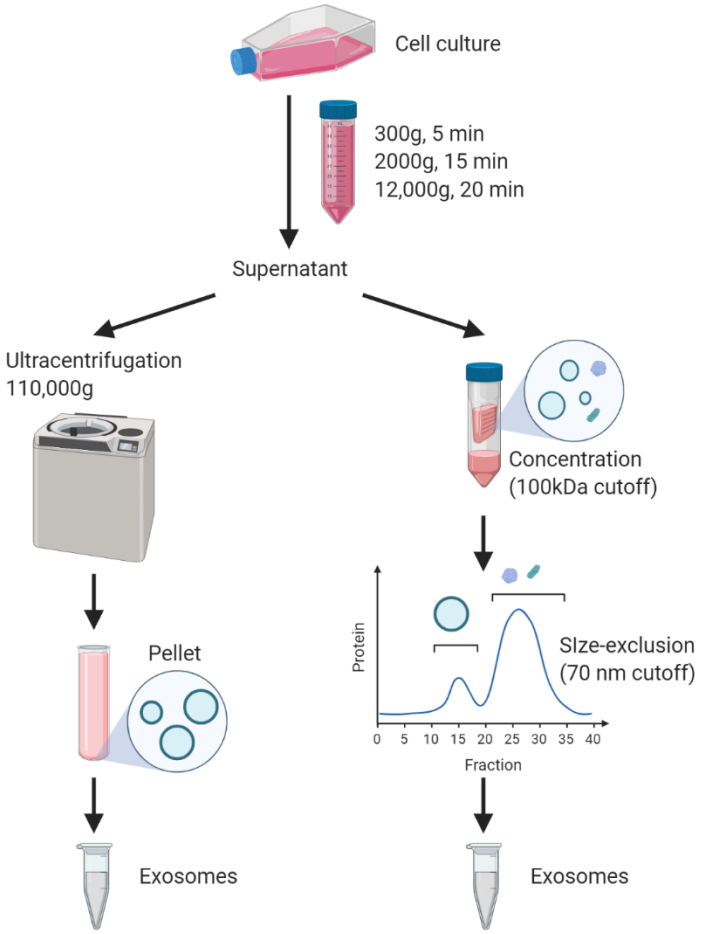

Figure 2.2. EV purification workflow using ultracentrifugation or size-exclusion methods. Created with BioRender.com.

We compared the yield of EVs obtained by ultracentrifugation vs. size-exclusion chromatography. While the size of the purified EVs (**Figure 2.3** A-B) and protein to particle ratios (**Figure 2.3** D) are similar in EVs purified using either method, we found that the fraction of particles recovered using SEC was higher than using ultracentrifugation (**Figure 2.3** C).

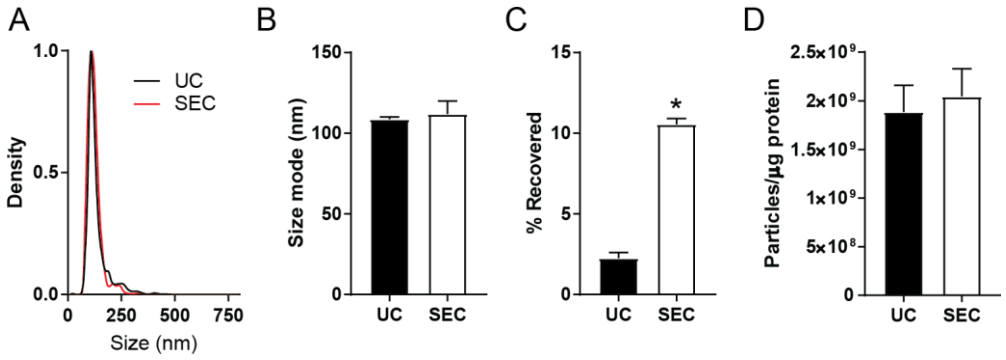

Figure 2.3. EVs purified using ultracentrifugation vs. size-exclusion chromatography. (A-E) Characterization of B16F10 EVs purified by ultracentrifugation (UC) vs. size-exclusion chromatography (SEC). Size distribution of particles (A), Particle size mode (B), percentage of particles recovered of total particles measured in starting cell-conditioned medium (C), particle number to protein ratio (D). n=2. Bars represent mean ± SEM. *p<0.05 using Student's t test.

EV purification from tumor cells *in vitro*, *in vivo* and *ex vivo*

EVs produced by cells of the tumor *in vivo* differ from *in vitro*-released EVs due to the heterogeneity of the cell types of the tumor microenvironment including tumor cells and host immune and stromal cells [19] as well as to the tissue biochemical and biomechanical properties [20]. We tested 3 strategies to harvest EVs released from tumor cells and cells of the tumor microenvironment *in vitro*, *in vivo* and *ex vivo* (**Figure 2.4** A). First, we purified EVs from *in vitro* cultures of B16F10 cell variants, and confirmed their enrichment in EV-specific proteins (Alix and TSG101) and low levels of GAPDH and endoplasmic reticulum-associated Calreticulin compared to cell lysates (**Figure 2.4** B). Then, B16F10 tumors were inoculated intradermally in mice, and tumors were harvested when they reached about 300 mm^3 (day 12-14 after inoculation). Tissues were dissociated by enzymatic digestion, cells were spun down, and digestion supernatants were collected for purification of EVs ("*in vivo*" EVs) by ultracentrifugation. Digested cells were plated in dishes for 48 hr after which EVs ("*ex vivo*"

EVs) were purified by ultracentrifugation. While the EV marker TSG101 was detected in both *in vivo* EVs and *ex vivo* EVs, the *ex vivo* EVs appeared to have a higher level of purity with higher levels of TSG101 and lower level of non-EV protein Calreticulin (**Figure 2.4** C).

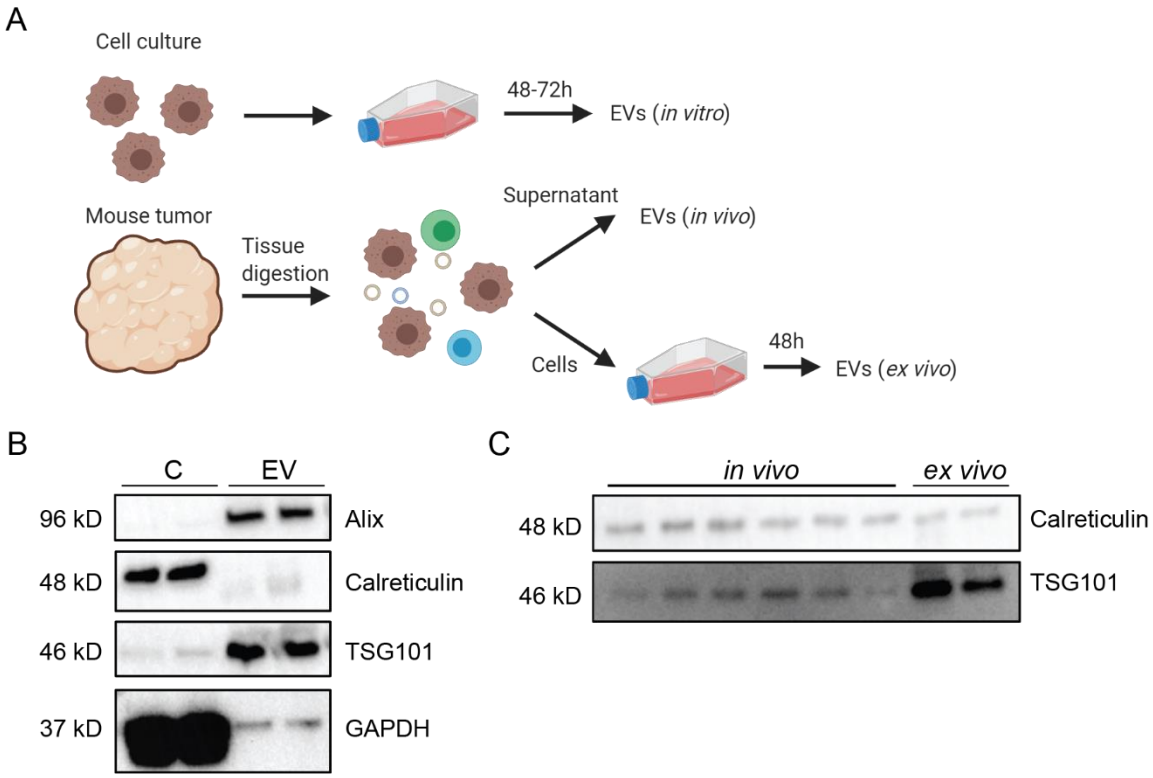

Figure 2.4. Characterization of EVs isolated from various sources. (A) Sources of tumor-derived EVs including *in vitro* cell culture, mouse tumors and *ex vivo* tumor derived-cell culture. (B) Protein composition of EVs (EV) from *in vitro* culture of B16F10 (+/-VEGFC) cells compared to cell lysate (C), 2 µg total protein loaded per lane. (C) Protein composition of EVs purified from B16F10 (+/-VEGFC) mouse tumors (*in vivo*) and *ex vivo* tumor cell culture supernatant (*ex vivo*), ~10 µg total protein loaded per lane.

Optimization of EV immunoaffinity bead capture for semiquantitative analysis

To complement NTA of particles, which quantifies all nanoparticles in solution including non-EV particles such as protein aggregates and lipoprotein particles, we sought to optimize a method to specifically measure levels of EVs by immunoaffinity. For this, we utilized biotin-

functionalized magnetic beads, namely Dynabeads, which we coated with EV-specific capture antibodies (anti-CD9, anti-CD63, anti-CD81 or a combination of all antibodies) through Streptavidin-Biotin interaction (**Figure 2.5** A). We first incubated the beads with EV solutions. Then, to detect EVs bound to beads, we used a combination of fluorescently labeled EV-specific antibodies (combination of anti-CD9-PE, anti-CD63-PE and anti-CD81-PE antibodies). We first tested the assay on solutions of purified B16F10 EVs, and detected concentration-dependent fluorescence intensity in the beads coated with single EV-specific antibodies or with a combination of three EV-specific antibodies (**Figure 2.5** B-C). The highest fluorescence signal was detected on beads coated with anti-CD9 antibody. As EV purification is associated with major and variable EV losses, it is desirable to quantify EV levels prior to purification. Therefore, we tested the potential of the assay to detect unpurified EVs in conditioned media (**Figure 2.5** D) and in plasma (**Figure 2.5** E). We detected fluorescence signal dependent on the dilution of both fluids, suggesting that this assay may provide a semi-quantitative analyses of EVs in complex fluids such as cell-conditioned media and plasma.

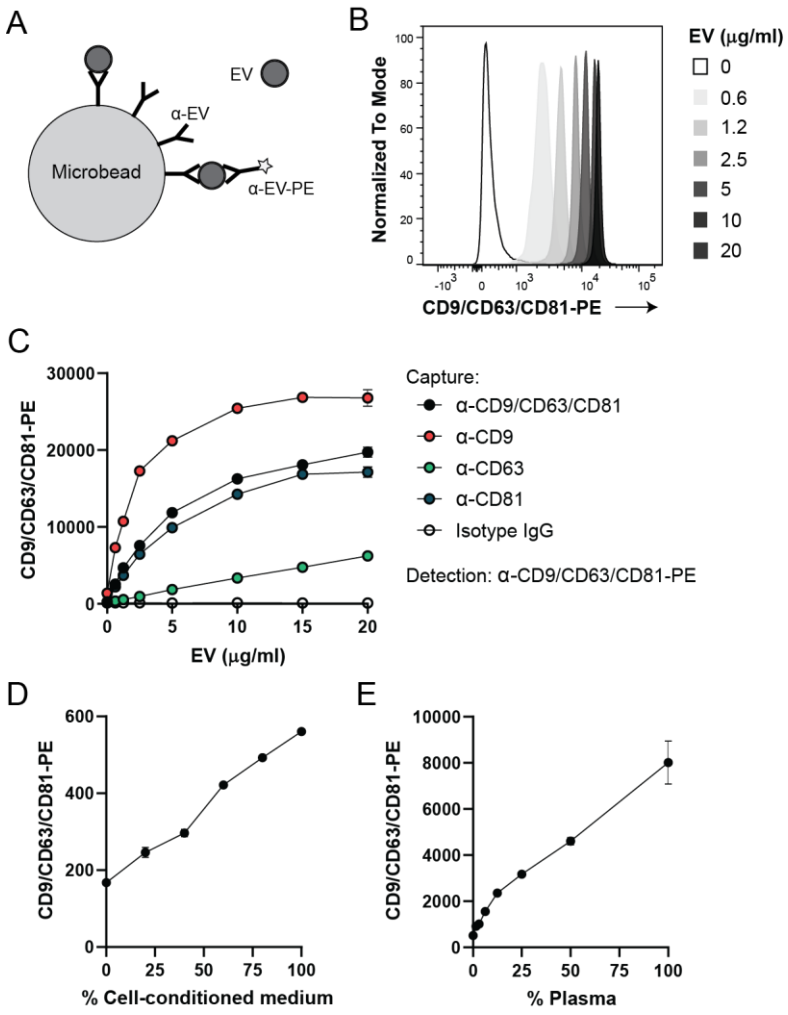

Figure 2.5. Semiquantitative analysis of EVs by flow cytometry. (A) Strategy for EV capture and labeling on microbeads using EV-specific antibodies (α-EV) for capture on beads, and Phycoerythrin (PE)-labeled, EV-specific antibodies (α-EV-PE) for detection. (B) Representative median fluorescence intensity (MFI) of purified B16F10 EVs at various concentrations captured on beads by a combination of anti-CD9, anti-CD63 and anti-CD81 antibodies, and stained with anti-CD9-PE, CD63-PE and CD81-PE. (C) MFI of purified B16F10 EVs captured by anti-CD9, anti-CD63, anti-CD81 or a combination of all antibodies, and detected by anti-CD9-PE, CD63-PE and CD81-PE (n=2). (D-E) MFI of non-purified EVs from (D) B16F10 cell-conditioned medium (n=2) and (E) naïve mouse plasma (n=3) at various concentrations captured on beads by a combination of anti-CD9, anti-CD63 and anti-CD81 antibodies, and stained with anti-CD9-PE, CD63-PE and CD81-PE. Data points represent mean ± SEM.

Fluorescence labeling of selected EV compartments

EVs possess multiple components that can be targeted for fluorescent labeling. We tested multiple strategies, including membrane labeling via lipid dyes (PKH and Di), protein labeling via amine reaction, and enzyme-dependent intra-EV labeling dye (CFSE, **Figure 2.6** A-B). We found that multiple dyes successfully led to fluorescent labeling of EVs as determined by flow cytometry (**Figure 2.6** C), and that they could be combined to simultaneously label two EV compartments (**Figure 2.6** D).

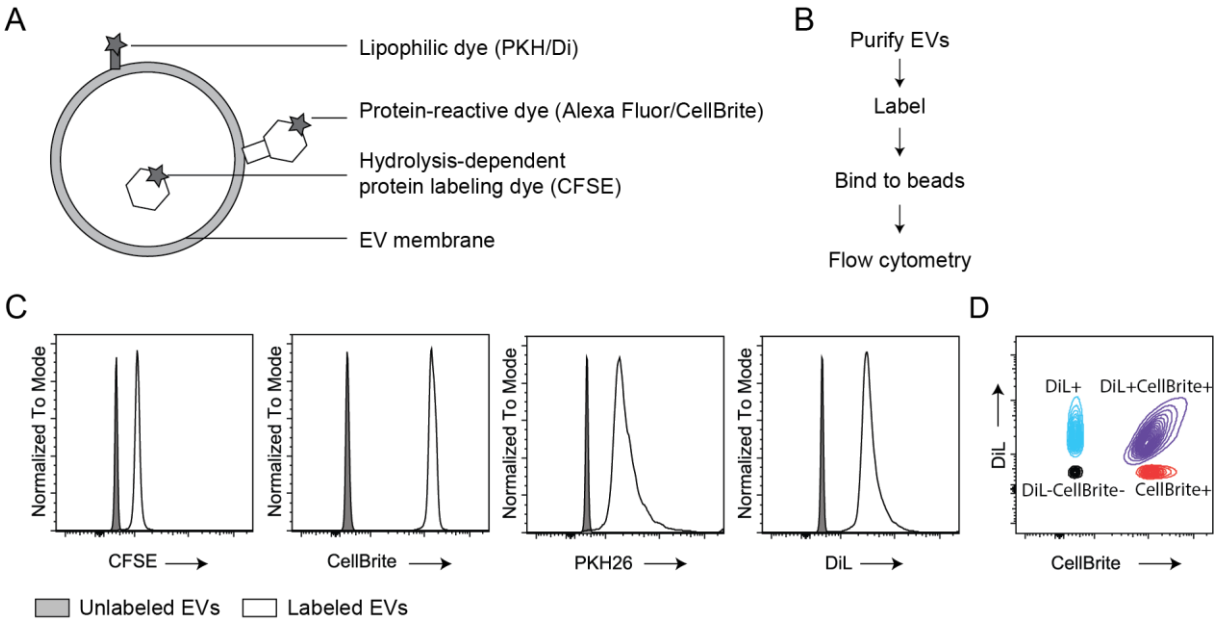

Figure 2.6. EV fluorescence labeling. (A) Overview of strategies to fluorescently label selected compartments of EVs. (B) Workflow for generation of fluorescently labeled EVs. (C-D) Flow cytometry analysis of EV fluorescence on beads. Analysis of exosomes labeled with one selected dye (C), analysis of EVs labeled for surface proteins (CellBrite) and/or membranes (DiL).

2.4. Discussion

We found that EVs are produced by tumor cells seeded at various cell densities and in under various serum levels, although in slightly different amounts. In order to maximize cell integrity and growth and prevent dead cell debris contamination in EV preparations, we produced EVs at serum levels of 2-5 % in subsequent experiments of this thesis.

EVs were purified based on their density and size via ultracentrifugation or size-exclusion chromatography. These methods were selected for their superior purity yields compared to precipitation reagents such as ExoQuick™ and Total Isolation Reagent™, as well as their capacity to purify EVs from larger volumes of conditioned media. Alternative methods would have enabled greater levels of purity, such as extra steps of purification using density gradient ultracentrifugation or immunoaffinity purification. However, these later methods lead to excessive EV loss and would have been difficult to scale up to reach required EV yields for EV distribution studies.

We saw that EVs purified from *in vitro* cultures of tumor cells were much richer in EV markers than EVs purified from *in vivo* or *ex vivo* tumor cells. This is likely due to increased cell viability and thus lower levels of cell debris contamination, as well as lower levels of non-tumor cell derived particles such as HDL, LDL and protein aggregates found *in vivo*. Therefore, additional purification steps may be particularly required when working with liquid biopsies and tissues. In Chapter 5, we describe the use of a combination of ultracentrifugation and size-exclusion methods to improve purity while maximizing EV yields from patient liquid biopsies.

EVs were labeled by lipid dyes or protein-reactive dyes. Lipid dyes are easy to use and bright. Protein labeling yields bright EVs as well and enables fixation for downstream fluorescence analysis. One limitation to protein labeling is that it may also label non-EV contaminating proteins.

Due to the complexity of the extracellular milieu and of the heterogeneity and nature of EVs, production, quantification and purification of EVs are not straight forward procedures. As multiple approaches are now available, it is necessary to select and optimize methods according to study needs. In this chapter, we have selected methods which enable to study bulk EV properties by producing, purifying, quantifying and labeling medium to large amounts of EVs with acceptable purity and yields from cell-culture conditioned media and tumor tissue materials.

2.5. Acknowledgments

I would like to thank Dr. Maria Broggi and Dr. Daniel Rabe for helpful discussions and technical assistance.

2.6. References

[1] M. Colombo, G. Raposo, C. Théry, Biogenesis, Secretion, and Intercellular Interactions of Exosomes and Other Extracellular Vesicles, Annu. Rev. Cell Dev. Biol. 30 (2014) 255–289. https://doi.org/10.1146/annurev-cellbio-101512-122326.

[2] C. Théry, A. Clayton, S. Amigorena, G. Raposo, Isolation and Characterization of Exosomes from Cell Culture Supernatants, Curr. Protoc. Cell Biol. Chapter 3 (2006) 1–29. https://doi.org/10.1002/0471143030.cb0322s30.

[3] J.B. Simonsen, What are we looking at? Extracellular vesicles, lipoproteins, or both?, Circ. Res. 121 (2017) 920–922. https://doi.org/10.1161/CIRCRESAHA.117.311767.

[4] C. Théry, K.W. Witwer, E. Aikawa, M.J. Alcaraz, J.D. Anderson, e t Al., Minimal information for studies of extracellular vesicles 2018 (MISEV2018): a position statement of the International Society for Extracellular Vesicles and update of the MISEV2014 guidelines, J. Extracell. Vesicles. 7 (2018).

https://doi.org/10.1080/20013078.2018.1535750.

[5] D.K. Jeppesen, A.M. Fenix, J.L. Franklin, J.N. Higginbotham, Q. Zhang, L.J. Zimmerman, D.C. Liebler, J. Ping, Q. Liu, R. Evans, W.H. Fissell, J.G. Patton, L.H. Rome, D.T. Burnette, R.J. Coffey, Reassessment of Exosome Composition, Cell. 177 (2019) 428-445.e18. https://doi.org/10.1016/j.cell.2019.02.029.

[6] A.N. Bo, E. Van Der Pol, A.E. Grootemaat, A.N. Böing, E. Van Der Pol, A.E. Grootemaat, A.W. Frank, A. Sturk, R. Nieuwland, A.N. Böing, E. Van Der Pol, A.E. Grootemaat, A.W. Frank, A.N. Bo, E. Van Der Pol, A.E. Grootemaat, Single-step isolation of extracellular vesicles by size-exclusion chromatography, J. Extracell. Vesicles. 1 (2014) 1–11. https://doi.org/10.3402/jev.v3.23430.

[7] H. Zhang, D. Freitas, H.S. Kim, K. Fabijanic, Z. Li, H. Chen, M.T. Mark, H. Molina, A.B. Martin, L. Bojmar, J. Fang, S. Rampersaud, A. Hoshino, I. Matei, C.M. Kenific, M. Nakajima, A.P. Mutvei, P. Sansone, W. Buehring, H. Wang, J.P. Jimenez, L. Cohen-gould, N. Paknejad, M. Brendel, K. Manova-todorova, J.R. Cubillos-ruiz, G. Galletti, P. Giannakakou, A.M. Cuervo, A. Magalhães, J.A. Ferreira, H. Osório, A.M. Silva, A. Massey, J.R. Cubillos-ruiz, G. Galletti, P. Giannakakou, A.M. Cuervo, J. Blenis, R. Schwartz, M.S. Brady, H. Peinado, J. Bromberg, H. Matsui, C.A. Reis, D. Lyden, A. Magalhães, J.A. Ferreira, H. Osório, A.M. Silva, A. Massey, J.R. Cubillos-ruiz, G. Galletti, P. Giannakakou, A.M. Cuervo, J. Blenis, R. Schwartz, M.S. Brady, H. Peinado, J. Bromberg, H. Matsui, C.A. Reis, D. Lyden, Identification of distinct nanoparticles and subsets of extracellular vesicles by asymmetric flow field-flow fractionation, Nat. Cell Biol. 20 (2018) 332–343. https://doi.org/10.1038/s41556-018-0040-4.

[8] H. Zhang, D. Lyden, Asymmetric-flow field-flow fractionation technology for exomere and small extracellular vesicle separation and characterization, Nat. Protoc. 14 (2019) 1027–1053. https://doi.org/10.1038/s41596-019-0126-x.

[9] M. Ostrowski, N.B. Carmo, S. Krumeich, I. Fanget, G. Raposo, A. Savina, C.F. Moita, K. Schauer, A.N. Hume, R.P. Freitas, B. Goud, P. Benaroch, N. Hacohen, M. Fukuda, C. Desnos, M.C. Seabra, F. Darchen, S. Amigorena, L.F. Moita, C. Thery, Rab27a and Rab27b control different steps of the exosome secretion pathway, Nat. Cell Biol. 12 (2009) 19–30. https://doi.org/10.1038/ncb2000.

[10] J. Kowal, G. Arras, M. Colombo, M. Jouve, J.P. Morath, B. Primdal-Bengtson, F. Dingli, D. Loew, M. Tkach, C. Théry, Proteomic comparison defines novel markers to characterize heterogeneous populations of extracellular vesicle subtypes, Proc. Natl. Acad. Sci. 113 (2016) 968–977. https://doi.org/10.1073/pnas.1521230113.

[11] J. Van Deun, P. Mestdagh, R. Sormunen, V. Cocquyt, K. Vermaelen, J. Vandesompele, M. Bracke, O. De Wever, A. Hendrix, The impact of disparate isolation methods for extracellular vesicles on downstream RNA profiling, J. Extracell. Vesicles. 3 (2014) 1–14. https://doi.org/10.3402/jev.v3.24858.

[12] J. Lötvall, A.F. Hill, F. Hochberg, E.I. Buzás, D. Di Vizio, C. Gardiner, Y.S. Gho, I. V. Kurochkin, S. Mathivanan, P. Quesenberry, S. Sahoo, H. Tahara, M.H. Wauben, K.W. Witwer, C. Théry, Minimal experimental requirements for definition of extracellular

vesicles and their functions: A position statement from the International Society for Extracellular Vesicles, J. Extracell. Vesicles. 3 (2014) 1–6. https://doi.org/10.3402/jev.v3.26913.

[13] J.L. Hood, R.S. San, S.A. Wickline, Exosomes Released by Melanoma Cells Prepare Sentinel Lymph Nodes for Tumor Metastasis, Cancer Res. 71 (2011) 3792–3801. https://doi.org/10.1158/0008-5472.CAN-10-4455.

[14] S. Srinivasan, F.O. Vannberg, J.B. Dixon, Lymphatic transport of exosomes as a rapid route of information dissemination to the lymph node, Sci. Rep. 6 (2016) 24436. https://doi.org/10.1038/srep24436.

[15] M. Santiana, S. Ghosh, B.A. Ho, V. Rajasekaran, W.L. Du, Y. Mutsafi, D.A. De Jésus-Diaz, S. V. Sosnovtsev, E.A. Levenson, G.I. Parra, P.M. Takvorian, A. Cali, C. Bleck, A.N. Vlasova, L.J. Saif, J.T. Patton, P. Lopalco, A. Corcelli, K.Y. Green, N. Altan-Bonnet, Vesicle-Cloaked Virus Clusters Are Optimal Units for Inter-organismal Viral Transmission, Cell Host Microbe. 24 (2018) 208-220.e8. https://doi.org/10.1016/j.chom.2018.07.006.

[16] V. Pospichalova, J. Svoboda, Z. Dave, A. Kotrbova, K. Kaiser, D. Klemova, L. Ilkovics, A. Hampl, I. Crha, E. Jandakova, L. Minar, V. Weinberger, V. Bryja, Simplified protocol for flow cytometry analysis of fluorescently labeled exosomes and microvesicles using dedicated flow cytometer, J. Extracell. Vesicles. 4 (2015) 25530. https://doi.org/10.3402/jev.v4.25530.

[17] H. Peinado, M. Alec, S. Lavotshkin, I. Matei, B. Costa-silva, G. Moreno-bueno, M. Hergueta-redondo, C. Williams, G. García-santos, C.M. Ghajar, A. Nitadori-hoshino, C. Hoffman, K. Badal, B.A. Garcia, M.K. Callahan, J. Yuan, V.R. Martins, J. Skog, R.N. Kaplan, M.S. Brady, J.D. Wolchok, P.B. Chapman, Y. Kang, Melanoma exosomes educate bone marrow progenitor cells toward a pro-metastatic phenotype through MET, Nat. Med. 18 (2012) 883–891. https://doi.org/10.1038/nm.2753.

[18] I. Keklikoglou, C. Cianciaruso, E. Güç, M.L. Squadrito, L.M. Spring, S. Tazzyman, L. Lambein, A. Poissonnier, G.B. Ferraro, L.M. Coussens, A. Bardia, R.K. Jain, J.W. Pollard, M. De Palma, C. Baer, A. Cassará, A. Guichard, M.L. Iruela-Arispe, C.E. Lewis, L.M. Coussens, A. Bardia, R.K. Jain, J.W. Pollard, M. De Palma, Chemotherapy elicits pro-metastatic extracellular vesicles in breast cancer models, Nat. Cell Biol. 21 (2019) 190–202. https://doi.org/10.1038/s41556-018-0256-3.

[19] C. Cianciaruso, T. Beltraminelli, F. Duval, S. Nassiri, R. Hamelin, A. Mozes, H. Gallart-Ayala, G. Ceada Torres, B. Torchia, C.H. Ries, J. Ivanisevic, M. De Palma, Molecular Profiling and Functional Analysis of Macrophage-Derived Tumor Extracellular Vesicles, Cell Rep. 27 (2019) 3062-3080.e11. https://doi.org/10.1016/j.celrep.2019.05.008.

[20] A. Villasante, A. Marturano-Kruik, S.R. Ambati, Z. Liu, A. Godier-Furnemont, H. Parsa, B.W. Lee, M.A.S. Moore, G. Vunjak-Novakovic, Recapitulating the Size and Cargo of Tumor Exosomes in a Tissue-Engineered Model, Theranostics. 6 (2016) 1119–1130. https://doi.org/10.7150/thno.13944.

CHAPTER 3

LYMPHATIC TRANSPORT OF EXTRACELLULAR VESICLES

3.1. Abstract

In this chapter, I investigated the contribution of lymphatic vessels to the transport of extracellular vesicles (EVs) from primary tumors to tumor-draining lymph nodes and distant sites. I produced and fluorescently labeled EVs from *in vitro* cultures of the mouse melanoma cell line B16F10. Upon injection into the mouse ear dermis, fluorescent EVs were observed within minutes in draining lymphatics, but not in surrounding blood vessels. Using the B16F10 melanoma model overexpressing the vascular endothelial growth factor C (VEGFC), I found that upon intratumoral injection of EVs, lymphatic endothelial cells within the tumor microenvironment abundantly take up EVs, and at higher levels than blood endothelial cells, delivering EVs to the draining lymph node and eventually to the blood. In transgenic mice lacking dermal lymphatics, EVs injected intratumorally were absent in the lymph nodes and present in far lower amounts in the blood compared to those injected into wild type mice. Additionally, while the density of endogenous blood exosomes increased upon tumor growth in wild type mice, no significant change in blood EV density was observed in transgenic mice. These findings suggested that lymphatic vessels constitute a major route of tumor EV distribution to the systemic circulation.

3.2. Introduction

Particulate transport in the interstitium

Upon release by cells into the interstitium, EVs are exposed to a complex, three-dimensional microenvironment. The extracellular space is shaped by the extracellular matrix (ECM) which provides mechanical support and plays important roles in signal transduction by directly providing mechanical and biochemical cues to cells, as well as by retaining

biomolecules and particulates via mechanical trapping or chemical interactions [1]. Additionally, the interstitium is constantly perfused by a slow fluid flow (typically 0.1-1 μm/s), named interstitial flow, which is primarily driven by plasma leaving blood capillaries and draining to initial lymphatic vessels [2]. Interstitial flow not only induces mechanical stress on cells and on the ECM, but also, importantly, contributes to the redistribution and transport of proteins and particulates within the interstitial space [3].

Diffusion is inversely related to particle size, while convection – the transport of particles along flow – becomes more important as particle size increases [1]. As such, interstitial flow constitutes the main driver of large particle distribution, which are primarily directed by virtue of convection towards lymphatic vessels rather than blood vessels [4]. Early studies showed that, after subcutaneous injection, liposomes of 70 nm were efficiently transported by lymphatics to the dLN and blood, 170 nm particles were transported to the dLN and blood but to a lesser extent to the blood. Importantly, 400 nm liposomes were not detected in the blood [5]. Our group obtained similar findings using polymer nanoparticles. Particles in the size range of 20-50 nm were very efficiently transported to dLNs, while larger (100 nm) were transported too, albeit less efficiently [6]. When such nanoparticles are injected intradermally in mice lacking dermal lymphatics, transport to the dLNs and blood is abrogated, showing that lymphatic vessels are required for nanoparticle distribution from the skin to the dLNs and blood [7].

Active transport functions of the lymphatic endothelium

Interstitial fluid and solutes are thought to be primarily transported into initial lymphatic vessels via hydraulic pressure gradients across the vessel wall. Initial lymphatic vessels are

blind-ended structures composed of a single layer of lymphatic endothelial cells (LECs) directly attached to the ECM by anchoring filaments. Upon increase in interstitial pressure, anchoring filaments stretch and exert radial pressure on initial lymphatics which increases their luminal volume and draws fluid into the vessel. Fluid can enter lymphatics through openings within discontinuous button-like structures without disrupting junction integrity [8]. As vessels fill, button-like junctions close and prevent fluid backflow into the interstitium. Space between "buttons" have been measured at around 3 μm [8] and constitute a potential route for particle entry into lymphatic vessels. In addition, fluids and solutes can also be transported transcellularly across the lymphatic endothelium via transcytosis mechanisms [9,10]. Lastly, particulates may be taken up by dendritic cells which can actively migrate into lymphatics [11].

LECs actively regulate trans-lymphatic transport by modulating both paracellular and transcellular transport pathways [10]. LEC permeability can be increased by inflammatory cues such as TNF-α, IL-1β, IL-6 and IFN-γ through cytoskeleton and cellular junction reorganization [12,13]. LEC permeability may also be reduced by microenvironment cues, which could help prevent viral dissemination and diet-induced obesity [14,15]. Interstitial flow was also shown to regulate fluid and solute transport across LECs, mostly by regulating vesicular, transcellular transport [9,10]. Many pathologies are associated with the growth of new lymphatic vessels, termed lymphangiogenesis [16]. Lymphangiogenesis often results in increased lymphatic transport, and thus provides an additional mechanism by which tissues may increase their communication with the draining lymph nodes and distant sites.

EV distribution to the draining lymph nodes and distant sites

Lymphatic vessels directly connect tissues with LNs, and as such efficiently deliver EVs sampled from healthy tissues and tumors to dLNs [17–19]. Early studies showed that intradermally injected EVs could mount potent immune responses, pointing towards the idea that EVs were efficiently transported to LNs [20]. Hood and colleagues reported that melanoma EVs could be picked up by cells of the dLN and remodel gene expression to support metastatic growth [17]. Subcapsular macrophages are highly exposed to EVs entering the LN, and constitute a physical barrier to partially prevent penetration of EVs into the node [18,21]. Nevertheless, EVs were shown to get access to deeper zones of the lymph nodes and to participate in immune response modulation. For example, tumor-derived EVs were found to present PD-L1 to inhibit T cell activation in the tumor-draining LN [22]. Finally, lymph in the thoracic duct – the main conduit driving lymph into the systemic circulation – was also found to contain tissue-derived EVs [18,23], suggesting that EVs may be transported beyond the LNs and eventually delivered to the blood.

In this chapter, we show that due to their size EVs do not diffuse in the extracellular space. As such, they are transported by convection with interstitial flow, making lymphatic vessels the primary route of EV transport. In this process, LECs partially take up EVs and actively regulate their transport. Lastly, LECs also produce their own EVs, which may contain solutes that they sampled from the extracellular space. Together, this chapter highlights a central role for lymphatic vessels in the regulation of EV production and distribution.

3.3. Materials and Methods

Reagents

Chemicals were purchased from Sigma-Aldrich, cell culture reagents were purchased from Gibco, flow cytometry antibodies were purchased from BioLegend, unless otherwise stated.

Cell lines

B16F10 melanoma cells (American Type Culture Collection) were maintained in high-glucose DMEM with L-glutamate supplemented with 10% heat-inactivated FBS. 4T1 breast cancer cells (American Type Culture Collection) were maintained in RPMI L-glutamate supplemented with 10% heat-inactivated FBS. For EV production, media were supplemented with 2-5% exosome-depleted FBS. Lentiviral vectors were used for stable expression of VEGFC, mCherry or control vectors. All cell lines were routinely tested negative for mycoplasma contamination. Human dermal lymphatic endothelial cells (Lonza or PromoCell) were maintained in EGM-2 medium (Lonza) and used at passage 5-9.

Animals

Wild type (WT) female mice (C57Bl/6J, Balb/cJ) were purchased from the Jackson Laboratory (Bar Harbor, Maine, USA) and used at age 8-12 weeks. K14-VEGFR3-Ig mice previously described [24] were maintained on a C57Bl/6 background and crossbred with C57Bl/6J mice from The Jackson Laboratory. K14-VEGFR3-Ig and wildtype littermates of both sexes were used at age 8-16 weeks. All experiments were performed with approval from the Veterinary Authority of the Institutional Animal Care and Use Committee at the University of Chicago under protocols no. 72530 and 72551.

Tumor models

250,000 B16F10 cells were inoculated intradermally in 30 µl PBS into the back flank of C57Bl/6J mice. Tumor growth was monitored with calipers and tumor volume was calculated as Volume = $4\pi*(x/2)*(y/2)*(z/2)/3$.

EV purification by size-exclusion

EVs were purified from 2- to 3-day cell–conditioned medium by concentration and size-exclusion separation. Briefly, cells and debris were cleared from supernatant by serial centrifugations 10 min at 300 g, 10 min at 2,000 g, and 20 min at 12,000 g. Then, the supernatant was concentrated to 500 µl using Amicon Ultra-15 Centrifugal Filter Units, and EVs were separated from free proteins using qEVoriginal Size Exclusion Columns (Izon).

Fluorescent labeling of EVs

EV membranes were labeled with PKH26 (Sigma-Aldrich), DiD or DiL (Invitrogen), and EV surface proteins were labeled with the Alexa Fluor 647 Protein Labeling Kit (Invitrogen) or CellBrite (Biotium) according to the manufacturer's protocols and purified from unbound dye using a qEVoriginal Size Exclusion Column or ultracentrifugation for 1 h 30 at 110,000 g.

Nanoparticle tracking analysis

NTA measurements were performed with a NanoSight NS300 (Malvern Instruments Ltd, Malvern, UK), equipped with a Low Volume Flow Cell Gasket and a 488 nm Blue Laser Module. The samples were injected manually with 1 ml tuberculin syringes (Excel) until the solution reached the tip of the nozzle, and then infused at constant flow rate using a syringe pump. The samples were measured for 60 s with manual shutter and gain adjustments. Three

measurements per sample were performed. The software used for capturing and analyzing the data was the NTA 3.2 Dev Build 3.2.16.

Western blot

EVs or cell lysates were mixed with Laemmli SDS sample buffer (Alfa Aesar), incubated 10 min at 95°C, and cooled to 4°C. Electrophoresis was performed on Mini-PROTEAN TGX Gels (Bio-Rad). Proteins were transferred to a polyvinylide difluoride membrane (Bio-Rad). After overnight blocking at 4°C in Tris-buffered saline (TBS) 5% milk, primary antibodies in TBS 1–5% milk were applied for 1 h at room temperature, and secondary, HRP-conjugated, antibodies were applied in TBS 1–5% milk for 1 h at RT. The following antibodies were used: anti-CD9 (1:500; C9993; Sigma-Aldrich), anti-CD63 (1:200; SC-15363; Santa Cruz Biotechnology), anti-CD81 (1:1,000; SAB 3500454; Sigma-Aldrich), and TSG101 (1:1,000; T5701; Sigma-Aldrich).

Tissue digestion

Tumors, lymph nodes and lungs were harvested from euthanized animals and digested as previously described [25]. Briefly, tissues were thinly cut, digested in DMEM medium supplemented with 1 mg/mL collagenase IV (Worthington-Biochem), 40 µg/ml DNAse I (Roche), 3.3 mg/ml collagenase D (Roche), 1.2 mM $CaCl_2$, 2-5% FBS for 1 h at 37°C with magnetic stirring or rotation. After repeated pipetting, enzymatic digestion was quenched with EDTA at a final concentration of 5 mM followed by addition of full medium. Lung cells were depleted of red blood cells using ACK lysis buffer for 3 min. Cells were then filtered through a 70 µm strainer, washed and analyzed. For splenocyte analysis, spleens were mashed through a 70 µm strainer, red blood cells were lysed for 3 min in ACK lysis buffer

(Gibco), and remaining cells were washed and analyzed. For blood analysis, 50 µl of blood collected in EDTA-coated tubes was used. Samples were depleted of red blood cells by 3 x 3 min incubation in ACK lysis buffer, washed and analyzed.

Flow cytometry

Single cell suspensions were stained with Fixable Viability Dye eFluor 455 UV (eBioscience) or Horizon Fixable Viability Stain 510 (BD Biosciences) for 15 min in PBS. Fc receptors were blocked with anti-CD16/32 antibodies (eBioscience) in FACS buffer (PBS 2% FBS) for 10 min at 4°C. Antibodies against surface markers were applied for 20 min in FACS buffer at 4°C. Cells were fixed in 2% paraformaldehyde (Affymetrix) for 15 min at 4°C, or using the Foxp3 fixation/permeabilization kit (eBioscience) following manufacturer's protocol. The following antibodies were used: CD31 ef450, gp38 AF488, and CD45 APC-Cy7. Cells were analyzed using a LSRFortessa X-20 flow cytometer (BD Biosciences), and data was processed using FlowJo software package v.10.6.1. LECs were defined as $CD45^{-}CD31^{+}gp38^{+}$, blood endothelial cells as $CD45^{-}CD31^{+}gp38^{-}$, cancer-associated fibroblasts and fibroblastic reticular cells as $CD45^{-}CD31^{-}gp38^{+}$, and other $CD45^{-}$ as $CD45^{-}CD31^{-}gp38^{-}$.

***In vitro* EV transport assay**

100,000 human, dermal LECs (PromoCell) were seeded on the underside of collagen coated 3 µm-pore cell culture inserts (Cat. 353096, Falcon). In order to induce ~0.1 µm/sec transmural flow, a medium pressure head was applied in the insert. Once cells reached confluence, labeled EVs were applied in the insert. Medium was collected in the bottom well at specific time points and fluorescence was measured by plate reader.

Immunofluorescence staining

Cells were fixed for 15 min in 2% PFA, washed in PBS, incubated for 10 min in TBS 0.1% Triton and 30 min in TBS casein 0.5% prior to immunostaining. They were then incubated with primary antibodies in TBS Casein 0.5% overnight at 4°C, followed by secondary antibodies for 1 h at RT. Cells were mounted with Prolong Gold Antifade Reagent with DAPI (Invitrogen) and imaged using a Leica DMi8 fluorescent microscope and 25x oil objective. Images were processed with ImageJ (NIH).

***In vivo* EV distribution**

5–10 μg of EVs in 10 μl were injected intradermally into each mouse hock (the lateral tarsal region just above the ankle). After 24 h, mice were sacrificed. Organs were homogenized in radioimmunoprecipitation assay buffer (Sigma-Aldrich) and centrifuged at 10,000 g for 10 min, and supernatant fluorescence was read by plate reader. To assess EV distribution from tumors, B16-VEGFC tumors were inoculated at day 0, 20–40 μg labeled EVs were injected intratumorally in 20 μl at day 11, and mice were euthanized at day 12 (i.e. 24 h after labeled EV injection).

EV drainage in ear dermis and whole mount imaging

1 μl of Alexa Fluor 647-labeled EVs were injected into mouse dorsal ear dermis. After 30 min, the mouse was euthanized and perfused with Ringer's solution followed by Zinc fixative (4.5 mM $CaCl_2$, 52 mM $ZnCl_2$, 32 mM $Zn(CF_3COO)_2$, 2 mM Tris, and 38 mM glycine, pH 6.5, 340 mOsm/liter). Whole mount staining was performed as described previously [26]. Ears were excised and fixed for 24 h in zinc fixative and 1% Triton X-100. The dorsal skin was isolated, washed in TBS, and blocked for 1 h in TBS 0.5% Casein. Then it was incubated with anti-VE-

cadherin antibody (BD Biosciences) and anti-podoplanin antibody (R&D Systems) for 24 h, washed in TBS 0.1% Tween, and incubated with secondary antibodies for 24 h. After washing in TBS Tween 0.1%, the tissue was dehydrated with 70% ethanol followed by 100% ethanol, cleared in 2:1 benzyl benzoate/benzyl alcohol solution and mounted on a glass slide. Fluorescence images were acquired with an Olympus IX2-DSU fluorescence microscope and a 63× lens. Image stacks were processed with ImageJ (National Institutes of Health).

Statistical analysis

Data were processed using Microsoft Excel v.16.0. Data were represented and statistics were computed using Prism v.8 (GraphPad). Numerical data are shown as mean ± SEM unless otherwise stated. Asterisks show groups statistically different and represent p values of specific statistical tests described in figure legends.

3.4. Results

EV transport is convection-mediated

Particles released by cells into the extracellular space may be transported via diffusion or interstitial flow-based convection [1]. The Peclet number (Pe) – a dimensionless ratio of convective transport over diffusion contribution to mass transport – was computed to determine which transport type dominates EV transport.

Pe is defined as:

$$Pe = \frac{L \cdot u_i}{D_i}$$

where u_i is the bulk convective velocity of the solute i, D_i is its diffusion coefficient, and L is the characteristic length (here the blood-lymphatic intercapillary distance).

The diffusion coefficient D_i was approximated using the Stokes-Einstein equation, assuming a dilute isotropic solution:

$$D_i = \frac{k_B T}{6 \pi \mu_i r_i}$$

where k_B is Bolzmann's constant, T is temperature, μ_j is solvent j viscosity, and r_i is the hydrodynamic radius of particle i.

In a tissue, the ECM may reduce transport due to steric hindrance and ionic interactions. We assumed that the ECM pore size (> 1 μm diameter [27]) was large enough to not trap EVs, and that due to their negative charge EVs have low electrostatic interactions with negatively charged ECM [28,29]. As such, these calculations assume that diffusion and

convection occur in free solution, and the bulk convective velocity of solutes is assumed to be equal to the fluid velocity.

Table 3.1. Parameters of particulate transport in the interstitium.

Interstitial fluid	
Temperature	37 °C
Viscosity	1.5 cP
Physiological flow rate	0.1-1 μm/s
Pathological flow rate	1-10 μm/s
Intercapillary distance	100 μm
Particulate	
Protein hydrodynamic diameter	1-10 nm
EV diameter	50-150 nm

Pe numbers were computed using the approximate values in **Table 3.1** as a function of velocity of interstitial flow (**Figure 3.1** A). Solutes in the size range of proteins (1-10 nm hydrodynamic diameter) are transported by a combination of diffusion and convection in physiological interstitial flow conditions (flowrate 0.1-1 μm/s) as shown with Peclet numbers in the range of 0.1-10, while convection starts dominating transport in pathological flow conditions (flowrate > 1 μm/s), as previously reported [3]. Strikingly, solutes in the size range of EVs (50-150 nm) are mostly transported by convection, as indicated by Pe > 10, both in physiological and pathological flow conditions. This suggests that, upon release into the interstitial space, EVs are largely transported by virtue of convection towards lymphatic vessels (**Figure 3.1** B).

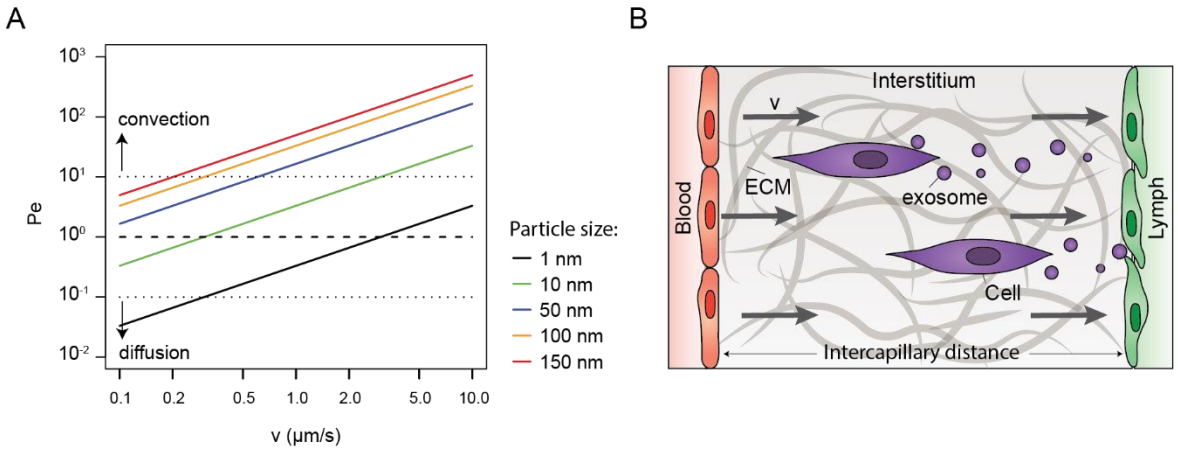

Figure 3.1. EV transport in the interstitum is mediated by convection. (A) Predicted Peclet numbers (Pe) for protein- and EV-size particles in the interstitial space as a function of interstitial flowrate (v) (B) Schematic of cell-released EV transport by virtue of convection toward lymphatic capillary.

Lymphatics are targeted by EVs, and lymphatic endothelial cells pick up large amounts of EVs

To determine whether EV transport toward lymphatic vessels occurred *in vivo*, we purified and fluorescently labeled EVs from *in vitro* cultures of the mouse melanoma cell line B16F10 and injected them into the mouse ear dermis. Minutes after injection, fluorescent EVs were observed in skin draining lymphatic vessels, but not in surrounding blood capillaries, supporting that lymphatics are targeted by EVs *in vivo* (Figure 3.2).

In contrast to healthy tissues, tumors are characterized by a poorly organized vasculature, which results in impaired lymphatic drainage. To determine whether lymphatic targeting by EVs could still occur in such conditions, we injected fluorescently labeled EVs intratumorally in VEGFC-overexpressing B16F10 tumors (B16F10-VEGFC) and measured uptake within cells of the tumor microenvironment (**Figure 3.3** A-C). While most of the cells

taking up EVs are CD45$^+$ immune cells, LECs make up a significant portion as well (**Figure 3.3** A). Additionally, LECs take up more EVs than blood endothelial cells (BECs), as shown by trends of higher percentages of EV-positive cells, and a higher cell fluorescence intensity (**Figure 3.3** B-C).

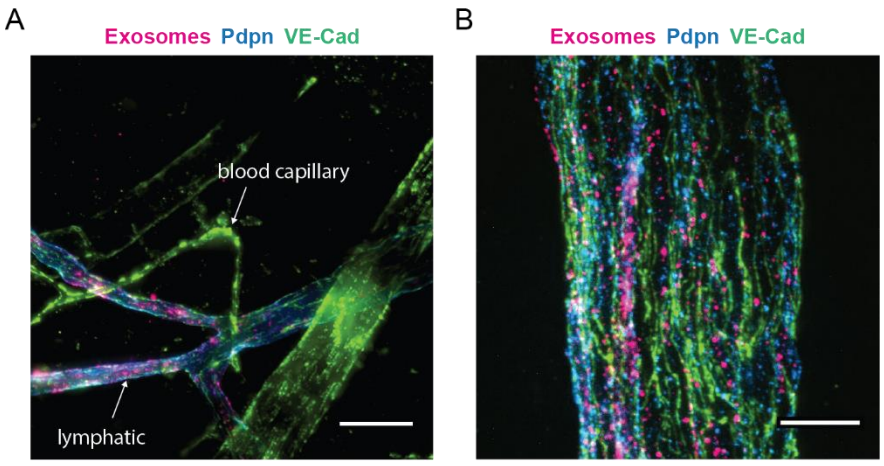

Figure 3.2. EVs are taken up by lymphatic endothelial cells in the skin. EV uptake by lymphatic (VE-cadherin$^+$ [VE-Cad$^+$, green] and podoplanin$^+$ [Pdpn$^+$, blue]), but not blood (VE-Cad$^+$Pdpn$^-$) endothelium, in the mouse ear dermis 30 min after intradermal injection of AF647-labeled EVs (pink). Bars, 50 μm (A) and 10 μm (B). Figure adapted from Broggi, Maillat et al. [19].

Lymphatic vessels deliver sampled fluids and particles from tumors to the tumor-draining lymph nodes (TDLN). As such, we detected large amounts of EVs in the TDLN (**Figure 3.3** D-F). Large portions of LECs in the TDLN took up EVs as well, pointing out to the fact that LECs are EV targets both in the periphery and in downstream draining LNs.

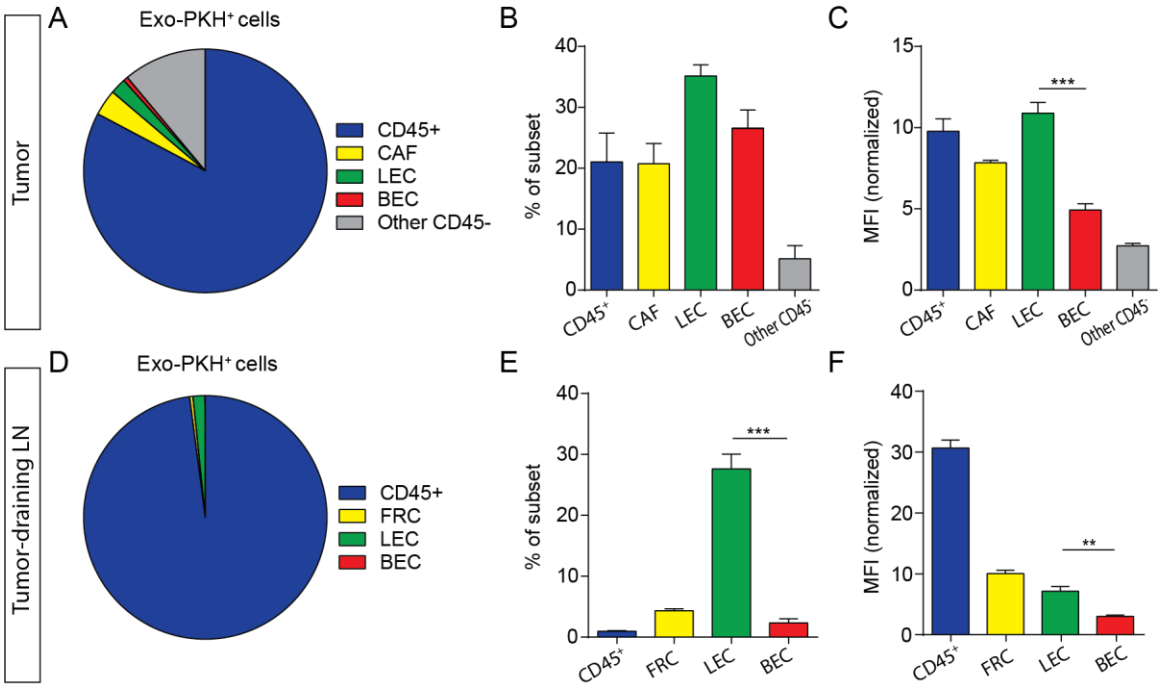

Figure 3.3. Cellular uptake of EVs after intratumoral injection. Distribution of EV-positive cells among total (A) tumor and (D) tumor-draining lymph node (TDLN) cell populations 24 h after intratumoral injection. Percentage of EV-positive cells within each cell subtype among (B) tumor and (E) TDLN cells. Mean fluorescence intensity of EV-positive cells within each cell subtype of the (C) tumor and (F) TDLN. For all data shown, n ≥ 4 per group. Bar plots represent mean ± SEM. Representative of 2 independent experiments. Figure adapted from Broggi, Maillat et al. [19].

EV transport from the skin to distant sites requires lymphatics

To determine the relative contribution of lymphatic vessels to EV distribution to distant sites, we used K14-VEGFR-3-Ig (transgenic [Tg]) mice lacking dermal lymphatics [24] and performed a biodistribution study 24 h after intradermal (i.d.) injection of labeled EVs into mouse hocks. We observed that while EVs injected i.d. into wild type (WT) mice were detected in dLNs, plasma, lungs, and liver, they were nearly undetectable in these tissues after i. d. injection into Tg mice (**Figure 3.4** A,B). Next, we injected labeled EVs directly into implanted B16-VEGFC melanomas, where again they were seen abundantly in WT mice and

to a much lesser extent in the dLNs and plasma of Tg mice (**Figure 3.4** C,D). To confirm that lymphatic vessels played a role in endogenous EV distribution from melanoma tumors, we analyzed the plasma of mice before tumor inoculation (day 0) and after B16-VEGFC tumor inoculation and growth (day 11). We observed that while the quantity of endogenous (non-labeled) EVs increased upon tumor growth in WT mice, no significant increase in EV levels was observed in Tg mice (**Figure 3.4** E).

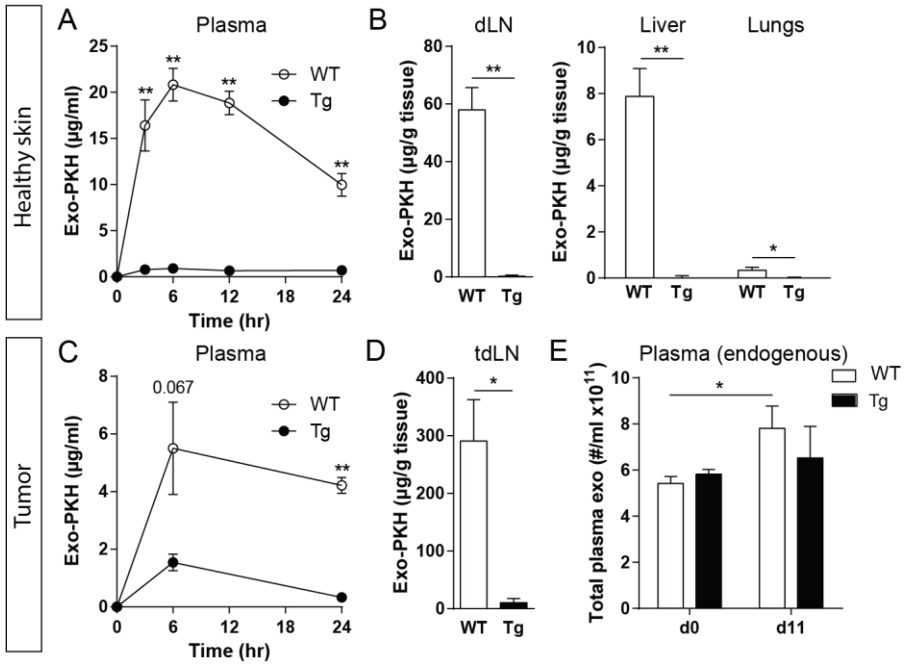

Figure 3.4. EV distribution from the skin and tumors to draining lymph nodes and distant sites require lymphatic vessels. (A-B) Biodistribution of PKH26-labeled EVs (Exo-PKH) after intradermal (i.d.) injection into wildtype (WT) mice and mice lacking dermal lymphatics (K14-VEGFR-3-Ig mice, Tg) in plasma (A) and (B) draining lymph nodes (dLN), liver, and lungs after 24 h. (C-D) EV biodistribution after intratumoral injections into B16-VEGFC tumors, (C) in plasma and (D) in dLN after 24 h. (E) Total endogenous particle concentration in plasma before tumor inoculation (d0) and after 11 days (d11) as determined by nanoparticle tracking analysis. For all data shown, $n \geq 4$ per group in at least two independent experiments; * $p < 0.05$, ** $p < 0.01$ by two-tailed unpaired Student's t test or one-way ANOVA. Data shown as mean $\pm$ SEM. Figure adapted from Broggi, Maillat et al. [19].

Lymphatic endothelial cells actively regulate EV transport *in vitro*

Lymphatic endothelial cells (LECs) have been shown to actively regulate macromolecular transport from the interstitial space into lymphatic vessels (Triacca et al., 2017). Knowing that EVs accumulate in LECs and are transported via lymphatics to the LN, we assessed *in vitro* whether LECs could actively regulate such mechanisms. First, we confirmed that EVs are actively taken up by LECs over time (**Figure 3.5** A, B). Indeed, incubation of LECs with EVs at 37°C but not at 4°C lead to EV accumulation in LECs (**Figure 3.5** A), and EVs accumulated within distinct intracellular compartments, partially in Lamp-1$^+$ late endosomal compartments (**Figure 3.5** B). Next, we cultured LECs on porous inserts to assess EV transport across LEC monolayers (**Figure 3.5** C). We found that upon cell fixation EV transport was reduced, and upon stimulation with inflammatory cytokines EV transport was increased as compared with untreated monolayers (**Figure 3.5** D). This indicates that EV transport is regulated by LEC permeability.

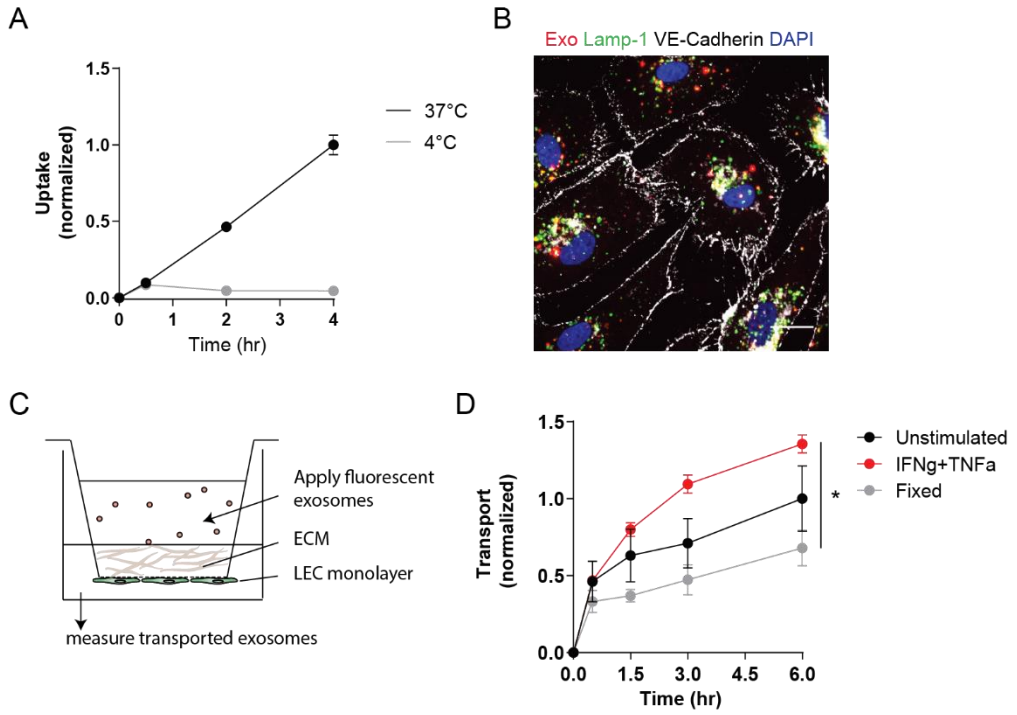

Figure 3.5. Lymphatic endothelial cells take up and transport EVs *in vitro*. (A) Time-dependent uptake of PKH-labeled EVs by human dermal LECs measured by flow cytometry (normalized mean fluorescence intensity, n=3), (B) z-projection of confocal microscopy images of LECs after 4h uptake of PKH-labeled EVs (exo, red), and stained for Lamp-1 (green), VE-cadherin (white) and DAPI (blue), scale = 10 μm, (C) schematic of transendothelial EV transport assay, (D) EV transport across unstimulated, IFNγ+TNFα, or PFA fixation (fixed) treated LEC monolayers (n=3). Data shown as mean ± SEM. * $p < 0.05$ using 2-way ANOVA with Tukey's correction.

Lymphatic endothelial cells produce EVs, and upregulate their production upon cytokine treatment

In addition to transporting EVs, LECs may also produce and release EVs in their vessel lumen for downstream transport. We found that human dermal LECs released EVs *in vitro* in the size-range of exosomes (**Figure 3.6** A), and that purified EVs were enriched for typical exosome marker proteins TSG101 and CD9 but not cellular protein GAPDH, and carried LEC marker podoplanin but not Lyve-1 (**Figure 3.6** B). When cultured on porous membrane

inserts, LECs released EVs mostly on their apical (lumen) side, suggesting a possible release of EVs in lymphatic vessel lumen (**Figure 3.6** C). Additionally, upon treatment with inflammatory cytokines IFNγ and TNFα, both of which can be found in the tumor microenvironment, LECs upregulated their production of EVs (**Figure 3.6** D-E). Together, this data suggests that LECs can contribute to EV-mediated communication not only by transporting EVs from tissues, but also by themselves producing EVs which can be directly released in the lymph and transported to downstream lymph nodes.

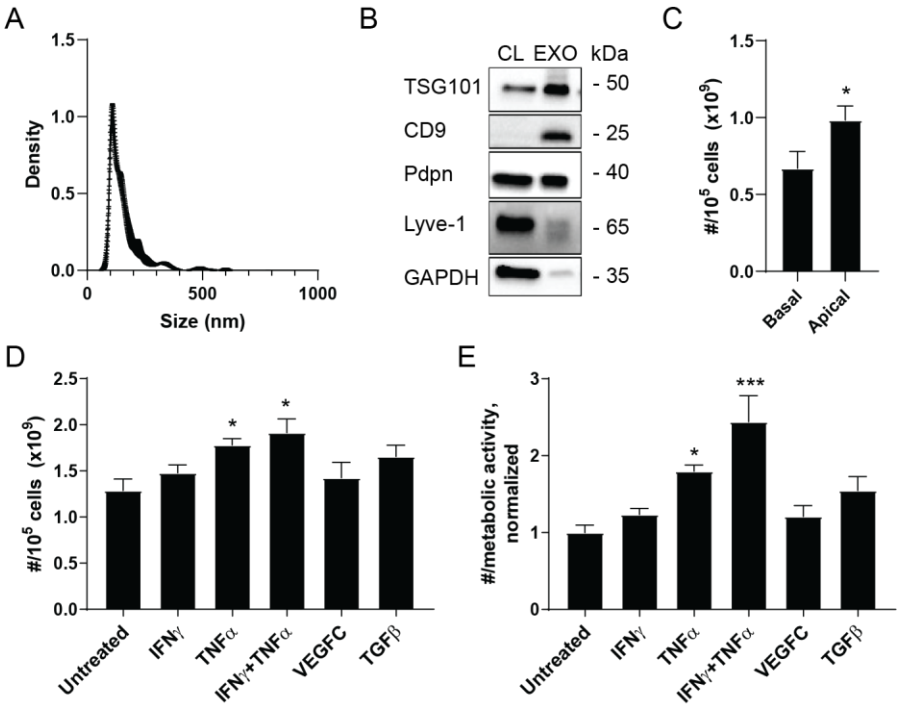

Figure 3.6. EV production by lymphatic endothelial cells *in vitro*. *In vitro* human dermal lymphatic endothelial cell-released EVs. (A) EV size distribution, (B) protein contents of purified EVs (EXO) as compared with cell lysates (CL), (C) vesicle release on LEC basal vs. apical side when cultured on porous membranes of transwell inserts, (D-E) EV production upon culture in presence of cytokines or VEGFC (D) per seeded cell number and (E) per metabolic activity. Data shown as mean ± SEM. *p<0.05, ***<0.005 by paired Student's t test (C) or one-way ANOVA with Dunnett's correction (D-E).

Lymphatic endothelial cells package exogenous proteins into EVs

As LEC can transport macromolecules via transcellular pathways [10] and produce EVs, we assessed the possibility that part of the macromolecules shuttled across LECs were packaged by LECs in EVs and released as such in the vessel lumen. We loaded LECs cultured *in vitro* with tumor cell proteins labeled fluorescently, washed them thoroughly and applied fresh media. After 48 h, we collected conditioned medium to analyze EVs by flow cytometry (**Figure 3.7** A, B). Fluorescent proteins were detected on beads functionalized with anti-CD63 antibodies and incubated with supernatants from lysate-loaded LECs, while IgG control-functionalized beads did not display any fluorescence (**Figure 3.7** C). Therefore, it appears that part of proteins being transcellularly shuttled across LECs can be packaged and released in EVs (**Figure 3.7** D).

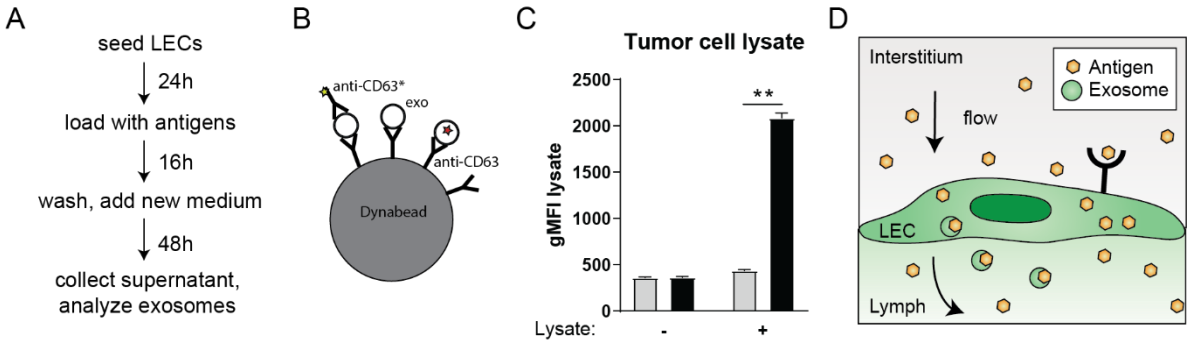

Figure 3.7. LEC packing of extracellular contents into EVs. (A) Experimental procedure, (B) schematic of EV binding to microbeads for downsteam flow cytometry analysis, (C) tumor cell lysate protein contents in EVs, (D) schematic of antigen transport and packing into EVs by LECs. Data shown as mean ± SEM. *p<0.05, **<0.01 by unpaired Student's t test.

3.5. Discussion

As EVs are transported through the interstitium, they may target various cells of the tissue microenvironment [30], be retained into the ECM via specific EV-ECM protein interactions [31] or transported to the draining lymph nodes or distant sites [17,18,32]. Here, we showed that EVs from the skin are transported preferentially by virtue of convection (**Figure 3.1**). As such, EVs are directed toward lymphatic vessels rather than blood vessels (**Figure 3.2**). Among EVs, exosomes have a size particularly suited for lymphatic targeting and transport: it is neither too big to get entrapped in the extracellular matrix fibers, nor too small to diffuse into blood capillaries. As such, exosomes may be more potent at distant cellular communication than larger EVs. It is also likely that extracellular particulates exomeres (< 50 nm) and small exosome populations as defined by Zhan et al. (50-90 nm) [28] are transported more efficiently to dLNs and to the blood than larger exosomes (90-120 nm) which may remain to a greater extent in their tissue of origin, although this remains to be investigated.

The extracellular microenvironment varies greatly between tissue types and is often modified in pathologies, which likely modulates EV transport. In particular, interstitial flow, the blood and lymphatic vasculature as well as ECM fiber organization, density and binding properties are known to play important roles in particulate biodistribution [33,34]. In inflammatory conditions, interstitial flow can increase in the order of 10-fold and increase lymphatic transport [35]. In contrary, in areas of leaky blood vasculature and nonfunctional lymphatics such as in the core of tumors, transport is impaired [35,36], which may lead to increased EV retention in the tissue. Nevertheless, EVs injected intratumorally were found to

be taken up in larger amounts by LECs than BECs, and partially transported to the tumor-draining lymph node (**Figure 3.3**). This indicates that even in conditions of poor vascular organization, lymphatics represent a significant route of EV distribution, and that blood vessels are less exposed to EVs.

We showed that not only immune cells, but also LN stromal cells – and particularly LECs – could pick up EVs within the draining LN. This signifies that EVs may reprogram LECs such as to enhance their contribution to the pre-metastatic niche. LECs from tumor-draining LNs exhibit an altered gene expression profile compared to LECs from healthy LNs [37]. Therefore, future studies on identifying the direct effects of EVs on LECs in the primary tumor and pre-metastatic niche would be relevant.

We showed that lymphatic vessels were required to deliver EVs from healthy skin and tumors to the systemic circulation, as mice lacking dermal lymphatics did not get EVs delivered from the skin to the blood (**Figure 3.4**). This finding has important implications for diagnosis and therapeutic interventions aimed at analyzing or targeting EV contents, respectively. EVs are increasingly investigated as a source of biomarkers as they reflect disease status. In parallel studies, we and others showed that the lymph of melanoma patients was enriched in tumor-associated EVs compared to plasma [19,38]. As such, lymph may represent a valuable source of EVs aimed at diagnosis and treatment response monitoring. Finally, as tumor-derived EVs are known to contribute to cancer metastasis, lymphatic transport routes may be therapeutically targeted to prevent EV delivery to distant sites.

We showed that LECs can regulate EV transport across the endothelium (**Figure 3.5**). This may occur via junction remodeling, as inflammatory cytokines may increase lymphatic permeability, and EVs themselves may carry junction-remodeling molecules such as ADAMs proteases [39] and microRNAs [40,41]. Given that EVs can be endocytosed into caveolae compartments and may be transcytosed by blood endothelial cells [42,43], transcellular transport of EVs may be an important mechanism of transport into lymphatic vessels as well.

In addition to transporting exogenous EVs from the tumor microenvironment, LECs also produce EVs themselves, which can be delivered into lymphatic vessels and transported to the TDLN and distant sites (**Figure 3.6**). As LECs are known to produce immune-modulatory and tumor-promoting factors [44], and we show here that LECs can also package exogenous factors into EVs (**Figure 3.7**), it is possible that LEC-secreted EVs may have tumor-promoting roles in the TDLN and at distant sites.

In summary, this chapter shows that the lymphatic vasculature represents the main route of EV distribution from the healthy skin and melanoma, and that LECs regulate both EV transport and production.

3.6. Acknowledgements

I would like to thank Dr. Lambert Potin, Dr. Maria Broggi and Dr. Witold Kilarski for technical assistance and helpful discussions. The K14-VEGFR3-Ig mice were kindly provided by Dr. Kari Alitalo (University of Helsinki). Parts of this chapter were published in the manuscript Broggi, Maillat et al. [19].

3.7. References

[1] M.A. Swartz, M.E. Fleury, Interstitial Flow and Its Effects in Soft Tissues, Annu. Rev. Biomed. Eng. 9 (2007) 229–256. https://doi.org/10.1146/annurev.bioeng.9.060906.151850.

[2] J.M. Rutkowski, M.A. Swartz, A driving force for change: interstitial flow as a morphoregulator, Trends Cell Biol. 17 (2007) 44–50. https://doi.org/10.1016/j.tcb.2006.11.007.

[3] M.E. Fleury, K.C. Boardman, M.A. Swartz, Autologous morphogen gradients by subtle interstitial flow and matrix interactions., Biophys. J. 91 (2006) 113–21. https://doi.org/10.1529/biophysj.105.080192.

[4] M.A. Swartz, The physiology of the lymphatic system, Adv. Drug Deliv. Rev. 50 (2001) 3–20. https://doi.org/https://doi.org/10.1016/S0169-409X(01)00150-8.

[5] C. Oussoren, J. Zuidema, D.J.A. Crommelin, G. Storm, Lymphatic uptake and biodistribution of liposomes after subcutaneous injection. II. Influence of liposomal size, lipid composition and lipid dose, Biochim. Biophys. Acta - Biomembr. 1328 (1997) 261–272. https://doi.org/10.1016/S0005-2736(97)00122-3.

[6] S.T. Reddy, A. Rehor, H.G. Schmoekel, J.A. Hubbell, M.A. Swartz, In vivo targeting of dendritic cells in lymph nodes with poly(propylene sulfide) nanoparticles, J. Control. Release. 112 (2006) 26–34. https://doi.org/10.1016/j.jconrel.2006.01.006.

[7] I.C. Kourtis, S. Hirosue, A. de Titta, S. Kontos, T. Stegmann, J.A. Hubbell, M.A. Swartz, Peripherally Administered Nanoparticles Target Monocytic Myeloid Cells, Secondary Lymphoid Organs and Tumors in Mice, PLoS One. 8 (2013). https://doi.org/10.1371/journal.pone.0061646.

[8] P. Baluk, J. Fuxe, H. Hashizume, T. Romano, E. Lashnits, S. Butz, D. Vestweber, M. Corada, C. Molendini, E. Dejana, D.M. McDonald, Functionally specialized junctions between endothelial cells of lymphatic vessels, J. Exp. Med. 204 (2007) 2349–2362. https://doi.org/10.1084/jem.20062596.

[9] D.O. Miteva, J.M. Rutkowski, J.B. Dixon, W. Kilarski, J.D. Shields, M.A. Swartz, Transmural flow modulates cell and fluid transport functions of lymphatic endothelium., Circ. Res. 106 (2010) 920–31. https://doi.org/10.1161/CIRCRESAHA.109.207274.

[10] V. Triacca, E. Güç, W.W. Kilarski, M. Pisano, M.A. Swartz, Transcellular Pathways in Lymphatic Endothelial Cells Regulate Changes in Solute Transport by Fluid Stress, Circ. Res. 120 (2017) 1440–1452. https://doi.org/10.1161/CIRCRESAHA.116.309828.

[11] G.J. Randolph, V. Angeli, M.A. Swartz, Dendritic-cell trafficking to lymph nodes through lymphatic vessels, Nat. Rev. Immunol. 5 (2005) 617–28. https://doi.org/10.1038/nri1670.

[12] Y. Kawai, M. Kaidoh, Y. Yokoyama, T. Ohhashi, Pivotal Roles of Lymphatic Endothelial Cell Layers in the Permeability to Hydrophilic Substances through Collecting Lymph Vessel Walls: Effects of Inflammatory Cytokines, Lymphat. Res. Biol. 12 (2014) 124–135. https://doi.org/10.1089/lrb.2014.0002.

[13] W.E. Cromer, S.D. Zawieja, B. Tharakan, E.W. Childs, M.K. Newell, D.C. Zawieja, The effects of inflammatory cytokines on lymphatic endothelial barrier function, Angiogenesis. 17 (2014) 395–406. https://doi.org/10.1007/s10456-013-9393-2.

[14] C.P. Loo, N.A. Nelson, R.S. Lane, J.L. Booth, S.C. Loprinzi Hardin, A. Thomas, M.K. Slifka, J.C. Nolz, A.W. Lund, Lymphatic Vessels Balance Viral Dissemination and Immune Activation following Cutaneous Viral Infection, Cell Rep. 20 (2017) 3176–3187. https://doi.org/10.1016/j.celrep.2017.09.006.

[15] F. Zhang, G. Zarkada, J. Han, J. Li, A. Dubrac, R. Ola, G. Genet, K. Boyé, P. Michon, S.E. Künzel, J.P. Camporez, A.K. Singh, G.H. Fong, M. Simons, P. Tso, C. Fernández-Hernando, G.I. Shulman, W.C. Sessa, A. Eichmann, Lacteal junction zippering protects against diet-induced obesity, Science (80-.). 361 (2018) 599–603. https://doi.org/10.1126/science.aap9331.

[16] K. Alitalo, T. Tammela, T. V. Petrova, Lymphangiogenesis in development and human disease, Nature. 438 (2005) 946–953. https://doi.org/10.1038/nature04480.

[17] J.L. Hood, R.S. San, S.A. Wickline, Exosomes Released by Melanoma Cells Prepare Sentinel Lymph Nodes for Tumor Metastasis, Cancer Res. 71 (2011) 3792–3801. https://doi.org/10.1158/0008-5472.CAN-10-4455.

[18] F. Pucci, C. Garris, C.P. Lai, A. Newton, C. Pfirschke, C. Engblom, D. Alvarez, M. Sprachman, C. Evavold, A. Magnuson, U.H. Von Andrian, K. Glatz, X.O. Breakefield, T.R. Mempel, R. Weissleder, M.J. Pittet, SCS macrophages suppress melanoma by restricting tumor-derived vesicle-B cell interactions, Science (80-.). 352 (2016) 242–246. https://doi.org/10.1126/science.aaf1328.

[19] M.A.S. Broggi, L. Maillat, C.C.C. Clement, N. Bordry, P. Corth, A. Auger, M. Matter, R. Hamelin, P. Corthésy, A. Auger, M. Matter, R. Hamelin, L. Potin, D. Demurtas, E. Romano, A. Harari, D.E. Speiser, L. Santambrogio, M.A. Swartz, Tumor-associated factors are enriched in lymphatic exudate compared to plasma in metastatic melanoma patients, J. Exp. Med. 216 (2019) 1–17. https://doi.org/10.1084/jem.20181618.

[20] L. Zitvogel, A. Regnault, A. Lozier, J. Wolfers, C. Flament, D. Tenza, P. Ricciardi-Castagnoli, G. Raposo, S. Amigorena, Eradication of established murine tumors using a novel cell-free vaccine: Dendritic cell-derived exosomes, Nat. Med. 4 (1998) 594–600. https://doi.org/10.1038/nm0598-594.

[21] S.C. Saunderson, A.C. Dunn, P.R. Crocker, A.D. Mclellan, CD169 mediates the capture of exosomes in spleen and lymph node, Blood. 123 (2014) 208–216.

[22] M. Poggio, T. Hu, C.-C. Pai, B. Chu, C.D. Belair, A. Chang, E. Montabana, U.E. Lang, Q. Fu,

L. Fong, R. Blelloch, Suppression of Exosomal PD-L1 Induces Systemic Anti-tumor Immunity and Memory, Cell. 177 (2019) 414-427.e13. https://doi.org/10.1016/j.cell.2019.02.016.

[23] A. Milasan, N. Tessandier, S. Tan, A. Brisson, E. Boilard, C. Martel, Extracellular vesicles are present in mouse lymph and their level differs in atherosclerosis, J. Extracell. Vesicles. 5 (2016) 1–9. https://doi.org/10.3402/jev.v5.31427.

[24] T. Mäkinen, L. Jussila, T. Veikkola, T. Karpanen, M.I. Kettunen, K.J. Pulkkanen, R. Kauppinen, D.G. Jackson, H. Kubo, S. Nishikawa, S. Ylä-Herttuala, K. Alitalo, Inhibition of lymphangiogenesis with resulting lymphedema in transgenic mice expressing soluble VEGF receptor-3., Nat. Med. 7 (2001) 199–205. https://doi.org/10.1038/84651.

[25] M.A.S. Broggi, M. Schmaler, N. Lagarde, S.W. Rossi, Isolation of Murine Lymph Node Stromal Cells, (2014) 1–6. https://doi.org/10.3791/51803.

[26] W.W. Kilarski, E. Güç, J.C.M. Teo, S.R. Oliver, A.W. Lund, M.A. Swartz, Intravital immunofluorescence for visualizing the microcirculatory and immune microenvironments in the mouse ear dermis, PLoS One. 8 (2013) e57135. https://doi.org/10.1371/journal.pone.0057135.

[27] K. Wolf, M. te Lindert, M. Krause, S. Alexander, J. te Riet, A.L. Willis, R.M. Hoffman, C.G. Figdor, S.J. Weiss, P. Friedl, Physical limits of cell migration: Control by ECM space and nuclear deformation and tuning by proteolysis and traction force, J. Cell Biol. 201 (2013) 1069–1084. https://doi.org/10.1083/jcb.201210152.

[28] H. Zhang, D. Freitas, H.S. Kim, K. Fabijanic, Z. Li, H. Chen, M.T. Mark, H. Molina, A.B. Martin, L. Bojmar, J. Fang, S. Rampersaud, A. Hoshino, I. Matei, C.M. Kenific, M. Nakajima, A.P. Mutvei, P. Sansone, W. Buehring, H. Wang, J.P. Jimenez, L. Cohen-gould, N. Paknejad, M. Brendel, K. Manova-todorova, J.R. Cubillos-ruiz, G. Galletti, P. Giannakakou, A.M. Cuervo, A. Magalhães, J.A. Ferreira, H. Osório, A.M. Silva, A. Massey, J.R. Cubillos-ruiz, G. Galletti, P. Giannakakou, A.M. Cuervo, J. Blenis, R. Schwartz, M.S. Brady, H. Peinado, J. Bromberg, H. Matsui, C.A. Reis, D. Lyden, A. Magalhães, J.A. Ferreira, H. Osório, A.M. Silva, A. Massey, J.R. Cubillos-ruiz, G. Galletti, P. Giannakakou, A.M. Cuervo, J. Blenis, R. Schwartz, M.S. Brady, H. Peinado, J. Bromberg, H. Matsui, C.A. Reis, D. Lyden, Identification of distinct nanoparticles and subsets of extracellular vesicles by asymmetric flow field-flow fractionation, Nat. Cell Biol. 20 (2018) 332–343. https://doi.org/10.1038/s41556-018-0040-4.

[29] H. Wiig, O. Kolmannskog, O. Tenstad, J.L. Bert, Effect of charge on interstitial distribution of albumin in rat dermis in vitro, J. Physiol. 550 (2003) 505–514. https://doi.org/10.1113/jphysiol.2003.042713.

[30] M. Mathieu, L. Martin-Jaular, G. Lavieu, C. Théry, Specificities of secretion and uptake of exosomes and other extracellular vesicles for cell-to-cell communication, Nat. Cell Biol. 21 (2019) 9–17. https://doi.org/10.1038/s41556-018-0250-9.

[31] K.R. Genschmer, D.W. Russell, C. Lal, T. Szul, P.E. Bratcher, B.D. Noerager, M. Abdul

Roda, X. Xu, G. Rezonzew, L. Viera, B.S. Dobosh, C. Margaroli, T.H. Abdalla, R.W. King, C.M. McNicholas, J.M. Wells, M.T. Dransfield, R. Tirouvanziam, A. Gaggar, J.E. Blalock, Activated PMN Exosomes: Pathogenic Entities Causing Matrix Destruction and Disease in the Lung, Cell. 176 (2019) 113–126. https://doi.org/10.1016/j.cell.2018.12.002.

[32] S. Srinivasan, F.O. Vannberg, J.B. Dixon, Lymphatic transport of exosomes as a rapid route of information dissemination to the lymph node, Sci. Rep. 6 (2016) 24436. https://doi.org/10.1038/srep24436.

[33] A.D. Theocharis, S.S. Skandalis, C. Gialeli, N.K. Karamanos, Extracellular matrix structure, Adv. Drug Deliv. Rev. 97 (2016) 4–27. https://doi.org/10.1016/j.addr.2015.11.001.

[34] H. Wiig, M.A. Swartz, Interstitial fluid and lymph formation and transport: physiological regulation and roles in inflammation and cancer., Physiol. Rev. 92 (2012) 1005–60. https://doi.org/10.1152/physrev.00037.2011.

[35] M.A. Swartz, A.W. Lund, Lymphatic and interstitial flow in the tumour microenvironment: linking mechanobiology with immunity., Nat. Rev. Cancer. 12 (2012) 210–9. https://doi.org/10.1038/nrc3186.

[36] N.A. Rohner, S.N. Thomas, Melanoma growth effects on molecular clearance from tumors and biodistribution into systemic tissues versus draining lymph nodes, J. Control. Release. 223 (2016) 99–108. https://doi.org/10.1016/j.jconrel.2015.12.027.

[37] C.D. Commerford, L.C. Dieterich, Y. He, T. Hell, J.A. Montoya-Zegarra, S.F. Noerrelykke, E. Russo, M. Röcken, M. Detmar, Mechanisms of Tumor-Induced Lymphovascular Niche Formation in Draining Lymph Nodes, Cell Rep. 25 (2018) 3554-3563.e4. https://doi.org/10.1016/j.celrep.2018.12.002.

[38] S. García-Silva, A. Benito-Martín, S. Sánchez-Redondo, A. Hernández-Barranco, P. Ximénez-Embún, L. Nogués, M.S. Mazariegos, K. Brinkmann, A.A. López, L. Meyer, C. Rodríguez, C. García-Martín, J. Boskovic, R. Letón, C. Montero, M. Robledo, L. Santambrogio, M.S. Brady, A. Szumera-Ciećkiewicz, I. Kalinowska, J. Skog, M. Noerholm, J. Muñoz, P.L. Ortiz-Romero, Y. Ruano, J.L. Rodríguez-Peralto, P. Rutkowski, H. Peinado, Use of extracellular vesicles from lymphatic drainage as surrogate markers of melanoma progression and BRAFV600E mutation, J. Exp. Med. 216 (2019) 1061–1070. https://doi.org/10.1084/jem.20181522.

[39] J.N. Higginbotham, M. Demory Beckler, J.D. Gephart, J.L. Franklin, G. Bogatcheva, G.J. Kremers, D.W. Piston, G.D. Ayers, R.E. McConnell, M.J. Tyska, R.J. Coffey, Amphiregulin exosomes increase cancer cell invasion, Curr. Biol. 21 (2011) 779–786. https://doi.org/10.1016/j.cub.2011.03.043.

[40] W. Zhou, M.Y. Fong, Y. Min, G. Somlo, L. Liu, M.R. Palomares, Y. Yu, A. Chow, S.T.F. O'Connor, A.R. Chin, Y. Yen, Y. Wang, E.G. Marcusson, P. Chu, J. Wu, X. Wu, A.X. Li, Z. Li, H. Gao, X. Ren, M.P. Boldin, P.C. Lin, S.E. Wang, Cancer-Secreted miR-105 destroys vascular endothelial barriers to promote metastasis, Cancer Cell. 25 (2014) 501–515.

https://doi.org/10.1016/j.ccr.2014.03.007.

[41] Z. Zeng, Y. Li, Y. Pan, X. Lan, F. Song, J. Sun, K. Zhou, X. Liu, X. Ren, F. Wang, J. Hu, X. Zhu, W. Yang, W. Liao, G. Li, Y. Ding, L. Liang, Cancer-derived exosomal miR-25-3p promotes pre-metastatic niche formation by inducing vascular permeability and angiogenesis, Nat. Commun. 9 (2018) 1–14. https://doi.org/10.1038/s41467-018-07810-w.

[42] G. Morad, C. V. Carman, E.J. Hagedorn, J.R. Perlin, L.I. Zon, N. Mustafaoglu, T.E. Park, D.E. Ingber, C.C. Daisy, M.A. Moses, Tumor-Derived Extracellular Vesicles Breach the Intact Blood-Brain Barrier via Transcytosis, ACS Nano. 13 (2019) 13853–13865. https://doi.org/10.1021/acsnano.9b04397.

[43] M. Grapp, A. Wrede, M. Schweizer, S. Hüwel, H.J. Galla, N. Snaidero, M. Simons, J. Bückers, P.S. Low, H. Urlaub, J. Gärtner, R. Steinfeld, Choroid plexus transcytosis and exosome shuttling deliver folate into brain parenchyma, Nat. Commun. 4 (2013) 1–13. https://doi.org/10.1038/ncomms3123.

[44] K. Maisel, M.S. Sasso, L. Potin, M.A. Swartz, Exploiting lymphatic vessels for immunomodulation: Rationale, opportunities, and challenges, Adv. Drug Deliv. Rev. 114 (2017) 43–59. https://doi.org/10.1016/j.addr.2017.07.005.

CHAPTER 4

ROLES OF LYMPHATIC VESSELS IN EXTRACELLULAR VESICLE-MEDIATED PREMETASTATIC NICHE FORMATION

4.1. Abstract

In this chapter, I investigated the consequence of tumor lymphangiogenesis on premetastatic niche formation. I found that tumor VEGFC overexpression leads to increased premetastatic niche features in tumor-draining lymph nodes and lungs such as increased expression of tumor-promoting genes and accumulation of neutrophils. While the production of EVs was similar in both control and VEGFC-overexpressing tumors, increased levels of EVs accumulated in the blood of VEGFC-overexpressing tumor-bearing mice. I found that EV transport from VEGFC-overexpressing tumors to the tumor-draining lymph node was higher than from control tumors. Additionally, reduction of EV production through CRISPR knockout of Rab27a which reduces EV production resulted in lower levels of neutrophils in the tumor, blood and lungs. Together, we suggest that lymphangiogenesis promotes metastasis via increased premetastatic niche formation, and that this process is partially mediated by EV transport.

4.2. Introduction

In a healthy tissue, cells work in concert to balance proliferation, differentiation and death for the maintenance of homeostasis. In contrast, cancer cells break the homeostatic barrier and shift the local tissue to a chaotic, growth-promoting state [1]. The tumor microenvironment, which is composed of cells, extracellular matrix (ECM) and factors that surround cancer cells, plays a major role in modulating the aggressiveness of solid tumors. Cells of the tumor microenvironment typically include stromal cells, such as blood endothelial cells, lymphatic endothelial cells and fibroblasts, as well as bone marrow-derived cells such as monocytes, granulocytes and lymphocytes (**Figure 4.1**). These cells may promote tumor progression and suppression of anti-tumor immune responses [1,2].

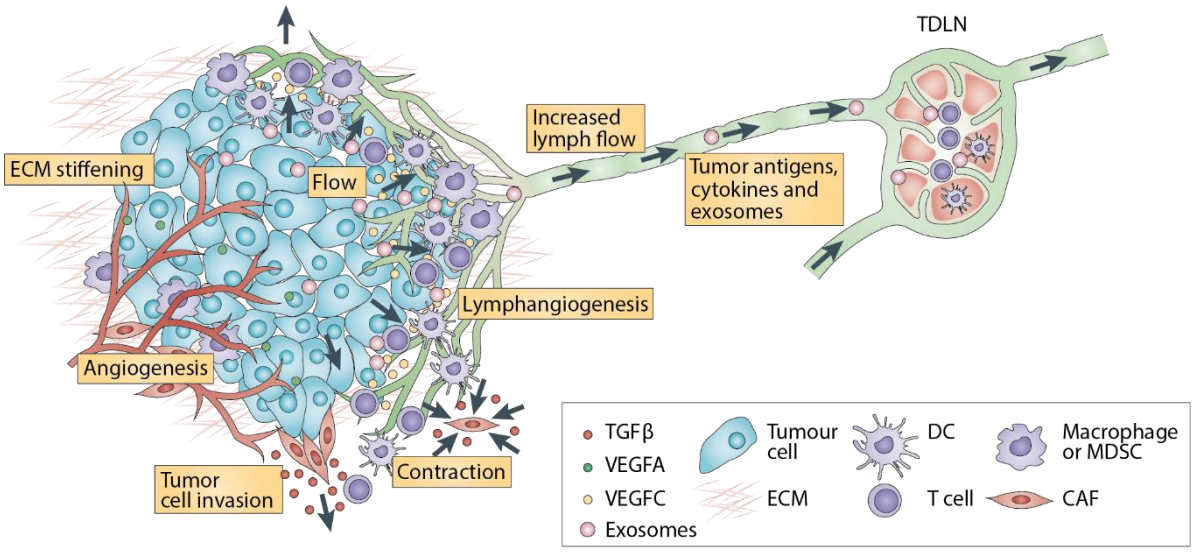

Figure 4.1. Tumor fluid pathways and lymphatic drainage. TDLN: tumor-draining lymph node, ECM: extracellular matrix, DC: dendritic cell, MDSC: myeloid-derived suppressor cell, CAF: cancer-associated fibroblast. Adapted from Swartz and Lund [3].

Lymphatic vessels constitute the main physical connection between the tumor and its draining lymph node(s) (LN, **Figure 4.1**). They constantly "bath" the tumor-draining lymph node (TDLN) with tumor cytokines, antigens and extracellular vesicles (EVs), negatively regulating the host anti-tumor immune response and remodeling the LN into a metastasis-promoting environment called premetastatic niche. Lymph flow from tumors is elevated compared to that from healthy tissue, due to poor vascular organization and vascular leakage. This not only increases communication with the TDLN, but also implies a high interstitial flow within the tumor. This interstitial flow induces mechanical stress on cells of the tumor microenvironment and on the ECM. The alteration of the tumor microenvironment further contributes to immunological changes, ECM stiffening and tumor invasiveness [3].

Tumor cells can migrate towards lymphatic vessels through autologous chemotaxis enabled by interstitial flow [4]. Additionally, lymphatic endothelial cells (LECs) express

chemokines such as CCL21 and adhesion molecules such as VCAM-1 and ICAM-1 which promote entry of tumor cells into lymphatic vessels and into the TDLNs [5]. As such, lymphangiogenesis can increase recruitment of tumor cells and their delivery to TDLNs [6]. Vascular endothelial growth factors C (VEGFC) and D (VEGFD) are often expressed by tumor cells or cells of the tumor microenvironment, and both promote tumor lymphangiogenesis and tumor metastasis in many cancer types [7,8].

Metastasis is a multi-step process in which tumor cells spread from the tumor of origin to distant organs. To form a metastasis, tumor cells and tumor factors use 3 main body fluids: blood, lymph and interstitial fluid. In most solid cancers, such as in melanoma, tumor cells first disseminate to the TDLNs via lymphatic vessels before reaching the blood and distant organs (**Figure 4.2**) [9]. LNs may constitute an intermediate station where cancer cells acquire additional mutations to increase their metastatic potential [2]. From the TDLNs, tumor cells can directly enter the bloodstream through LN blood vessels, or alternatively travel further via lymphatics to the thoracic duct after which they enter the blood circulation [10,11].

Prior to metastasis to TDLNs and distant sites, tumor cells secrete and induce the production of a variety of factors, including lymphangiogenic growth factors, which prepare the LN and distant organs for metastasis [12–14]. Tumor-associated lymphatics contribute to immune suppression and pre-metastatic niche formation by delivering tumor-derived factors to cells of the TDLN. For example, the TDLN lymphatic and blood vasculature undergoes expansion and remodeling [15,16]. Additionally, the TDLN is more immune

suppressed than non-draining LNs, and VEGFC expression by the tumor further contributes to immunosuppression [16,17].

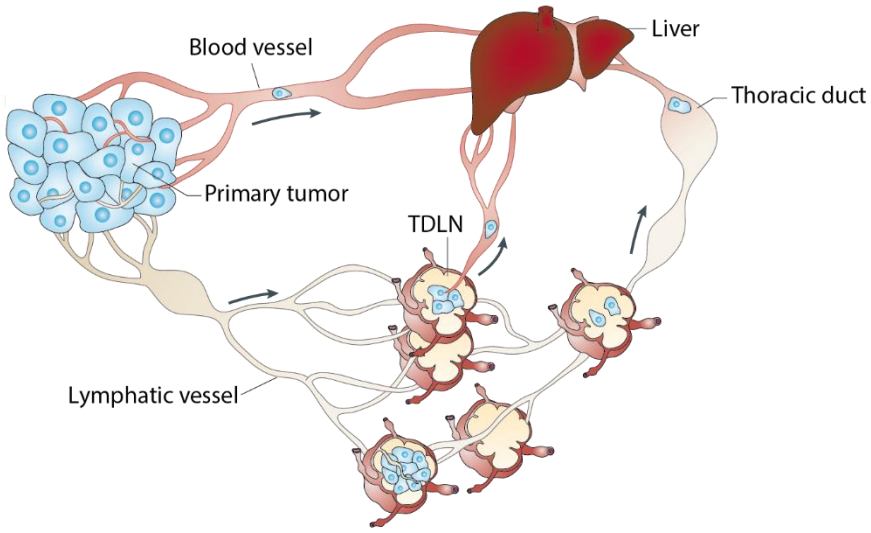

Figure 4.2. Routes for tumor cell metastasis. TDLN: tumor-draining lymph node. Adapted from Stacker et al. [18].

Tumor reprogramming of LECs in the TDLN results in lymphatic network expansion and upregulation of a variety of genes involved in chemoattraction and immune modulation and participate in the premetastatic niche [19,20]. For example, tumor-secreted VEGFC induces the expression of integrin α4β1 by lymphatic endothelial cells (LECs) of the LNs, which promotes LEC expansion and adhesion of $VCAM^+$ tumor cells, thus promoting LN metastasis [21]. Tumors can also induce the production of VEGFC and VEGFD by macrophages and dendritic cells in the TDLN through COX-2-derived prostaglandin, which in turn drives lymphangiogenesis [22]. Midkine is another pro-tumorigenic factor that can be secreted by melanoma and induce lymphangiogenesis at distant sites resulting in increased

metastasis [23]. Additionally, LN lymphangiogenesis may also enhance metastasis from the LN to distant sites [24,25].

EVs play important roles in inducing premetastatic niches as they transport and transfer bioactive molecules to distant sites. EVs were shown to induce TDLN and distant organ remodeling which include immune suppression, extracellular matrix deposition, vascular permeability and angiogenesis, and bone marrow-derived cell recruitment. EVs can be transported by lymphatics to TDLNs, where they are largely taken up by subcapsular sinus macrophages which limits further penetration into the TDLN [26]. EVs can reprogram TDLN cells to express metastasis-promoting genes [27] and contribute to immunosuppression, for example via their surface PDL1 [28,29].

Although it is known that both tumor lymphangiogenesis and EV delivery to TDLNs and distant sites promote metastasis, it remains unknown whether both mechanisms are interconnected. As we found in chapter 3 that EVs were mainly transported by lymphatic vessels, it is likely that lymphatic growth affects EV distribution. In this chapter, we suggest that tumor lymphangiogenesis results in increased transport of EVs from tumors to the TDLN and distant organs, and therefore promote the formation of premetastatic niches.

4.3. Methods

Materials

Chemicals were purchased from Sigma-Aldrich, cell culture reagents were purchased from Invitrogen, flow cytometry antibodies were purchased from Biolegend, unless otherwise stated.

Cell lines

B16-F10 melanoma cells (American Type Culture Collection) were maintained in high-glucose DMEM with L-glutamate supplemented with 10% heat-inactivated FBS. 4T1 breast cancer cells (American Type Culture Collection) were maintained in RPMI with L-glutamate supplemented with 10% heat-inactivated FBS. For EV production, media were supplemented with 2 to 5% exosome-depleted FBS. Lentiviral vectors were used for stable expression of VEGFC or control vectors. Protein levels of VEGFC in cell supernatant were confirmed by ELISA (VEGFC duoset ELISA; R&D). All cell lines were routinely tested negative for mycoplasma contamination.

Animals

Wild-type (WT) female mice (C57Bl/6J, Balb/c) were purchased from the Jackson Laboratory (Bar Harbor, Maine, USA) and used at age 8-12 weeks. Rag-deficient mice (C57Bl/6J $Rag^{-/-}$) and heterozygous littermates were obtained by breading C57Bl/6J $Rag^{-/-}$ and C57Bl/6J $Rag^{+/+}$ from the Jackson Laboratory. All experiments were performed with approval from the Veterinary Authority of the Institutional Animal Care and Use Committee at the University of Chicago under protocols no. 72530 and 72551.

Tumor models

250,000 B16-F10 cells were inoculated intradermally in 30 µl PBS into the back flank of C57Bl/6J mice. 200,000 4T1 cells were inoculated in 40 µl PBS into the lower left mammary fat pad of Balb/c mice. Tumor growth was monitored with calipers and tumor volume was calculated as Volume = 4π*(x/2)*(y/2)*(z/2)/3. For experimental metastasis models,

250,000 tumor cells were injected intravenously in 100 µl PBS, and mice were sacrificed after 14 days.

EV purification by ultracentrifugation

EVs were purified from 2- to 3-day cell‑conditioned medium. Cells and debris were cleared from supernatant by serial centrifugations 10 min at 300 g, 10 min at 2,000 g, and 30 min at 12,000 g at 4°C. Supernatants were then centrifuged 1h30 at 110,000 g, pellets were resuspended in PBS, centrifuged again 1h30 at 110,000 g and resuspended in PBS. EV concentration was quantified by Nanoparticle tracking analysis (NTA) and protein contents were quantified by BCA assay (Thermo).

EV fluorescent labeling

EV membranes were labeled with DiD or DiL (Invitrogen), and EV surface proteins were labeled with Cellbrite (Biotium) according to the manufacturers protocols and purified from unbound dye using a qEVoriginal Size Exclusion Column or ultracentrifugation for 1h30 at 110,000g.

Nanoparticle tracking analysis

NTA measurements were performed with a NanoSight NS300 (Malvern Instruments Ltd, Malvern, UK), equipped with a Low Volume Flow Cell Gasket and a 488 nm Blue Laser Module. The samples were injected manually with 1 ml tuberculin syringes (Excel) until the solution reached the tip of the nozzle, and then infused at constant flow rate using a syringe pump. The samples were measured for 60 s with manual shutter and gain adjustments. Three measurements per sample were performed. The software used for capturing and analyzing the data was the NTA 3.2 Dev Build 3.2.16.

Western blot

EVs or cell lysates were mixed with Laemmli SDS sample buffer (Alfa Aesar), heated for 10 min at 95°C, and cooled to 4°C. Electrophoresis was performed on Mini-PROTEAN TGX Gels (Bio-Rad). Proteins were transferred to a polyvinylide difluoride membrane (Bio-Rad). After 1 h blocking in Tris-buffered saline (TBS) 5 % milk, primary antibodies in TBS 1‑5 % milk were applied for 1 h at room temperature (RT) or overnight at 4°C, and secondary, HRP-conjugated, antibodies were applied in TBS 1‑5 % milk for 1 h at RT. The following antibodies were used: anti-CD9(1:500; C9993; Sigma-Aldrich), anti-CD63 (1:200; SC-15363; Santa Cruz Biotechnology), anti-CD81 (1:1,000; SAB 3500454; Sigma-Aldrich), and TSG101 (1:1,000; T5701; Sigma-Aldrich).

TEM

Grids (continuous carbon on 200-mesh copper grids - EMS CF200-CU) were first glow discharged for 30 seconds. 3.5 µl of EV sample was applied to the grid for 1 minute. The excess sample was blotted off. The grids were stained with 2 washes and then 45 seconds of 0.75% uranyl formate (EMS 22450). Excess stain was blotted off at each step. Grids were imaged on a Technai G2 F30 (FEI) electron microscope operating at 300kV.

Tissue digestion

Tumors, lymph nodes and lungs were harvested from euthanized animals and digested as previously described (Broggi et al., Jove). Briefly, tissues were thinly cut, digested in DMEM medium supplemented with 1 mg/mL collagenase IV (Worthington-Biochem), 40 µg/mL DNAse I (Roche), 3.3 mg/mL collagenase D (Roche), 1.2mM $CaCl_2$, 2-5% FBS for 1 h at 37°C with magnetic stirring. After repeated pipetting, enzymatic digestion was quenched with

EDTA at a final concentration of 5 mM followed by addition of full medium. Lung cells were depleted of red blood cells using ACK lysis buffer for 3 min. Cells were then filtered through a 70 µm strainer, washed and analyzed. For splenocyte analysis, spleens were mashed through a 70 µm strainer, red blood cells were lysed for 3 min in ACK lysis buffer, and remaining cells were washed and analyzed. For blood analysis, 50 µL of blood collected in EDTA-coated tubes was used. Samples were depleted of red blood cells by 3 x 3 min incubation in ACK lysis buffer, washed and analyzed.

Flow cytometry

Single cell suspensions were stained with Fixable Viability Dye eFluor 455 UV (eBioscience) or Horizon Fixable Viability Stain 510 (BD Biosciences) for 15 min in PBS. Fc receptors were blocked with anti-CD16/32 antibodies in FACS buffer (PBS 2% FBS) for 10 min at 4°C. Antibodies against surface markers were applied for 20 min in FACS buffer at 4°C. The following antibodies were used: CD45-APCCy7, CD11b-BUV396, Ly6G-PacBlue, Siglec-f-PE, CD11c-PE-Cy7, F4/80-FITC, Ly6C-BV605, CD3e-BUV396, CD31-ef450, gp38-AF488. Cells were then fixed in 2% paraformaldehyde (Affymetrix) for 15 min at 4°C.

Cells were analyzed using a LSRFortessa X-20 flow cytometer (BD Biosciences), and data was processed using FlowJo software package v.10.6.1. LECs were defined as $CD45^{-}CD31^{+}gp38^{+}$, blood endothelial cells as $CD45^{-}CD31^{+}gp38^{-}$, neutrophils as $CD45^{+}CD11b^{+}Ly6G^{+}$, eosinophils as $CD45^{+}CD11c^{-}Siglec\text{-}f^{+}$, T cells as $CD45^{+}CD3e^{+}$, monocytes as $CD45^{+}CD11b^{+}F4/80^{+}Ly6C^{+}$.

RT-PCR

RNA was extracted using a RNeasy Plus Mini Kit (Qiagen) and reversed-transcribed using GoScript™ Reverse Transcriptase kit (Promega) following manufacturer's protocols.

Quantitative PCR was performed using FastStart Essential DNA Green Master (Roche) following manufacturer's protocol and a LightCycler® 96 Instrument (Roche). Gene expression was normalized using the $\Delta\Delta$Cq method and housekeeping gene Beta-actin (*Actb*). The following primer pairs were used (Integrated DNA Technologies):

Gene	Forward primer	Reverse primer
Prox1	TGTTCTTTTACACCCGCTACCC	CTCACGGAAATTGCTGAACCAC
Ccl21	CCCTGGACCCAAGGCAGT	AGGCTTAGAGTGCTTCCGGG
Tgfb	CACCGGAGAGCCCTGGATA	TGTACAGCTGCCGCACACA
Tnfa	ACGCTCTTCTGTCTACTGAACTTCG	GATGATCTGAGTGTGAGGGTCTGG
Hif1a	ATGGTAGCCACAATTGCACA	AAATGCCACATACCTTCCAGA
Fn1	TGGTGGCCACTAAATACGAA	GGAGGGCTAACATTCTCCAG
S100a8	TGGTCACTACTGAGTGTCCT	CTACTCCTTGTGGCTGTCTT
S100a9	CCTTCTCAGATGGAGCGCAG	TGTCCAGGTCCTCCATGATG
Actb	TGGAATCCTGTGGCATCCATGAAAC	TAAAACGCAGCTCAGTAACAGTCCG

Immunofluorescence staining

Tumor and lung samples were fixed in 10% formalin, embedded in paraffin and cut into 6 µm-thick sections. After deparaffinization, slides were incubated for 40 min in citrate buffer (10 mM citric acid, 0.05% Tween 20, pH 6.0) at 100°C for antigen retrieval. LNs were fixed with zinc fixative (BD Biosciences) and incubated for at least 2 days in Tris-Buffered Saline (TBS) 15% sucrose followed by TBS 30% sucrose. Tissues were embedded in Tissue-Tek® OCT Compound (Electron Microscopy Sciences) and frozen before being cut into 7 µm sections. All sections were incubated for 10 min in TBS 10 % dimethylsulfoxide, 10 min in TBS 0.1 % Triton, 30 min in TBS casein 0.5 % prior to immunostaining. They were then incubated with primary antibodies in TBS Casein 0.5 % overnight at 4°C, followed by secondary antibodies for 1 h at RT. Sections were mounted with Prolong Gold Antifade

Reagent with DAPI (Invitrogen) and imaged using a Leica DMi8 fluorescent microscope and 25x oil objective. Images were processed with ImageJ (NIH).

In vivo EV distribution

5–10 μg EVs in 10 μl was injected intradermally into the mouse hock (the lateral tarsal region just above the ankle) or into tumors. After 6-24 h, mice were sacrificed. Organs were homogenized in radioimmunoprecipitation assay buffer (Sigma-Aldrich) and centrifuged at 10,000 g for 10 min, and supernatant fluorescence was read by plate reader. Alternatively, organs were digested and analyzed by flow cytometry.

Statistical analysis

Data were processed using Microsoft Excel v.16.0. Data were represented and statistics were computed using Prism v.8 (GraphPad). Numerical data are shown as mean ± SEM unless otherwise stated. Asterisks show groups statistically different and represent p values of specific statistical tests described in figure legends.

4.4. Results

Tumor VEGFC overexpression leads to increased premetastatic niche formation and metastasis

In order to study the consequences of tumor lymphangiogenesis on the premetastatic niche, we used B16F10 melanoma tumor cells lentivirally transduced to express the lymphangiogenic growth factor VEGFC (B16F10-VEGFC), and B16F10 cells transduced with a control vector (B16F10-Ctrl), as previously reported [30]. Upon intradermal injection in the mouse flank, both B16F10-Ctrl and B16F10-VEGFC tumors developed at a similar rate (**Figure 4.3** A). As indicated by flow cytometry analysis, B16F10-Ctrl tumors contained very

low levels of lymphatic endothelial cells (LECs, gated as $CD45^{-}gp38^{+}CD31^{+}$), while B16F10-VEGFC tumors showed a marked increase in LEC numbers (**Figure 4.3** B-D). In contrast, B16F10-Ctrl and B16F10-VEGFC tumors contained similar levels of blood endothelial cells (BECs, gated as $CD45^{-}gp38^{-}CD31^{+}$).

We first analyzed the consequence of tumor growth and VEGFC overexpression on tumor-draining lymph nodes 2 weeks after primary tumor inoculation (**Figure 4.4**). While both B16F10-Ctrl and B16F10-VEGFC TDLNs were larger than naïve LNs, no significant weight difference was observed between TDLNs draining the two tumor types (**Figure 4.4** A). However, B16F10-VEGFC TDLNs showed higher densities of lymphatic vessels upon section immunostaining for LEC marker Lyve-1 (**Figure 4.4** B), and higher expression of LEC transcription factor Prospero homeobox protein 1 (*Prox1)* and VEGFC receptor Vascular endothelial growth factor receptor 3 (*Vegfr3*). Crucially, multiple genes associated with the premetastatic niche were found significantly upregulated in B16F10-VEGFC TDLNs but not in B16F10-Ctrl TDLNs such as *Ccl21* and *Tgfb* (**Figure 4.4** D). Of note, B16F10 tumor antigen tyrosinase-related protein 2 (*Trp2*) was undetected at this time point, indicating that tumor cells have not formed LN metastases yet (**Figure 4.4** E). Because of the fast growth of B16F10 tumors, we could not detect LN or lung metastases prior to experimental endpoint based on poor mouse health or tumor size reaching 1 cm^3 (not shown). In order to confirm that VEGFC overexpression results in increased metastasis, we surgically removed primary tumors prior to experimental endpoint, and allowed metastases to form for 4 weeks (**Figure 4.4** F). Then, we found that while B16F10-Ctrl tumors did not form metastases in the TDLN, 3 out of 9 mice bearing B16F10-VEGFC tumors developed metastases (**Figure 4.4** G). Of note, no lung metastases were observed (not shown).

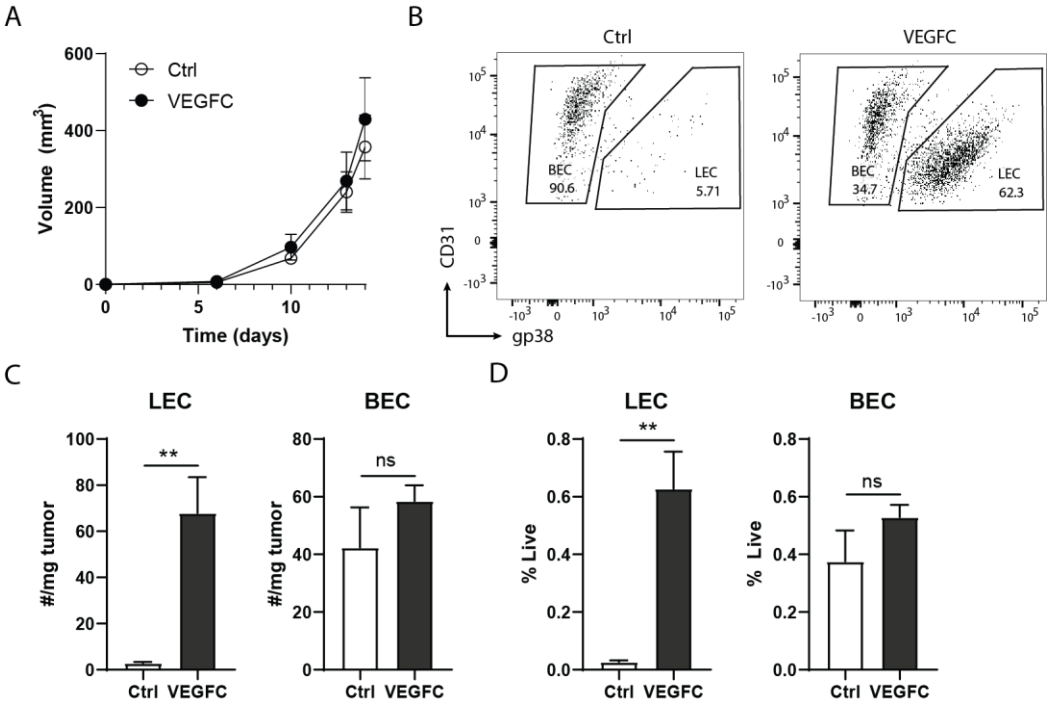

Figure 4.3. VEGFC overexpression in B16-F10 induces tumor lymphangiogenesis. (A) B16-F10 control (Ctrl) and B16-F10 VEGFC (VEGFC) tumor growth upon injection of 250,000 cells intradermally in mouse flank. n=7-8. (B-D) Lymphatic endothelial cells (LEC) and blood endothelial cells (BEC) in Ctrl and VEGFC B16-F10 tumors. (B) representative gating on LEC ($CD31^+gp38^+$) and BEC ($CD31^+gp38^-$) within tumor $CD45^-CD31^+$ cells. (C) LEC and BEC number per milligram of tumor. (D) LEC and BEC as percentage of live cells. n=6-7. Bar charts represent mean ± SEM. ** $p<0.01$ using unpaired, 2-tailed Student's t test.

Despite the absence of metastases two weeks after tumor inoculation, we next sought to determine whether tumor VEGFC overexpression might affect premetastatic remodeling at distant sites. For this, we analyzed lungs of tumor-bearing mice, as lungs represent a common organ of melanoma and breast cancer metastasis. First, we analyzed lymphangiogenesis by staining for VEGFR3, as it is known to be induced in the premetastatic lungs and lead to the formation so called lymphovascular niches [23]. While both B16F10-Ctrl and B16F10-VEGFC appeared to induce increased VEGFR3 expression in lungs, we did not see differences in VEGFR3 expression between the two tumor groups (**Figure 4.5** A-B).

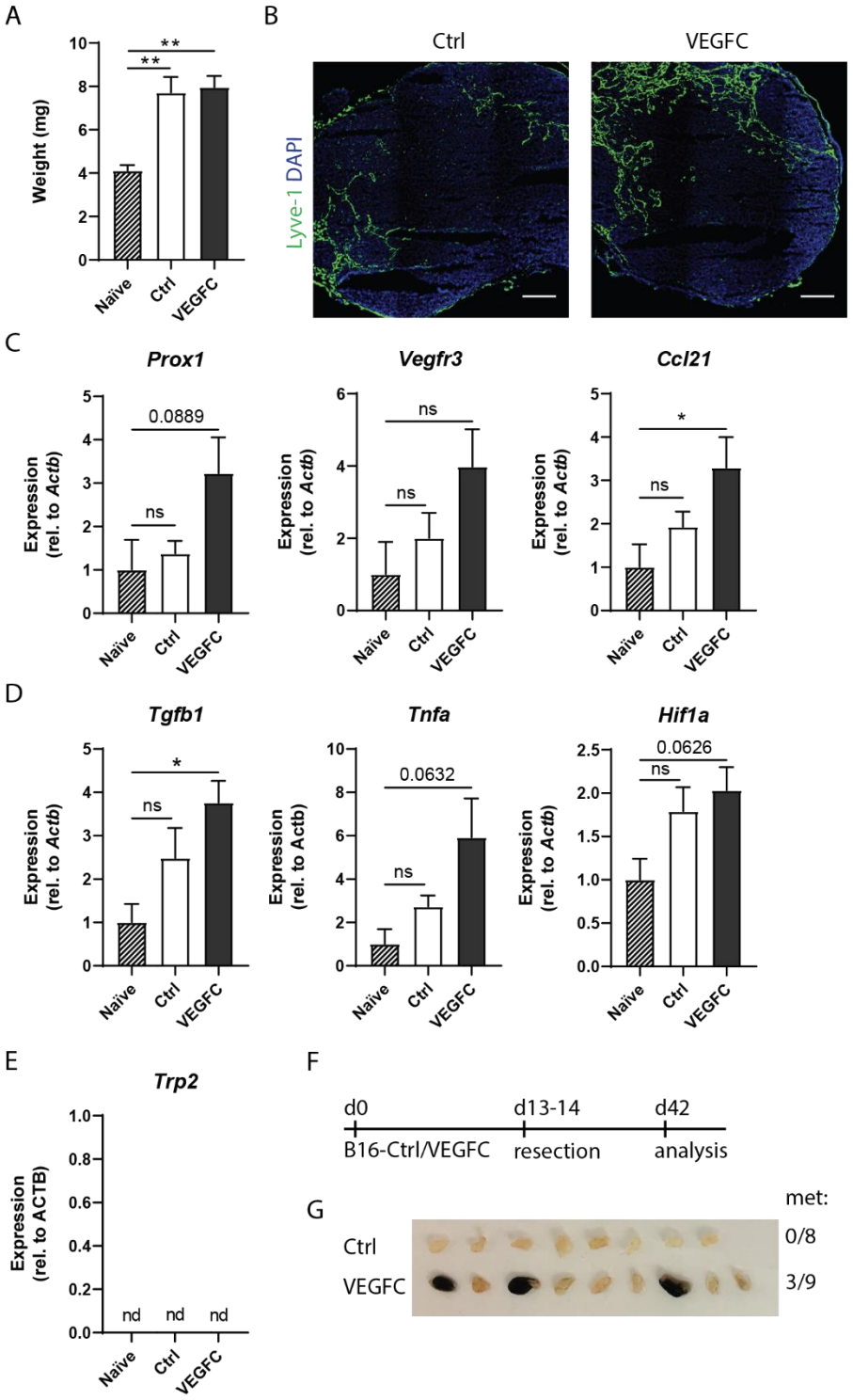

Figure 4.4. Tumor VEGFC overexpression induces lymph node lymphangiogenesis and the expression of tumor-promoting genes prior to metastasis. (A-E) Naïve mouse LN and B16-F10 Control (Ctrl)- and B16-F10 VEGFC (VEGFC)-tumor draining lymph nodes (TDLN) analyzed at day 15 after tumor inoculation. n=4-6. (A) Naïve mouse LN and TDLN weight.

Figure 4.4, continued. (B) TDLN sections stained for Lyve-1 (green) and DAPI (blue). Scale bar: 200 μm. Naïve and TDLN (C) lymphatic and (D) tumor-promoting gene expression determined by RT-PCR. (E) Tumor antigen Tyrosinase-related protein-2 (Trp2) gene expression. (F-G) B16F10 metastasis after tumor resection (n=4-5). F) Experimental design G) Picture of tumor-draining LNs at endpoint and number of metastatic LNs of total number (met). Representative of 2 independent experiments. Bar charts represent mean ± SEM. * $p<0.05$, ** $p<0.01$ using one-way ANOVA with Tukey's test.

Next, we analyzed immune infiltration in lungs which may participate in the premetastatic niche, in particular neutrophils [31,32]. We found increased relative density of neutrophils, decreased levels of eosinophils and monocytes and unchanged levels of T cells in B16F10-VEGFC tumor-bearing mice compared to B16F10-Ctrl tumor-bearing mice (**Figure 4.5** C). In addition, we detected increased expression of premetastatic niche-associated chemokines *S100a8* and *S100a9,* which can be produced by neutrophils [33](**Figure 4.5** D). We also detected higher levels of neutrophils in the blood of B16F10-VEGFC tumor-bearing mice, suggesting a systemic increase in neutrophil mobilization or survival (**Figure 4.5** E).

In order to assess whether our observations linking tumor VEGFC signaling and the induction of the premetastatic niche were model-agnostic, we employed an additional model, namely the 4T1 triple negative breast cancer. Here, cell lines were either transduced with an empty lentiviral vector (4T1-Ctrl) or a VEGFC vector (4T1-VEGFC). We observed a similar increase in neutrophil levels in lungs of 4T1-VEGFC tumor-bearing mice compared to lungs of 4T1-Ctrl tumor-bearing ones (**Figure 4.5** F). Here, T cell infiltration was decreased in lungs of VEGFC-overexpressing tumors compared to control tumors.

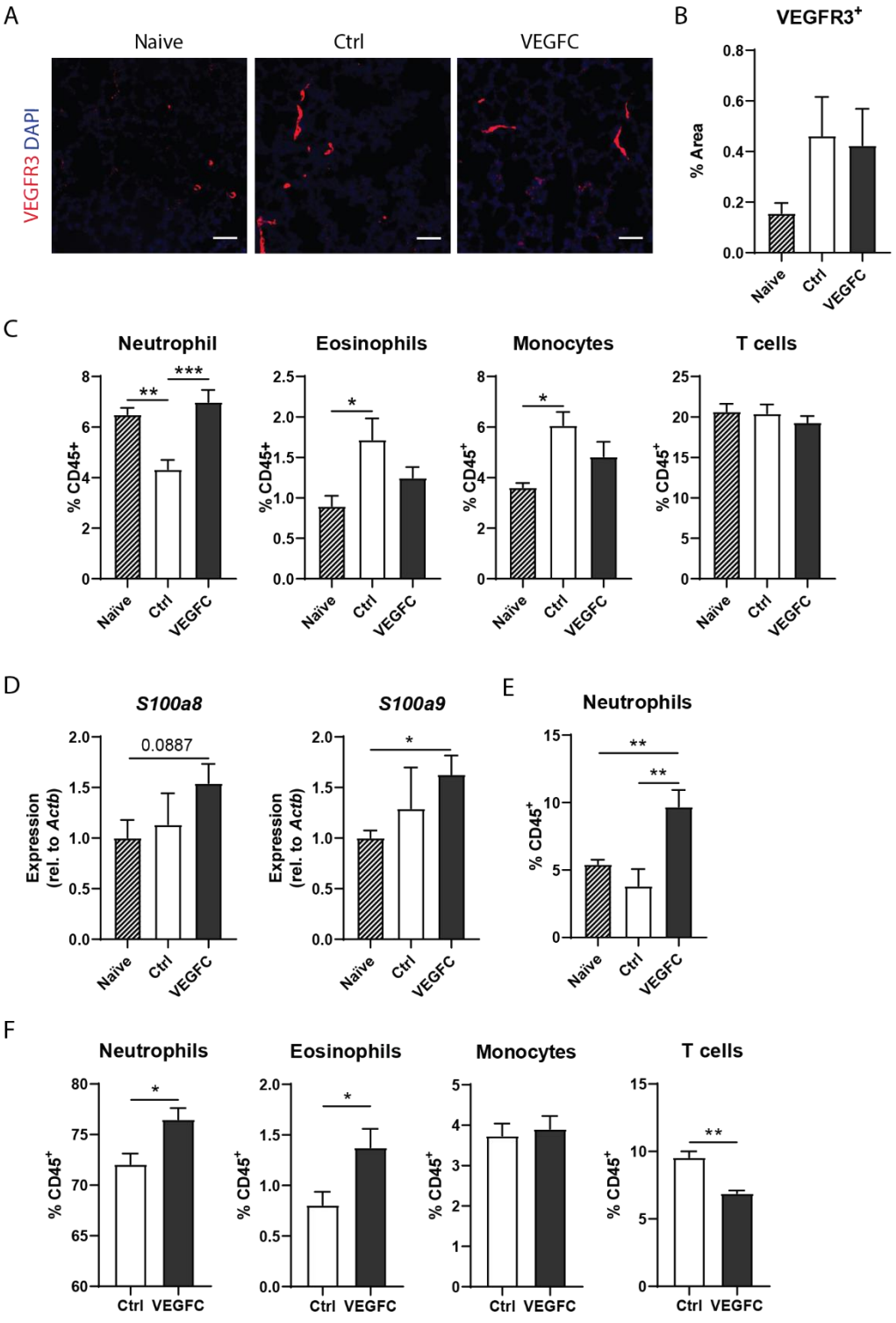

Figure 4.5. VEGFC overexpression in B16-F10 and 4T1 tumors lead to neutrophil accumulation in lungs. (A-E) Analysis of naïve and Control (Ctrl) or VEGFC overexpressing (VEGFC) B16-F10 tumor-bearing mice 2 weeks after tumor inoculation. (A) Lung sections stained for VEGFR3 (red) and DAPI (blue). Scale bar: 50 μm.

Figure 4.5, continued. (B) quantification of VEGFR3$^+$ percent area of lung sections, (C) Immune cell infiltration in lungs as percentage of CD45$^+$ cells. (D) *S100a8* and *S100a9* gene expression in the lungs, normalized to *Beta-actin* (*Actb*). (E) Neutrophils in blood as percentage of CD45$^+$ cells. (F) Lung analysis in 4T1 tumor-bearing mice analyzed at day 18 after tumor inoculation. Immune cell infiltration in lungs percentage of CD45+ cells. Data represent mean ± SEM. * $p<0.05$, ** $p<0.01$ using one-way ANOVA (C-D) or Student's t test (F).

VEGFC tumors remodel distant organs to promote tumor cell invasion and seeding

In order to determine whether the differences in premetastatic niches induced by VEGFC-overexpressing tumors played roles in subsequent metastasis formation, we analyzed lung permeability and metastasis formation in primary tumor-bearing mice (**Figure 4.6**). First, we found a trend towards increased immediate infiltration of mCherry$^+$ tumor cells into the lungs of B16F10-VEGFC tumor-bearing mice compared to control after intravenous injection, as indicated by flow cytometry analysis of fluorescent cells in the lungs (**Figure 4.6** A-C). This may be due to increased permeability of the lung as we also saw increased accumulation of dextran in lung cells after intravenous injection (**Figure 4.6** D-F). To determine whether primary B16F10-VEGFC tumor conditioning affected the formation of metastatic lesions, we surgically resected primary tumors, injected tumor cells intravenously and sacrificed mice 2 weeks later. We found increased numbers of macroscopic metastatic nodules in mice with prior B16F10-VEGFC tumors compared with B16F10-Ctrl tumors (**Figure 4.6** G-J). These lesions are likely mostly composed of intravenously-injected B16F10-mCherry$^+$ tumor cells, as opposed to primary tumor-derived tumor cells, as we detected high numbers of mCherry$^+$ cells in lungs, with trends of more mCherry$^+$ cells in B16F10-VEGFC tumor-bearing mice (**Figure 4.6** K). Additionally, in prior experiments where we did not inject tumor cells

intravenously after tumor resection, we did not detect the formation of metastatic nodules in lungs (**Figure 4.4** F-G).

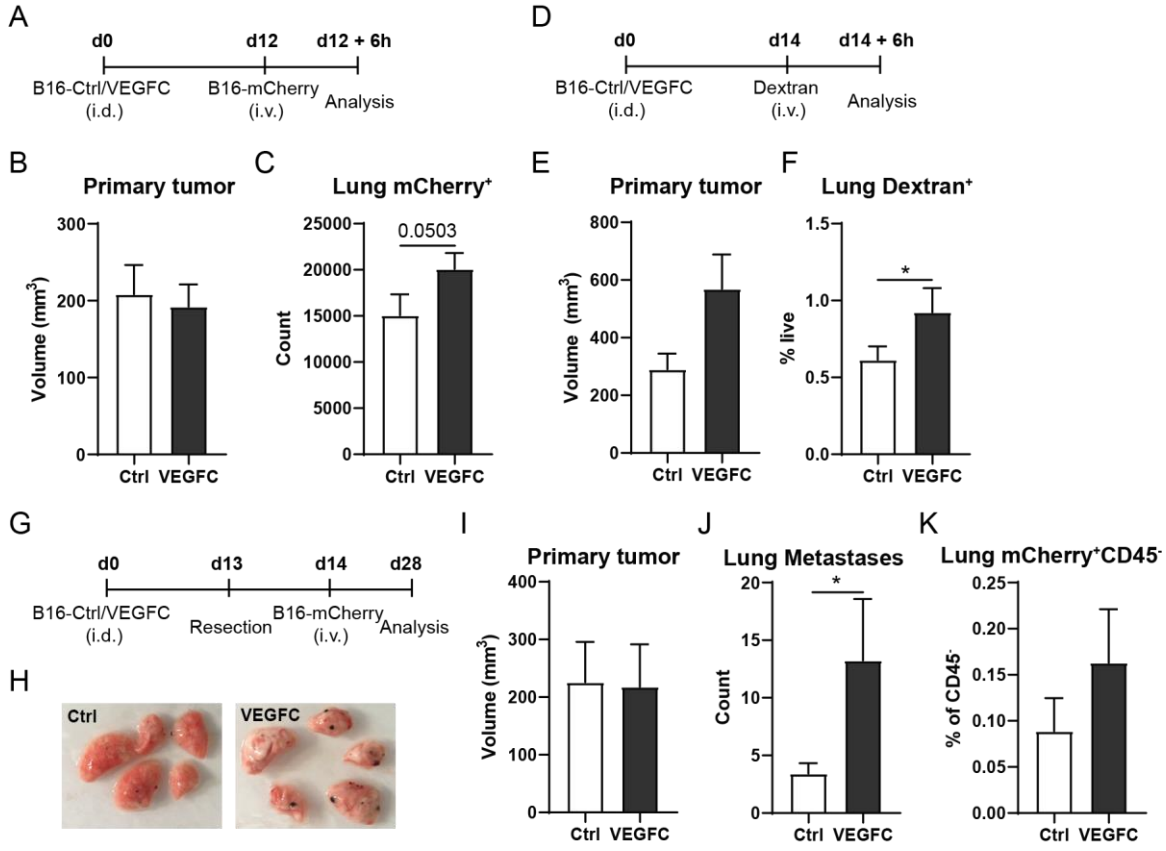

Figure 4.6. VEGFC overexpression by B16-F10 primary tumor favors metastatic seeding in the lungs. (A-C) B16F10-mCherry (B16-mCherry) tumor cells infiltrated in lungs 6 h after intravenous (i.v.) injection in B16-F10-Control (B16-Ctrl, n=5) or B16-F10-VEGFC (B16-VEGFC, n=6) tumor-bearing mice. (A) Experimental schedule, (B) Primary tumor volume at experimental endpoint, (C) Total count of mCherry-positive cells in 3 lung lobes. (D-F) Cellular uptake of 70 kDa Dextran-Texas Red in the lungs 6h after i.v. injection in B16-Ctrl (n=8) or B16-VEGFC (n=6) tumor-bearing mice. (D) Experimental schedule, (E) Primary tumor volume at experimental endpoint, (F) Percentage of lung cells positive for Dextran. (G-K) Metastasis formation by i.v.-injected B16-mCherry cells after B16-Ctrl (n=10) or B16-VEGFC (n=9) primary tumor resection in Rag2-deficient mice. (G) Experimental schedule, (H) Representative image of lung lobes at experimental endpoint. (I) Primary tumor volume at resection. (J) Count of total lung surface metastases. (K) $mCherry^{+}CD45^{-}$ cells in the lung as percentage of CD45-negative cells. Data represent mean ± SEM. * $p<0.05$ using unpaired, one-tailed Student's t test.

Tumor VEGFC leads to increased EV transport to the tumor-draining lymph node

Because EVs contribute to the induction of the pre-metastatic niche [34,35], we asked whether EVs might be involved in premetastatic remodeling by B16F10-VEGFC primary tumors. Importantly, we found that the levels of EVs was significantly increased in B16F10-VEGFC tumor-bearing mouse blood compared to naïve mice, but not in B16F10-Ctrl tumor-bearing mice (**Figure 4.7** A). This observation could not be attributed to a difference in EV production between cell lines, as *in vitro* both B1610-VEGFC and B16F10-Ctrl cell lines produced similar amounts of EVs (**Figure 4.7** B-C). Moreover, cells from B16F10-Ctrl and VEGFC mouse tumor digestions produced similar amounts of EVs *ex vivo* as well (**Figure 4.7** D-E).

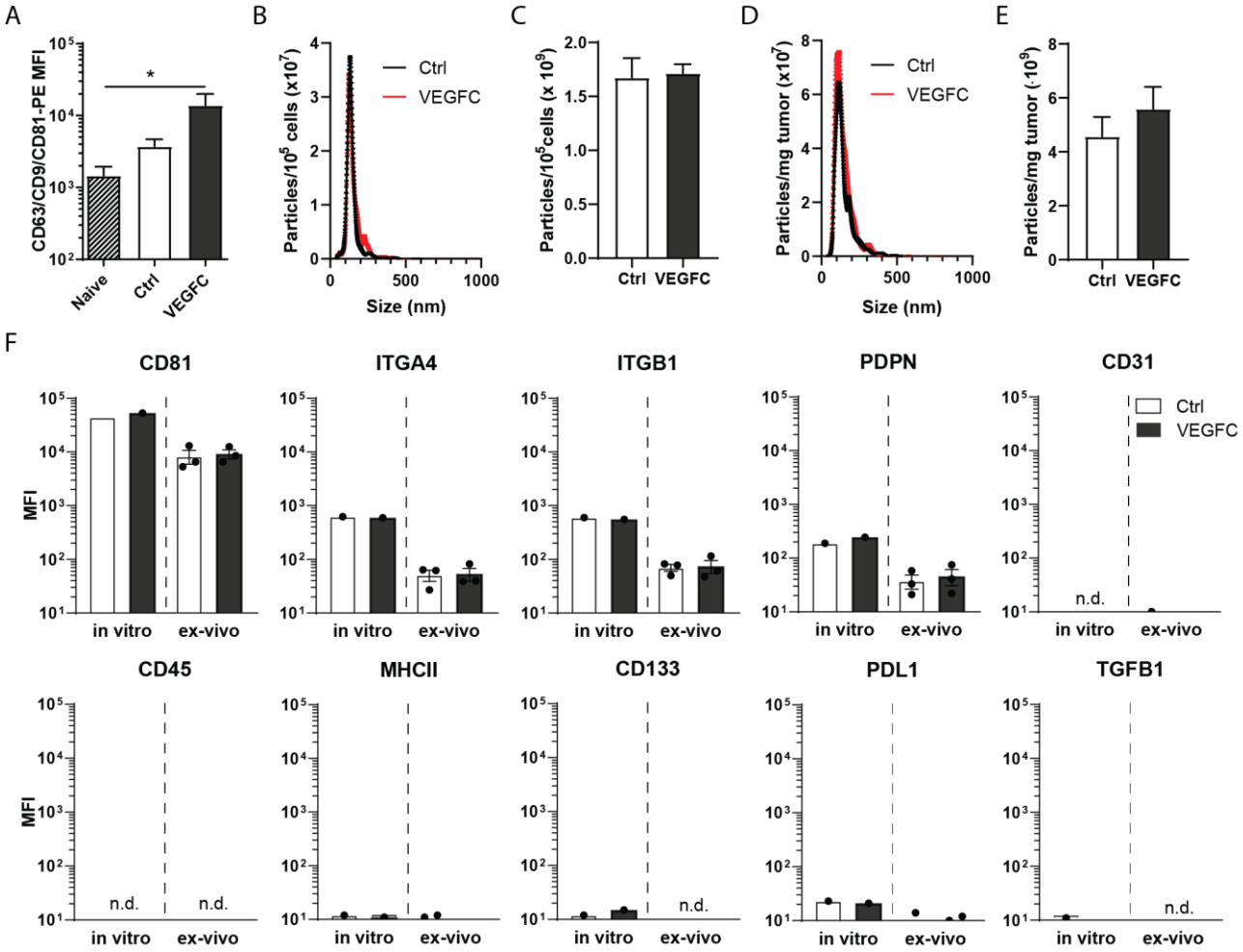

Figure 4.7. Blood levels of EVs is higher upon tumor VEGFC overexpression although VEGFC overexpression does not affect the amount of EV production by tumor cells. (A) Levels of tetraspanins CD63, CD9, CD81 on beads functionalized with CD63, CD9, CD81 antibodies and incubated with plasma of naïve, B16-F10 Control (Ctrl) and B16-F10 VEGFC tumor-bearing mice 2 weeks after inoculation. (B-C) EV production by B16-F10 Ctrl and VEGFC tumor cells in vitro over 48h. (B) representative particle density as a function of size, (C) total particle production per cells. (D-E) EV production by cells digested from B16-F10 Ctrl and VEGFC tumors over 48h ex-vivo. (D) representative particle density as a function of size, (E) total particle production per cells. (F) Surface protein levels on CD81/CD9/CD63 bead-captured EVs from in vitro and ex-vivo tumor cell cultures.

We then selected 10 EV surface proteins, and found no differences in surface levels between B16F10-Ctrl and B16F10-VEGFC EVs, both *in vitro* and *ex vivo* (Figure 4.7 F). In all tumor cell-derived EVs, common marker of EVs CD81 was detected at high level. Additionally,

we detected Integrin alpha 4, Integrin beta 1 which were reported at high levels in B16F10 EVs and may contribute to specific cell and organ targeting [36,37]. Additionally, we detected medium levels of podoplanin, which can be expressed by tumor cells, fibroblasts and lymphatic endothelial cells and contribute to cancer progression [38]. In contrast, we did not detect endothelial marker CD31, or immune markers CD45, MHCII. We did not detect proteins associated with cancer progression such as CD133, PDL1 and TGFβ. Taken together, these data suggest that the EVs were overall quantatively similar between B16F10-Ctrl and B16F10-VEGFC, both *in vitro* and *ex vivo,* although we cannot exclude that deeper analyses may reveal differences in EV contents between B16F10-Ctrl and B16F10-VEGFC tumors.

As tumor EV production appeared to be unchanged upon VEGFC overexpression, we asked whether the increased levels of EVs observed in the blood of B16F10-VEGFC tumor-bearing mice could be due to increased transport from primary tumors. We injected fluorescently labeled EVs intratumorally into B16F10-Ctrl and B16F10-VEGFC tumors, and found higher levels of fluorescence in LNs draining B16F10-VEGFC tumors than in LNs draining B16F10-Ctrl tumors (**Figure 4.8** A). This was associated with a higher percentage of LN cells that picked up EVs (**Figure 4.8** B). To confirm that the increased levels of EVs in B16F10-VEGFC TDLNs was due to increased transport as opposed to increased retention of EVs within the LN, we injected labeled EVs into non-tumor skin draining to the TDLN, and found no difference in EV levels in B16F10-Ctrl compared with B16F10-VEGFC TDLNs (**Figure 4.8** C).

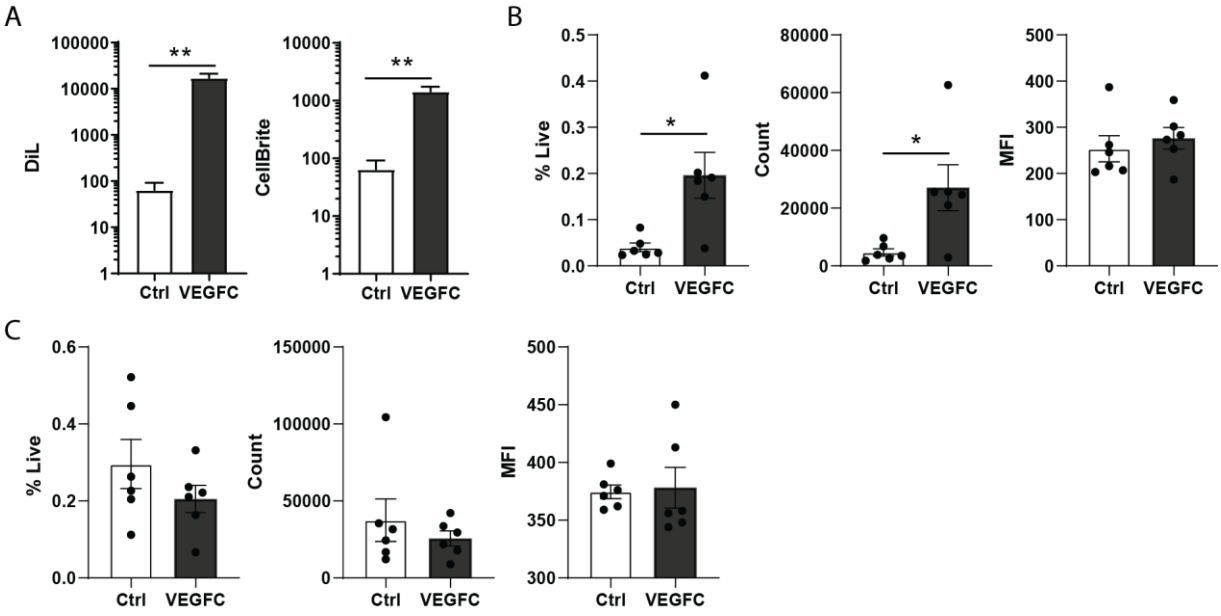

Figure 4.8. Tumor lymphangiogenesis leads to increased EV transport to the tumor-draining lymph node. (A) EV fluorescence intensity in TDLN homogenate, 6 h after intratumoral injection of Cellbrite- and DiL-labeled exosomes (n=6-7). (B) and (C) Percentage, count and mean fluorescence intensity (MFI) of exosome-positive cells in the TDLN, 6h after B) intratumoral and C) intradermal (hock) injection of Di-labeled exosomes (n=6). Data represent mean ± SEM. * $p<0.05$, ** $p<0.01$ using two-tailed, unpaired Student's t test.

Blocking exosomes reduces neutrophil infiltration in tumors and at distant sites

To assess the contribution of EVs in premetastatic remodeling by VEGFC-overexpressing tumors, we used B16F10 tumor cell lines in which Ras-related protein Rab-27a (Rab27a) was knocked out ($Rab27a^{-/-}$). Rab27a knockout has been reported to reduce EV production by cells including B16F10 [31]. $Rab27a^{-/-}$ tumors tended to grow slightly more slowly than Rab27a-competent tumors ($Rab27a^{+/+}$), particularly in B16F10-Ctrl tumors as previously reported [31] (**Figure 4.9** A). LEC density was elevated both in B16F10-VEGFC $Rab27a^{+/+}$ and in B16F10-VEGFC $Rab27a^{-/-}$ tumors, and low in both B16F10-Ctrl $Rab27a^{+/+}$ and in B16F10-Ctrl $Rab27a^{-/-}$ tumors, while blood endothelial cell and immune cell infiltration

remained unchanged overall (**Figure 4.9** B). Strikingly, neutrophil density in tumors, blood, lungs and spleens were not only reduced upon Rab27a knockout in B16F10-Ctrl tumor-bearing mice as previously reported [31], but also and even more strikingly in B16F10-VEGFC tumor-bearing mice (**Figure 4.9** C).

Finally, we sought to determine the possibility of reducing EV production as a therapeutic approach to prevent metastasis of VEGFC-overexpressing tumors in the 4T1 tumor model. For this, we used the sphingomyelinase inhibitor GW4869, which has been shown to reduce EV production *in vitro* and *in vivo* upon intraperitoneal injection [39,40]. We started daily intraperitoneal treatment upon appearance of tumor mass, 7 days after tumor inoculation into mammary fat pads, until experimental endpoint (**Figure 4.9** D). As expected, 4T1-VEGFC tumors formed increased metastatic nodules in lungs than 4T1-Ctrl tumors (**Figure 4.9** E). In addition, GW4869 treatment trended to reduce lung metastatic nodules in both 4T1-Ctrl and in 4T1-VEGFC tumor.

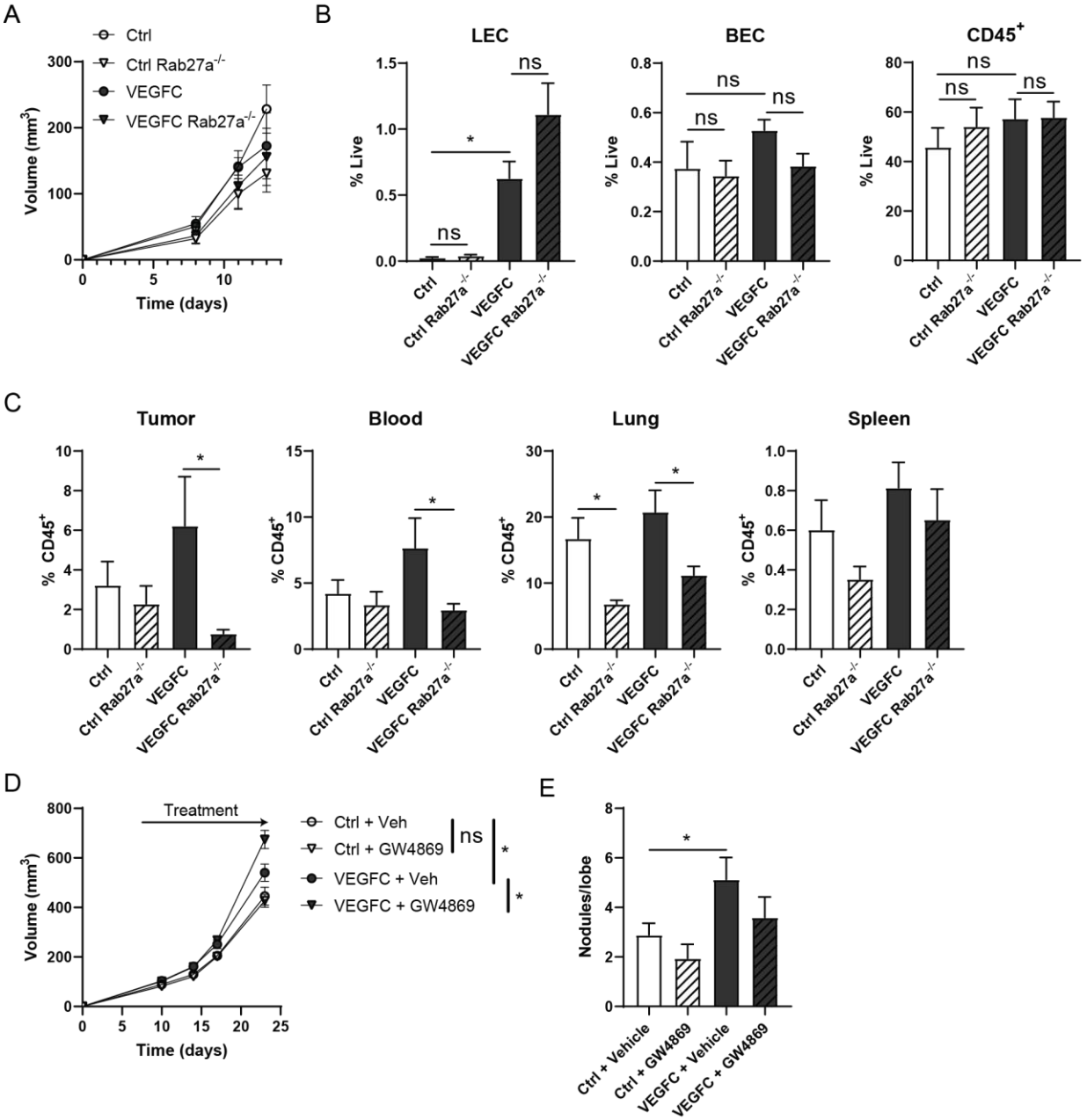

Figure 4.9. Reduction of extracellular vesicle production in VEGFC overexpressing tumors leads to lower neutrophil mobilization. (A-C) Control (Ctrl), Rab27a-deficient (Rab27a$^{-/-}$) Ctrl, VEGFC overexpressing (VEGFC) or Rab27a$^{-/-}$ VEGFC B16-F10 tumors were inoculated intradermally and mice were analyzed 2 weeks after tumor inoculation. (A) Tumor growth, (B) Lymphatic endothelial cells (LEC), blood endothelial cells (BECs) and immune cell (CD45^{+}) infiltration in tumors, as percentage of live cells, (C) Neutrophil density in tumor, blood, lung and spleen as percentage of CD45^{+} cells. (D-E) Ctrl or VEGFC overexpressing 4T1 tumors were injected into the mouse mammary fat pad and treated with vehicle or GW4869 sphingomyelinase inhibitor from day 7. (D) Tumor growth, (E) lung macrometastasis count at day 24 after tumor inoculation. Data represent mean ± SEM. * $p<0.05$, ** $p<0.01$ using one-way ANOVA.

4.5. Discussion

In this chapter, we analyzed the consequences of VEGFC expression in tumors on the formation of premetastatic niches. For this, we used the B16F10 mouse melanoma model. As previously reported, unmodified B16F10 cells do not produce VEGFC at detectable levels *in vitro*, and tumors implanted *in vivo* develop very low densities of lymphatic vessels [17,30]. In contrast, VEGFC overexpression by these tumors leads to lymphatic endothelial cell growth in tumors characterized by high densities of intratumoral and peritumoral lymphatic vessels (**Figure 4.3** and [30]). We suggest that both B16F10-Ctrl and B16F10-VEGFC tumors represent a range of lymphatic densities that may occur in human melanoma, where lymphatic vessel density was reported to vary between ~0.1% to 4% of tumor area [41].

Although lymphangiogenesis has been associated with the premetastatic niche, both in LNs [13,22,42] and in lungs [23,43], the contributions of primary tumor lymphangiogenesis to the process of premetastatic niche formation remained poorly understood. Our group has shown that B16F10-VEGFC TDLNs were more immune suppressed than B16F10-Ctrl TDLNs, and has suggested that such effect may be due to tolerogenic properties of LN LECs, which can cross-present tumor-associated antigens to tumor-specific $CD8^+$ T cells to tolerize them [17]. Additionally, LN LECs have been suggested to contribute to the metastatic process by upregulating adhesion molecules upon tumor factor conditioning [44]. In lungs, local induction of lymphangiogenesis was found to increase metastatic growth [43]. In this work, we suggest that VEGFC may not only contribute directly to the premetastatic niche by inducing lymphangiogenesis in the TDLN and distant sites but may also indirectly promote the premetastatic niche through induction of tumor lymphangiogenesis and resulting enhanced transport of tumor-derived factors to the

premetastatic niche. In turn, transported tumor-derived factors may play a variety of roles in the formation of the premetastatic niche in addition to the induction of lymphangiogenesis.

Higher levels of neutrophils were observed in lungs and blood of B16F10-VEGFC tumor-bearing mice than in B16F10-Ctrl tumor-bearing mice. Neutrophils have long been identified as a hallmark of the premetastatic niche [32,45,46]. Additionally, EVs have been shown to play key roles in their mobilization from the bone marrow and chemoattraction into premetastatic organs [31,32]. We hypothesize that the increased levels of neutrophils observed upon overexpression of VEGFC in tumors may be due to the increased amounts of tumor-derived EVs transported into the blood and distant organs. However, it is possible that additional mechanisms play roles. For example, lymphatic endothelial cells may produce chemokines or adhesion molecules favoring neutrophil mobilization and survival. Additionally, we cannot exclude that VEGFC may have a direct effect on bone vascular niches and as a result affect neutrophil mobilization. Nevertheless, our findings on the reduction of neutrophil levels in Rab27a-deficient B16F10-Ctrl and B16F10-VEGFC tumor-bearing mice suggest that tumor-derived EVs contribute, at least partially, in this process.

In addition to neutrophil accumulation, we have found that several genes associated with the premetastatic niche are upregulated in LNs or in lungs of B16F10-VEGFC tumor-bearing mice (**Figure 4.4** and **Figure 4.5**). This suggests that VEGFC overexpression in tumors may lead to an overall enhancement of multiple mechanisms involved in premetastatic remodeling. Future studies would be necessary to determine whether tumor VEGFC leads to the activation of specific pro-tumorigenic pathways. We found that tumor VEGFC overexpression leads to increased seeding of tumor cells in the lungs (**Figure 4.6**). Because we see increased infiltration of tumor cells and of dextran at early time points after

intravenous injection, we suggest that lungs may be more pro-metastatic due to enhanced permeability to tumor cells or to enhanced chemoattraction of tumor cells into the lungs. Endothelial permeability may be induced by various tumor-derived factors, including tumor EVs. For example, tumor EVs were reported to be picked up by blood endothelial cells of the lungs and to induce tight junction remodeling via miRNAs resulting in increased permeability and tumor cell invasion [47]. Chemoattraction is another hallmark of the premetastatic niche whereby lung cells increase expression of chemokines and adhesion molecules to enhance recruitment of bone-marrow-derived cells and tumor cells [35]. Among these chemokines, S100A8 and S100A9 for example play important roles and can be induced by EVs [31,33,48] and were shown to be expressed at high levels in the lungs of B16F10-VEGFC tumor-bearing mice (**Figure 4.5**).

We did not observe significant differences in the amount and quality of EV production by VEGFC overexpressing tumors compared to control (**Figure 4.7**). However, as we only measured selected surface protein markers, and the quantification methods used did not allow a high level of precision, we cannot rule out the fact that EVs may different. In fact, as VEGFC overexpressing tumors develop high densities of lymphatic vessels, and we have also previously reported that it leads to enhanced recruitment of immune cells such as T cells and dendritic cells, it is likely that EVs produced by these cells of the tumor microenvironment may contribute to changes in EVs quality and quantity. Nevertheless, as we have previously observed that tumor cells present the majority of total cells of the tumors (not shown), more advanced methods may be required to detect markers of LEC and immune cell-derived EVs.

We observed higher levels of EVs transported to TDLNs from VEGFC-overexpressing tumors (**Figure 4.8**). Due to the aggressiveness of the B16F10 model, the process of

lymphangiogenesis, the biomechanical properties of the tumor microenvironment and the time course of premetastatic niche formation likely differ significantly from human melanoma. However, increased transport upon lymphangiogenesis is not unique to EV transport nor to the B16F10 melanoma model. Our group and others reported that lymphangiogenesis contributes to enhanced transport of macromolecules and cells to the draining lymph nodes in tumors and in skin wounds [17,49]. Therefore, it is likely that EV transport would be increased upon tissue lymphangiogenesis in other contexts, including different tumor types and other physiological contexts. Future work to further investigate the implications of tumor lymphangiogenesis on premetastatic niche formation could employ other melanoma tumor models suited to the study of metastasis and biomechanical properties of tumors, such as the autochthonous $Braf^{V600E}$-$PTEN^{-/-}$ melanoma model [50]. In this model, VEGFC signaling and EV production can be modulated through injections of a VEGFR3 blocking antibody [30] and injections of GW4869, respectively.

The knock-out of Rab27a in tumor cells led to lower neutrophil mobilization both in control and VEGFC-overexpressing tumor-bearing mice (**Figure 4.9**). This is consistent with a prior study from Dr. Lyden and colleagues on B16F10 tumors [31], and suggests that the same mechanisms apply to VEGFC-overexpressing tumors as well. Moreover, broadly blocking EV formation using the sphingomyelinase inhibitor GW4869 trended to reduce metastasis both in control and VEGFC-overexpressing 4T1 tumors. It is not surprising to see a subtle difference in resulting metastasis. First, the inhibitor is expected to reduce only partially EV production as the inhibitor does not inhibit all pathways of EV production but only the ceramide pathway. Additionally, non-EV tumor-derived factors are involved in premetastatic niche formation as well and are likely to play roles even in absence of EVs.

In conclusion, the findings of this chapter suggest that tumor lymphangiogenesis may not only enhance metastasis by providing additional routes for tumor cells to travel to the TDLN and to the systemic circulation, but may also enhance metastasis through transport of tumor-derived factors and priming of the premetastatic niche.

4.6. Acknowledgements

I would like to thank Dr. Lambert Potin, Rachel Gleyzer, Dr. Priscilla Briquez, Ha-Na Shim, Peyman Hosseinchi, Trevin Kurtanich, Dr. Maria Stella Sasso, Dr. Nikolaos Mitrousis, Mindy Nguyen and Ani Solanki for technical assistance and helpful discussions. The Rab27a-knockout cell lines were kindly provided by Dr. David Lyden (Cornell University).

4.7. References

[1] D. Hanahan, R.A. Weinberg, Hallmarks of cancer: the next generation., Cell. 144 (2011) 646–74. https://doi.org/10.1016/j.cell.2011.02.013.

[2] J.A. Joyce, J.W. Pollard, Microenvironmental regulation of metastasis, Nat. Rev. Cancer. 9 (2009) 239–252. https://doi.org/10.1038/nrc2618.

[3] M.A. Swartz, A.W. Lund, Lymphatic and interstitial flow in the tumour microenvironment: linking mechanobiology with immunity., Nat. Rev. Cancer. 12 (2012) 210–9. https://doi.org/10.1038/nrc3186.

[4] J.D. Shields, M.E. Fleury, C. Yong, A.A. Tomei, G.J. Randolph, M.A. Swartz, Autologous chemotaxis as a mechanism of tumor cell homing to lymphatics via interstitial flow and autocrine CCR7 signaling., Cancer Cell. 11 (2007) 526–38. https://doi.org/10.1016/j.ccr.2007.04.020.

[5] M. Kim, Y.J. Koh, K.E. Kim, B.I. Koh, D.H. Nam, K. Alitalo, I. Kim, G.Y. Koh, CXCR4 signaling regulates metastasis of chemoresistant melanoma cells by a lymphatic metastatic niche, Cancer Res. 70 (2010) 10411–10421. https://doi.org/10.1158/0008-5472.CAN-10-2591.

[6] T. Hoshida, N. Isaka, J. Hagendoorn, E. Di Tomaso, Y.-L.L. Chen, B. Pytowski, D. Fukumura, T.P. Padera, R.K. Jain, E. Tomaso, Y.-L.L. Chen, B. Pytowski, D. Fukumura, T.P. Padera, R.K. Jain, D. Fukumura, J. Hagendoorn, R.K. Jain, T. Hoshida, E. Di Tomaso, Imaging Steps of Lymphatic Metastasis Reveals That Vascular Endothelial Growth Factor-C Increases Metastasis by Increasing Delivery of Cancer Cells to Lymph Nodes: Therapeutic Implications, Cancer Res. 66 (2006) 8065–8075.

https://doi.org/10.1158/0008-5472.can-06-1392.

[7] S.S. Dadras, T. Paul, J. Bertoncini, L.F. Brown, A. Muzikansky, D.G. Jackson, U. Ellwanger, C. Garbe, M.C. Mihm, M. Detmar, Tumor lymphangiogenesis: A novel prognostic indicator for cutaneous melanoma metastasis and survival, Am. J. Pathol. 162 (2003) 1951–1960. https://doi.org/10.1016/S0002-9440(10)64328-3.

[8] A. Alitalo, M. Detmar, Interaction of tumor cells and lymphatic vessels in cancer progression., Oncogene. 31 (2012) 4499–508. https://doi.org/10.1038/onc.2011.602.

[9] G. Follain, D. Herrmann, S. Harlepp, V. Hyenne, N. Osmani, S.C. Warren, P. Timpson, J.G. Goetz, Fluids and their mechanics in tumour transit: shaping metastasis, Nat. Rev. Cancer. 20 (2019) 107–124. https://doi.org/10.1038/s41568-019-0221-x.

[10] E.R. Pereira, D. Kedrin, G. Seano, O. Gautier, E.F.J. Meijer, D. Jones, S.M. Chin, S. Kitahara, E.M. Bouta, J. Chang, E. Beech, H.S. Jeong, M.C. Carroll, A.G. Taghian, T.P. Padera, Lymph node metastases can invade local blood vessels, exit the node, and colonize distant organs in mice, Science (80-.). 359 (2018) 1403–1407. https://doi.org/10.1126/science.aal3622.

[11] M. Brown, F.P. Assen, A. Leithner, J. Abe, H. Schachner, G. Asfour, Z. Bago-Horvath, J. V. Stein, P. Uhrin, M. Sixt, D. Kerjaschki, Lymph node blood vessels provide exit routes for metastatic tumor cell dissemination in mice, Science (80-.). (2018) 1408–1411. https://doi.org/10.1126/science.aal3662.

[12] R.H. Farnsworth, M.G. Achen, S.A. Stacker, The evolving role of lymphatics in cancer metastasis, Curr. Opin. Immunol. 53 (2018) 64–73. https://doi.org/10.1016/j.coi.2018.04.008.

[13] N. Wakisaka, Y. Hasegawa, S. Yoshimoto, K. Miura, A. Shiotani, J. Yokoyama, Primary Tumor-Secreted Lymphangiogenic Factors Induce Pre-Metastatic Lymphvascular Niche Formation at Sentinel Lymph Nodes in Oral Squamous Cell Carcinoma, PLoS One. 10 (2015) 144056. https://doi.org/10.1371/journal.pone.0144056.

[14] R.N. Kaplan, S. Rafii, D. Lyden, Preparing the ‘“ Soil ”’: The Premetastatic Niche, (2006) 11089–11094. https://doi.org/10.1158/0008-5472.CAN-06-2407.

[15] C.N. Qian, B. Berghuis, G. Tsarfaty, M.B. Bruch, E.J. Kort, J. Ditlev, I. Tsarfaty, E. Hudson, D.G. Jackson, D. Petillo, J. Chen, J.H. Resau, B.T. Teh, Preparing the “soil”: The primary tumor induces vasculature reorganization in the sentinel lymph node before the arrival of metastatic cancer cells, Cancer Res. 66 (2006) 10365–10376. https://doi.org/10.1158/0008-5472.CAN-06-2977.

[16] L. Jeanbart, M. Ballester, A. De Titta, Enhancing Efficacy of Anticancer Vaccines by Targeted Delivery to Tumor-Draining Lymph Nodes Enhancing Ef fi cacy of Anticancer Vaccines by Targeted Delivery to Tumor-Draining Lymph Nodes, (2014) 436–447. https://doi.org/10.1158/2326-6066.CIR-14-0019-T.

[17] A.W.W. Lund, F.V. V. Duraes, S. Hirosue, V.R.R. Raghavan, C. Nembrini, S.N.N. Thomas,

A. Issa, S. Hugues, M.A.A. Swartz, A. Issa, S. Hugues, M.A.A. Swartz, VEGF-C promotes immune tolerance in B16 melanomas and cross-presentation of tumor antigen by lymph node lymphatics., Cell Rep. 1 (2012) 191–199. https://doi.org/10.1016/j.celrep.2012.01.005.

[18] S.A. Stacker, S.P. Williams, T. Karnezis, R. Shayan, S.B. Fox, M.G. Achen, Lymphangiogenesis and lymphatic vessel remodelling in cancer, Nat. Rev. Cancer. 14 (2014) 159–72. https://doi.org/10.1038/nrc3677.

[19] S. Hirakawa, S. Kodama, R. Kunstfeld, K. Kajiya, L.F. Brown, M. Detmar, VEGF-A induces tumor and sentinel lymph node lymphangiogenesis and promotes lymphatic metastasis., J. Exp. Med. 201 (2005) 1089–99. https://doi.org/10.1084/jem.20041896.

[20] C.D. Commerford, L.C. Dieterich, Y. He, T. Hell, J.A. Montoya-Zegarra, S.F. Noerrelykke, E. Russo, M. Röcken, M. Detmar, M. Ro, C.D. Commerford, L.C. Dieterich, Y. He, T. Hell, J.A. Montoya-Zegarra, M. Detmar, Mechanisms of Tumor-Induced Lymphovascular Niche Formation in Draining Lymph Nodes Report Mechanisms of Tumor-Induced Lymphovascular Niche Formation in Draining Lymph Nodes, Cell Rep. 25 (2018) 3554–3563. https://doi.org/10.1016/j.celrep.2018.12.002.

[21] B. Garmy-Susini, C.J. Avraamides, J.S. Desgrosellier, M.C. Schmid, P. Foubert, L.G. Ellies, A.M. Lowy, S.L. Blair, S.R. Vandenberg, B. Datnow, H.Y. Wang, D.A. Cheresh, J. Varner, PI3Ka activates integrin α4ß1 to establish a metastatic niche in lymph nodes, Proc. Natl. Acad. Sci. U. S. A. 110 (2013) 9042–9047. https://doi.org/10.1073/pnas.1219603110.

[22] F. Ogawa, H. Amano, K. Eshima, Y. Ito, Y. Matsui, K. Hosono, H. Kitasato, A. Iyoda, K. Iwabuchi, Y. Kumagai, Y. Satoh, S. Narumiya, M. Majima, Prostanoid induces premetastatic niche in regional lymph nodes, J. Clin. Invest. 124 (2014) 4882–4894. https://doi.org/10.1172/JCI73530.

[23] D. Olmeda, D. Cerezo-Wallis, E. Riveiro-Falkenbach, P.C. Pennacchi, M. Contreras-Alcalde, N. Ibarz, M. Cifdaloz, X. Catena, T.G. Calvo, E. Cañón, D. Alonso-Curbelo, J. Suarez, L. Osterloh, O. Graña, F. Mulero, D. Megías, M. Cañamero, J.L. Martínez-Torrecuadrada, C. Mondal, J. Di Martino, D. Lora, I. Martinez-Corral, J.J. Bravo-Cordero, J. Muñoz, S. Puig, P. Ortiz-Romero, J.L. Rodriguez-Peralto, S. Ortega, M.S. Soengas, Whole-body imaging of lymphovascular niches identifies pre-metastatic roles of midkine, Nature. 546 (2017) 676–680. https://doi.org/10.1038/nature22977.

[24] S. Hirakawa, L.F. Brown, S. Kodama, K. Paavonen, K. Alitalo, M. Detmar, VEGF-C-induced lymphangiogenesis in sentinel lymph nodes promotes tumor metastasis to distant sites, Blood. 109 (2007) 1010–1017. https://doi.org/10.1182/blood-2006-05-021758.

[25] A. Gogineni, M. Caunt, A. Crow, C. V. Lee, G. Fuh, N. Van, W. Ye, R.M. Weimer, N. van Bruggen, W. Ye, R.M. Weimer, Inhibition of VEGF-C Modulates Distal Lymphatic Remodeling and Secondary Metastasis, PLoS One. 8 (2013) 68755.

https://doi.org/10.1371/journal.pone.0068755.

[26] F. Pucci, C. Garris, C.P. Lai, A. Newton, C. Pfirschke, C. Engblom, D. Alvarez, M. Sprachman, C. Evavold, A. Magnuson, U.H. Von Andrian, K. Glatz, X.O. Breakefield, T.R. Mempel, R. Weissleder, M.J. Pittet, SCS macrophages suppress melanoma by restricting tumor-derived vesicle-B cell interactions, Science (80-.). 352 (2016) 242–246. https://doi.org/10.1126/science.aaf1328.

[27] J.L. Hood, R.S. San, S.A. Wickline, Exosomes Released by Melanoma Cells Prepare Sentinel Lymph Nodes for Tumor Metastasis, Cancer Res. 71 (2011) 3792–3801. https://doi.org/10.1158/0008-5472.CAN-10-4455.

[28] G. Chen, A.C. Huang, W. Zhang, G. Zhang, M. Wu, W. Xu, Z. Yu, J. Yang, B. Wang, H. Sun, H. Xia, Q. Man, W. Zhong, L.F. Antelo, B. Wu, X. Xiong, X. Liu, L. Guan, T. Li, S. Liu, R. Yang, Y.Y. Lu, L. Dong, S. McGettigan, R. Somasundaram, R. Radhakrishnan, G. Mills, Y.Y. Lu, J. Kim, Y.H. Chen, H. Dong, Y. Zhao, G.C. Karakousis, T.C. Mitchell, L.M. Schuchter, M. Herlyn, E.J. Wherry, X. Xu, W. Guo, Exosomal PD-L1 contributes to immunosuppression and is associated with anti-PD-1 response, Nature. 560 (2018) 382–386. https://doi.org/10.1038/s41586-018-0392-8.

[29] M. Poggio, T. Hu, C.-C. Pai, B. Chu, C.D. Belair, A. Chang, E. Montabana, U.E. Lang, Q. Fu, L. Fong, R. Blelloch, Suppression of Exosomal PD-L1 Induces Systemic Anti-tumor Immunity and Memory, Cell. 177 (2019) 414–427. https://doi.org/10.1016/j.cell.2019.02.016.

[30] M. Fankhauser, M.A.S. Broggi, L. Potin, N. Bordry, L. Jeanbart, A.W. Lund, E. Da Costa, S. Hauert, M. Rincon-Restrepo, C. Tremblay, E. Cabello, K. Homicsko, O. Michielin, D. Hanahan, D.E. Speiser, M.A. Swartz, Tumor lymphangiogenesis promotes T cell infiltration and potentiates immunotherapy in melanoma, Sci. Transl. Med. 9 (2017) 1–13. https://doi.org/10.1126/scitranslmed.aal4712.

[31] H. Peinado, M. Alec, S. Lavotshkin, I. Matei, B. Costa-silva, G. Moreno-bueno, M. Hergueta-redondo, C. Williams, G. García-santos, C.M. Ghajar, A. Nitadori-hoshino, C. Hoffman, K. Badal, B.A. Garcia, M.K. Callahan, J. Yuan, V.R. Martins, J. Skog, R.N. Kaplan, M.S. Brady, J.D. Wolchok, P.B. Chapman, Y. Kang, Melanoma exosomes educate bone marrow progenitor cells toward a pro-metastatic phenotype through MET, Nat. Med. 18 (2012) 883–891. https://doi.org/10.1038/nm.2753.

[32] Y. Liu, Y. Gu, Y. Han, Q. Zhang, Z. Jiang, X. Zhang, B. Huang, X. Xu, J. Zheng, X. Cao, Tumor Exosomal RNAs Promote Lung Pre-metastatic Niche Formation by Activating Alveolar Epithelial TLR3 to Recruit Neutrophils, Cancer Cell. 30 (2016) 243–256. https://doi.org/10.1016/j.ccell.2016.06.021.

[33] S. Hiratsuka, A. Watanabe, H. Aburatani, Y. Maru, Tumour-mediated upregulation of chemoattractants and recruitment of myeloid cells predetermines lung metastasis, Nat. Cell Biol. 8 (2006) 1369–1375. https://doi.org/10.1038/ncb1507.

[34] H. Peinado, H. Zhang, I.R. Matei, B. Costa-Silva, A. Hoshino, G. Rodrigues, B. Psaila, R.N. Kaplan, J.F. Bromberg, Y. Kang, M.J. Bissell, T.R. Cox, A.J. Giaccia, J.T. Erler, S. Hiratsuka, C.M. Ghajar, D. Lyden, Pre-metastatic niches: Organ-specific homes for metastases,

Nat. Rev. Cancer. 17 (2017) 302–317. https://doi.org/10.1038/nrc.2017.6.

[35] I. Wortzel, S. Dror, C.M. Kenific, D. Lyden, Exosome-Mediated Metastasis: Communication from a Distance, Dev. Cell. 49 (2019) 347–360. https://doi.org/10.1016/J.DEVCEL.2019.04.011.

[36] H. Zhang, D. Freitas, H.S. Kim, K. Fabijanic, Z. Li, H. Chen, M.T. Mark, H. Molina, A.B. Martin, L. Bojmar, J. Fang, S. Rampersaud, A. Hoshino, I. Matei, C.M. Kenific, M. Nakajima, A.P. Mutvei, P. Sansone, W. Buehring, H. Wang, J.P. Jimenez, L. Cohen-gould, N. Paknejad, M. Brendel, K. Manova-todorova, J.R. Cubillos-ruiz, G. Galletti, P. Giannakakou, A.M. Cuervo, A. Magalhães, J.A. Ferreira, H. Osório, A.M. Silva, A. Massey, J.R. Cubillos-ruiz, G. Galletti, P. Giannakakou, A.M. Cuervo, J. Blenis, R. Schwartz, M.S. Brady, H. Peinado, J. Bromberg, H. Matsui, C.A. Reis, D. Lyden, Identification of distinct nanoparticles and subsets of extracellular vesicles by asymmetric flow field-flow fractionation, Nat. Cell Biol. 20 (2018) 332–343. https://doi.org/10.1038/s41556-018-0040-4.

[37] A. Hoshino, B. Costa-Silva, T.-L. Shen, G. Rodrigues, A. Hashimoto, M. Tesic Mark, H. Molina, S. Kohsaka, A. Di Giannatale, S. Ceder, S. Singh, C. Williams, N. Soplop, K. Uryu, L. Pharmer, T. King, L. Bojmar, A.E. Davies, Y. Ararso, T. Zhang, H. Zhang, J. Hernandez, J.M. Weiss, V.D. Dumont-Cole, K. Kramer, L.H. Wexler, A. Narendran, G.K. Schwartz, J.H. Healey, P. Sandstrom, K. Jørgen Labori, E.H. Kure, P.M. Grandgenett, M.A. Hollingsworth, M. de Sousa, S. Kaur, M. Jain, K. Mallya, S.K. Batra, W.R. Jarnagin, M.S. Brady, O. Fodstad, V. Muller, K. Pantel, A.J. Minn, M.J. Bissell, B.A. Garcia, Y. Kang, V.K. Rajasekhar, C.M. Ghajar, I. Matei, H. Peinado, J. Bromberg, D. Lyden, Tumour exosome integrins determine organotropic metastasis, Nature. 527 (2015) 329–335. https://doi.org/10.1038/nature15756.

[38] P. Carrasco-Ramírez, D.W. Greening, G. Andrés, S.K. Gopal, E. Martín-Villar, J. Renart, R.J. Simpson, M. Quintanilla, Podoplanin is a component of extracellular vesicles that reprograms cell-derived exosomal proteins and modulates lymphatic vessel formation, Oncotarget. 7 (2016). https://doi.org/10.18632/oncotarget.7445.

[39] K. Trajkovic, C. Hsu, S. Chiantia, L. Rajendran, D. Wenzel, F. Wieland, P. Schwille, B. Brügger, M. Simons, Ceramide triggers budding of exosome vesicles into multivesicular endosomes., Science. 319 (2008) 1244–1247. https://doi.org/10.1126/science.1153124.

[40] S. Faict, J. Muller, K. De Veirman, E. De Bruyne, K. Maes, L. Vrancken, R. Heusschen, H. De Raeve, R. Schots, K. Vanderkerken, J. Caers, E. Menu, Exosomes play a role in multiple myeloma bone disease and tumor development by targeting osteoclasts and osteoblasts, Blood Cancer J. 8 (2018). https://doi.org/10.1038/s41408-018-0139-7.

[41] N. Bordry, M.A.S. Broggi, K. de Jonge, K. Schaeuble, P.O. Gannon, P.G. Foukas, E. Danenberg, E. Romano, P. Baumgaertner, M. Fankhauser, N. Wald, L. Cagnon, S. Abed-Maillard, H.M. El Hajjami, T. Murray, K. Ioannidou, I. Letovanec, P. Yan, O. Michielin, M. Matter, M.A. Swartz, D.E. Speiser, Lymphatic vessel density is associated with CD8+ T cell infiltration and immunosuppressive factors in human melanoma, Oncoimmunology. 7 (2018) 1–13.

https://doi.org/10.1080/2162402X.2018.1462878.

[42] R. Evans, F. Flores-Borja, S. Nassiri, E. Miranda, K. Lawler, A. Grigoriadis, J. Monypenny, C. Gillet, J. Owen, P. Gordon, V. Male, A. Cheung, F. Noor, P. Barber, R. Marlow, E. Francesch-Domenech, G. Fruhwirth, M. Squadrito, B. Vojnovic, A. Tutt, F. Festy, M. De Palma, T. Ng, Integrin-Mediated Macrophage Adhesion Promotes Lymphovascular Dissemination in Breast Cancer, Cell Rep. 27 (2019) 1967-1978.e4. https://doi.org/10.1016/j.celrep.2019.04.076.

[43] Q. Ma, L.C. Dieterich, K. Ikenberg, S.B. Bachmann, J. Mangana, S.T. Proulx, V.C. Amann, M.P. Levesque, R. Dummer, P. Baluk, D.M. McDonald, M. Detmar, Unexpected contribution of lymphatic vessels to promotion of distant metastatic tumor spread, Sci. Adv. 4 (2018) 1–11. https://doi.org/10.1126/sciadv.aat4758.

[44] E. Lee, E.J. Fertig, K. Jin, S. Sukumar, N.B. Pandey, A.S. Popel, Breast cancer cells condition lymphatic endothelial cells within pre-metastatic niches to promote metastasis, Nat. Commun. 5 (2014) 1–16. https://doi.org/10.1038/ncomms5715.

[45] S.K. Wculek, I. Malanchi, Neutrophils support lung colonization of metastasis-initiating breast cancer cells, Nature. 528 (2015) 413–417. https://doi.org/10.1038/nature16140.

[46] L. Yang, Q. Liu, X. Zhang, X. Liu, B. Zhou, J. Chen, D. Huang, J. Li, H. Li, F. Chen, J. Liu, Y. Xing, X. Chen, S. Su, E. Song, DNA of neutrophil extracellular traps promotes cancer metastasis via CCDC25, Nature. (2020) 1–6. https://doi.org/10.1038/s41586-020-2394-6.

[47] W. Zhou, M.Y. Fong, Y. Min, G. Somlo, L. Liu, M.R. Palomares, Y. Yu, A. Chow, S.T.F. O'Connor, A.R. Chin, Y. Yen, Y. Wang, E.G. Marcusson, P. Chu, J. Wu, X. Wu, A.X. Li, Z. Li, H. Gao, X. Ren, M.P. Boldin, P.C. Lin, S.E. Wang, Cancer-Secreted miR-105 destroys vascular endothelial barriers to promote metastasis, Cancer Cell. 25 (2014) 501–515. https://doi.org/10.1016/j.ccr.2014.03.007.

[48] S. Hiratsuka, A. Watanabe, Y. Sakurai, S. Akashi-Takamura, S. Ishibashi, K. Miyake, M. Shibuya, S. Akira, H. Aburatani, Y. Maru, The S100A8–serum amyloid A3–TLR4 paracrine cascade establishes a pre-metastatic phase, Nat. Cell Biol. 10 (2008) 1349–1355. https://doi.org/10.1038/ncb1794.

[49] E. Güç, P.S. Briquez, D. Foretay, M.A. Fankhauser, J.A. Hubbell, W.W. Kilarski, M.A. Swartz, Local induction of lymphangiogenesis with engineered fibrin-binding VEGF-C promotes wound healing by increasing immune cell trafficking and matrix remodeling, Biomaterials. 131 (2017) 160–175. https://doi.org/10.1016/j.biomaterials.2017.03.033.

[50] D. Dankort, D.P. Curley, R.A. Cartlidge, B. Nelson, A.N. Karnezis, W.E. Damsky, M.J. You, R.A. DePinho, M. McMahon, M. Bosenberg, BrafV600E cooperates with Pten loss to induce metastatic melanoma, Nat. Genet. 41 (2009) 544–552. https://doi.org/10.1038/ng.356.

CHAPTER 5

ANALYSIS OF LIPOASPIRATE FLUID AS A SOURCE OF BIOMARKERS IN LIPEDEMA

5.1. Introduction

Lipedema

Lipedema is a disease of the adipose tissue of unknown etiology that affects about 10% of women worldwide [1]. It is characterized by bilateral enlargement of the buttocks, hips, legs and often arms due to adipose tissue expansion. The lipedema adipose tissue is highly resistant to exercise and diet, and patients suffer from pain, reduced mobility, hematoma, edema and psychosocial distress. Lipedema evolves in 3 stages: Stage 1 is characterized by normal skin over pearl-sized nodules in a hypertrophic fat layer, stage 2 is characterized by skin indentations and up to apple-size nodules in the hypertrophic fat layer, and stage 3 is characterized by large extrusions of adipose tissue causing limb deformations [2]. Despite its high incidence, lipedema is understudied, and reliable and consistent diagnostic criteria have not been established yet. As a result, lipedema is often misdiagnosed as lifestyle-induced obesity or lymphedema [3]. There is therefore a clear unmet medical need in differentiating the adipose tissue in lipedema and diet-induced obese patients.

The adipose microenvironment

The adipose tissue is the largest endocrine organ and has the main function of storing and releasing energy in the form of lipids. Fatty acids are metabolized to triglycerides in response to caloric intake, which are hydrolyzed back into fatty acids and transported into the blood stream to be used by tissues of the body [4]. The adipose tissue secretes numerous types of factors that participate in intercellular communication within the tissue and at distant sites and play roles in the maintenance of glucose, lipid, energy and immune homeostasis. When the adipose tissue expands in metabolic disorders, its microenvironment is altered and is often associated with hypoxia, vascular dysfunction and chronic inflammation [5].

A variety of secreted factors play roles in adipose tissue homeostasis and pathology. Adipose tissue-secreted cytokines, termed adipokines, play crucial roles. Abundant adipokines include adiponectin and leptin which have critical functions in the maintenance of adipose tissue homeostasis [6,7]. Additionally, recent studies have suggested that extracellular vesicles (EVs) can be secreted by adipocytes and cells of the adipose microenvironment and play crucial roles in intercellular communication within the adipose tissue and at distance [5,8,9]. In fact, it appears that the majority of EV-derived microRNAs found in the blood are derived from adipose tissues, and that adipose-derived EVs have a broad influence on tissue and whole-body metabolism [10]. In obesity, adipose tissue-derived EVs can drive disease through various mechanisms such as modulation of glucose metabolism [11], macrophage polarization [12,13], and modulation of dietary lipid uptake [14].

Microenvironmental cues in lipedema

While the intricacies of the adipose tissue between lipedema and diet-induced obese patients are not fully elucidated, an emerging body of work has emerged over the past few years. Notably, the lipedema adipose tissue is characterized by hypertrophic adipocytes, macrophage infiltration, dilation of subdermal blood and lymphatic vessels and tissue fibrosis [15,16]. Although the lymphatic vasculature is believed to be altered in lipedema, the mechanisms of lymphatic dysfunction and its roles in disease progression remain unclear [15,17,18]. Interestingly, the level of VEGFC is increased in the plasma of lipedema patients compared to control, while VEGF and VEGF-D levels are unchanged [16]. Recent work has investigated functional differences in adipose-derived stem cells (ASCs) from lipedema compared to healthy patients. For example, lipedema ASCs were shown to increase

expression of leptin and of adipogenic genes Adiponectin, Lipoprotein lipase, Peroxisome proliferator-activated receptor gamma and Glucose transporter type 4 [2,19]. Additionally, *in vitro*-differentiated adipocytes from lipedema ASCs appear to produce increased levels of EV-associated miRNAs miR–16-5p, miR-29a-3p, miR-24-3p, miR-454-p, miR–144-5p, miR-130a-3p and let-7c-5p compared to healthy, body mass index (BMI)-matched control ASCs [3].

In addition to participating in disease progression, secreted factors of the lipedema adipose microenvironment may be found in the blood and serve as disease biomarkers. Blood-based liquid biopsies are an attractive source of disease biomarkers as they are easily accessible and enable repeated measurement over time [20]. However, one limitation is that pathological tissue-derived factors are highly diluted and may be challenging to identify among healthy-tissue derived factors. The emergence of high throughput sequencing and analysis partially overcame that issue, but not all pathologies benefitted from such technological advances.

In this chapter, we analyzed infranatant as a rich source of adipose microenvironment factors to delineate its characteristics between lipedema and diet-induced obese patients, with the goal of ultimately identifying systemically available yet lipedema-specific biomarkers. For this, we analyzed tumescent fluid from liposuction, named infranatant, as a source of interstitial fluid, solutes and EVs of the adipose microenvironment. Infranatant contains the solution injected into the adipose tissue for the liposuction the procedure (saline supplemented with local anesthetic and epinephrine), as well as interstitial fluid and solutes from the suctioned tissue. As such, we hypothesized that it would be rich in adipose tissue-derived factors. Additionally, such factors in interstitial fluid can potentially be transported

by lymphatic vessels into the systemic circulation where they could be measured as biomarkers.

5.2. Materials and methods

Participants

20 lipedema patients and 10 non-lipedema subjects participated in this study. All participants provided informed consent before undergoing an elective liposuction procedure. The study was conducted in accordance with the Declaration of Helsinki and the protocols were approved by the Human Research and Protection Program at the University of Arizona (Institutional Review Board protocol 1602399502) and the University of Chicago (Institutional Review Board protocol IRB18-0304).

Lipoaspirate processing

Lipoaspirates were obtained from thigh and/or abdomen of lipedema and control participants. Lipoaspirates were centrifuged for 10 min at 250 x g, and the infranatant portion was separated and centrifuged further 10 min at 500 x g to remove cells. Then, cOmplete™ Protease Inhibitor Cocktail (Roche) was added according to manufacturer's instructions, and infranatants were stored overnight at 4°C. Infranatant was cleared further by 30 min centrifugation at 2,000 x g, and 45 min centrifugation at 12,000 x g.

Adipokine analysis

Protein concentration was determined by BCA assay. Adipokine levels were determined using a LEGENDplex Human Adipokine assay (BioLegend).

Nanoparticle tracking analysis (NTA)

NTA measurements were performed with a NanoSight NS300 (Malvern Instruments Ltd, Malvern, UK), equipped with a Low Volume Flow Cell Gasket and a 488 nm Blue Laser Module. The samples were injected manually with 1 ml tuberculin syringes (Excel) until the solution reached the tip of the nozzle, and then infused at constant flow rate using a syringe pump. The samples were measured for 60 s with manual shutter and gain adjustments. Three measurements per sample were performed. The software used for capturing and analyzing the data was the NTA 3.2 Dev Build 3.2.16.

EV purification

EVs were purified from infranatant by ultracentrifugation and size-exclusion separation. Cleared infranatant was centrifuged for 90 min at 110,000 x g, and EV-enriched pellets were resuspended in PBS. EVs were separated from proteins and particles smaller than 70 nm using qEV size-exclusion columns (Izon). Then, the sample was applied to a 0.22 μm filter. Finally, the preparation was centrifuged at 110,000 x g for 90 min. Pellets were resuspended in 200 μl PBS. EV concentration was determined by NTA and protein contents were quantified by BCA assay (Thermo).

Western blot

EVs or whole infranatant samples were mixed with Laemmli SDS sample buffer (Alfa Aesar), incubated 10 min at 95°C, and cooled to 4°C. Electrophoresis was performed on Mini-PROTEAN TGX Gels (Bio-Rad). Proteins were transferred to a polyvinylide difluoride membrane (Bio-Rad). After overnight blocking at 4°C in Tris-buffered saline (TBS) 5% milk, primary antibodies in TBS 1–5% milk were applied for 1 h at room temperature, and secondary, HRP-conjugated, antibodies were applied in TBS 1–5% milk for 1 h at RT. The

following antibodies were used: anti-TSG101 (1:1,000; T5701; Sigma-Aldrich), anti-ApoA1 (1:500; 11A-G2B; Academy Bio-Med), anti-ApoB (1:500; sc-13538; Santa Cruz).

TEM

Grids (continuous carbon on 200-mesh copper grids - EMS CF200-CU) were first glow discharged for 30 seconds. 3.5 µl of EV sample was applied to the grid for 1 minute. The excess sample was blotted off. The grids were stained with 2 washes and then 45 seconds of 0.75% uranyl formate (EMS 22450). Excess stain was blotted off at each step. Grids were imaged on a Technai G2 F30 (FEI) electron microscope operating at 300kV.

Shotgun proteomics

5 µg purified EVs were used for trypsin digestion. Samples were denatured by heating at 65°C and reduced with 5mM dithiothreitol (DTT) for 1 h, alkylated with 15 mM iodoacetamide for 30 min at room temperature in the dark, and excess iodoacetamide was quenched with an additional 5 mM DTT. Samples were digested with trypsin (Promega, Madison, WI) at 1:20 w/w ratio overnight at 37°C with mixing. After digestion, SDC was precipitated by addition of 1 % trifluoroacetic acid and insoluble material was removed by centrifugation at 14,000 x g for 10 min. Samples were then desalted by solid phase extraction using Oasis HLB 96-well µElution Plate, dried down, stored at -80°C, and reconstituted with 0.1 % formic acid in 5 % acetonitrile to a peptide concentration of 0.1 µg/µL for LC-MS analysis.

LC/MS analyses

Digested peptides were injected onto a trap column (40 x 0.1 mm, Reprosil C18, 5 µm, Dr.Maisch, Germany), desalted for 5 min at a flow of 4 µL/min, and separated on a pulled tip analytical column (700 x 0.075 mm, Reprosil C18, 5 µm, Dr.Maisch, Germany) with a 3

segment linear gradient of acetonitrile, 0.1 % FA (B) in water, 0.1 % FA (A) as follows: 0-2 min 1-5 % B, 2-60 min 5-25 % B, 60-70 min 25-35 % B followed by column wash at 80 % B and re-equilibration at a flow rate 0.4 µL/min (Waters NanoACQUITY UPLC). Tandem MS/MS spectra were acquired on Orbitrap Fusion Lumos (Thermo Scientific) operated in data-dependent mode on charge states 2-4 with 2s cycle time, dynamic exclusion of 30s, HCD fragmentation (NCE 30%) and MS/MS acquisition in the Orbitrap. MS spectra were acquired at a resolution 120,000 and MS/MS spectra (precursor selection window 1.6 Da) at a resolution of 30,000 (for PMN media) or 15,000 (in-gel digests, recombinant peptides). Peptides and proteins were identified using the Comet search engine33 with PeptideProphet and ProteinProphet validation. Search criteria included a 20 ppm tolerance window for precursors and products, fixed Cys alkylation, and variable Met oxidation.

Statistical analysis

Data were processed using Microsoft Excel v.16.0. Data were represented and statistics were computed using Prism v.8 (GraphPad). Numerical data are shown as mean ± SEM unless otherwise stated. Asterisks show groups statistically different and represent p values of specific statistical tests described in figure legends.

5.3. Results

Patient demographic

We processed liposuction samples from thigh and/or abdomen of lipedema patients and BMI-matched non-lipedema control patients (**Figure 5.1** A-C). All patients enrolled in the study were females. Of note, within lipedema patients, age slightly increased and BMI significantly increased with disease stage (**Figure 5.1** D-E).

A

Characteristic	Control	Lipedema			
Stage	0	1	2	3	1/2/3
Number	10	8	7	5	20
Sex	Female	Female	Female	Female	Female
Age (years)	42 ± 15	37 ± 8	41 ± 5	54 ± 9	43 ± 10
BMI (kg/m²)	34 ± 7	26 ± 3	32 ± 3	47 ± 5	33 ± 9

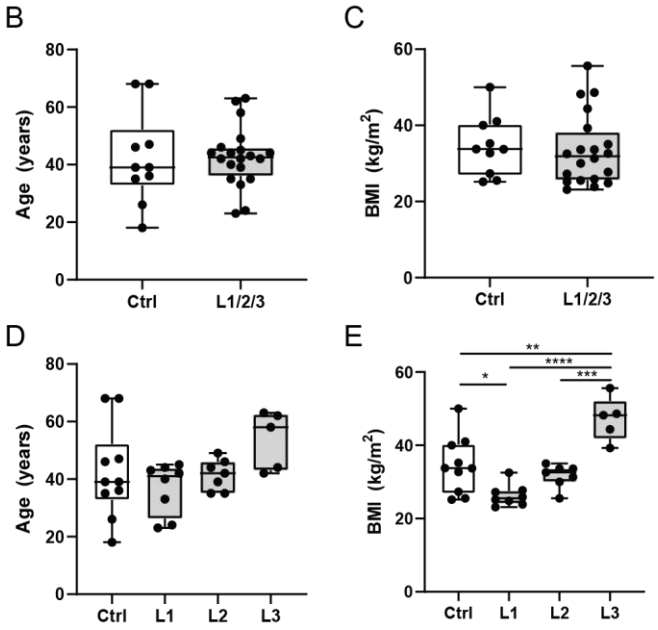

Figure 5.1. Patient cohort demographic. (A) Patient characteristics, with lipedema disease stage, number of patients, sex, age and body mass index (BMI) as mean ± standard derivation. (B) Age and (C) BMI in control vs. lipedema patients all stages combined (L1/2/3). (D) Age and (E) BMI per disease stage in control (Ctrl), lipedema stage 1 (L1), 2 (L2) and 3 (L3) patients.

Adipokines levels are different in lipedema infranatant

Immediately following liposuction procedures, lipoaspirates were centrifuged at low speed and infranatant fluid was separated from adipose tissue, lipid and cell fractions. Infranatant was then stored at 4°C with protease inhibitors and cleared further from large debris by centrifugation. We first measured total protein levels and found all infranatant samples to contain on average 680.6 ± 494.6 µg/ml protein (all groups combined), without significant differences in concentration between lipedema and control infranatant samples (**Figure 5.2**

A). Next, we measured a panel of adipokines and computed their relative protein abundance (**Figure 5.2** B). Some adipokines such as Adiponectin, CXCL10, MCP-1 and IFNγ were mostly unchanged in lipedema compared to control infranatant, both in abdomen and thigh. In contrast, homeostasis-associated adipokine Adipsin levels were significantly lower in lipedema infranatant, while levels of pro-inflammatory cytokines IL-1β and TNFα were significantly higher in lipedema than in controls. Leptin levels trended to be higher in thigh lipedema infranatant, and IL-10 levels were higher as well.

Infranatant contains high amounts of extracellular vesicles

Next, we measured nanoparticle levels in infranatant by nanoparticle tracking analysis (NTA). Infranatant samples contained a high concentration of nanoparticles in the size range of 70-500 nm (**Figure 5.3** A). The size mode of particle population was on average 106.8 ± 17.56 nm (all groups combined), and no significant differences in size mode was observed between control and lipedema infranatant from abdomen nor thigh (**Figure 5.3** B). Particle concentration trended to be increased in lipedema infranatant, particularly from thigh (**Figure 5.3** C). However, the ratio of particles to protein was unchanged in lipedema (**Figure 5.3** D).

Nanoparticles measured in infranatant may include EVs as well as lipoprotein particles, such as HDL and LDL. HDL particles have a density similar to EVs, while LDL have a lower density but size similar to EVs [21]. Therefore, to selectively purify EVs, we optimized a protocol combining density-based enrichment of EVs, namely ultracentrifugation, with size-based enrichment of EVs, namely by size-exclusion chromatography and filtration (**Figure 5.4**).

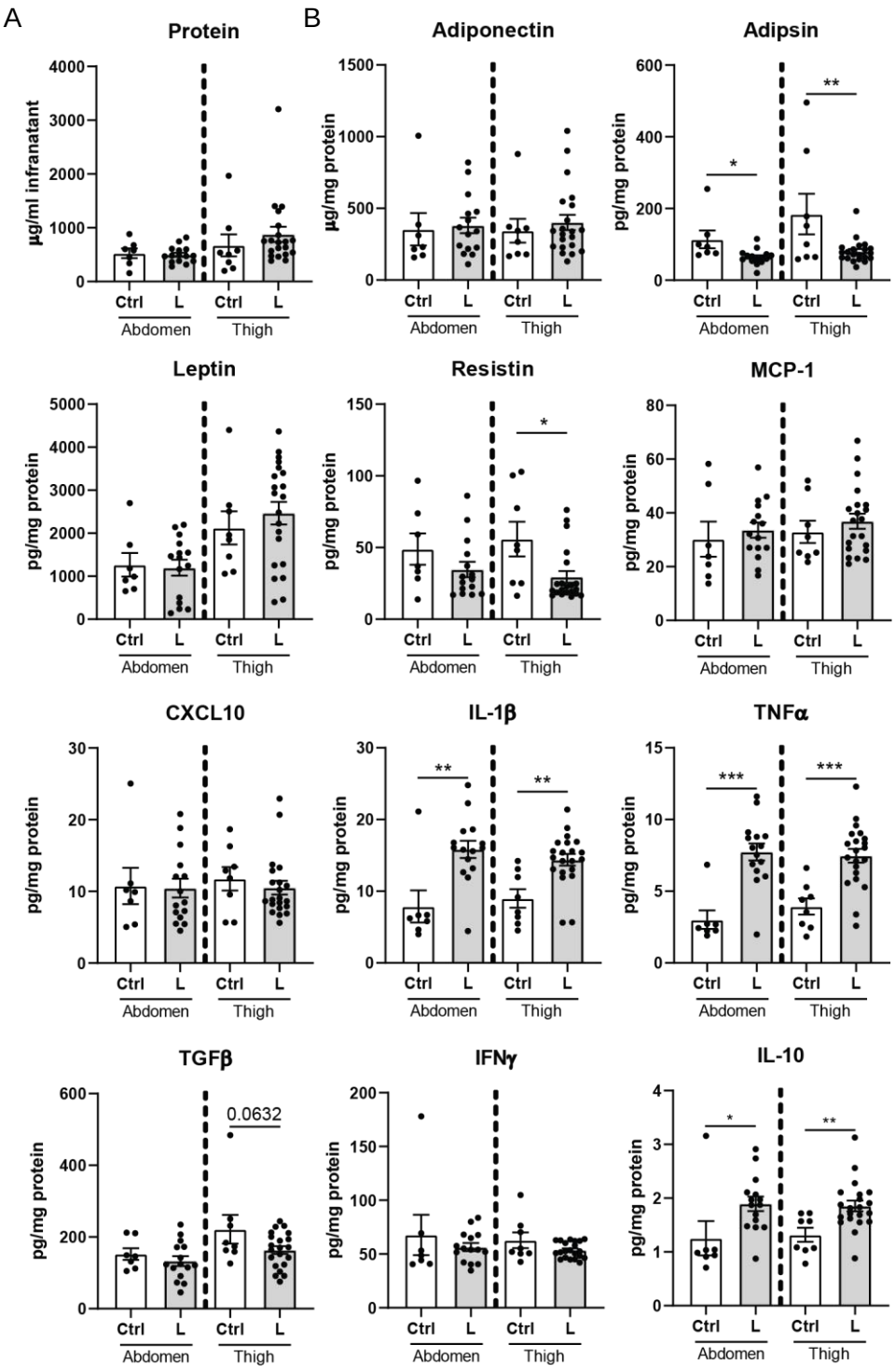

Figure 5.2. Adipokine levels differ between lipedema and control patient infranatant. (A) Total protein concentration in infranatant of control (Ctrl) and lipedema (L) patients. (B) Fraction of selected adipokines per total protein in infranatant.

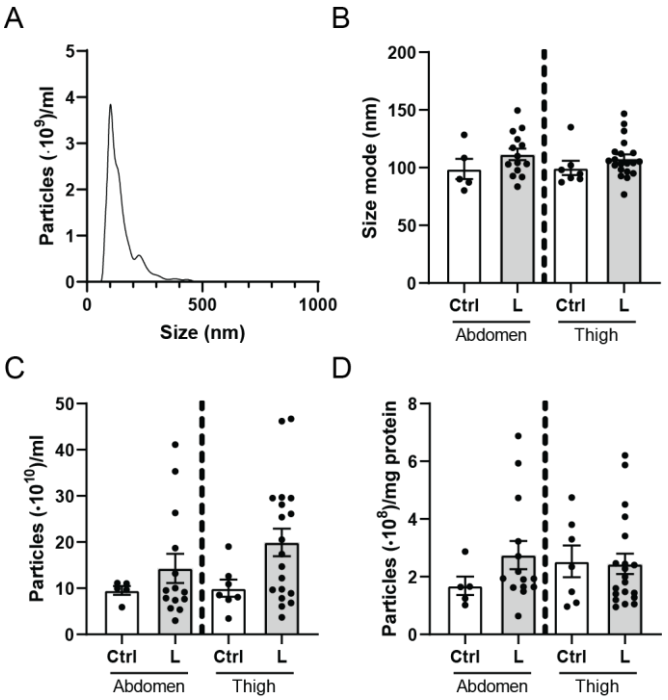

Figure 5.3. Liposuction infranatant contains nanoparticles. (A-D) Nanoparticle tracking analysis of infranatant from control (Ctrl) and lipedema (L) patient thigh and abdomen. (A) Representative measurement of particles in infranatant. (B) Size mode of infranatant nanoparticles. (C) Particle concentration in infranatant. (D) Particles per total protein content in infranatant.

We obtained particles in the size range (**Figure 5.5** A) and morphology (**Figure 5.5** B) of EVs. The protein content of EVs was similar between group, with trends of higher protein to particle contents in thigh lipedema EV samples (**Figure 5.5** C). Importantly, this method enabled selective enrichment of EVs, as shown with EV marker TSG101, and dilution of HDL component Apolipoprotein A1 (ApoA1) and LDL component ApoB (**Figure 5.5** D).

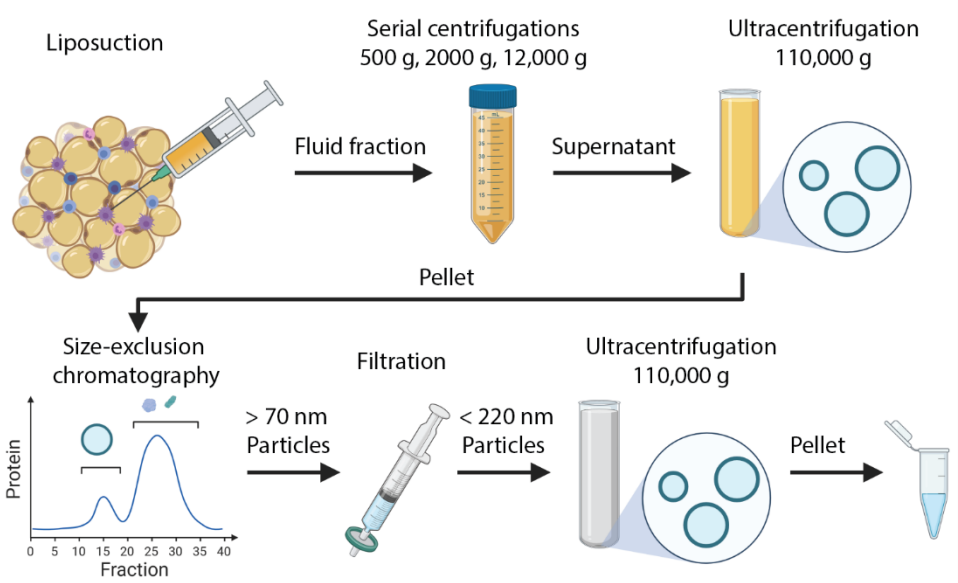

Figure 5.4. EV purification workflow. Infranatant is cleared from dead cell and debris by centrifugation, after which EVs are enriched by ultracentrifugation, size-exclusion chromatography to select particles larger than 70 nm, and filtration to select particles smaller than 220 nm.

Next, we performed a high dimensional protein analysis of purified EVs by mass spectrometry. Over 2000 proteins were detected with high confidence in EV samples, including proteins typical of exosomes such as Tetraspanin CD81, Integrin alpha 1 (ITA1), Alix and Flotinin-1 (**Figure 5.6** A). Additionally, markers of cells and EVs of the adipose microenvironment such as endothelial cell protein PECAM-1, adipocyte proteins Adiponectin and Perilipin-1, and macrophage CD14 and MRC-1 were detected (**Figure 5.5** B). Importantly, proteins typically contained in exosomes and from the adipose tissues were found at equivalent levels between lipedema and control patients.

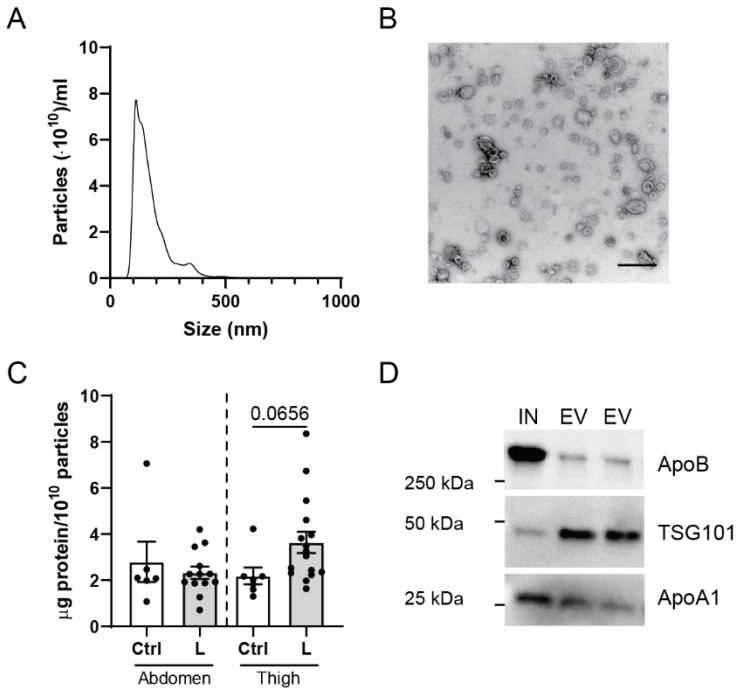

Figure 5.5. Enrichment of EVs after purification procedure from infranatants. (A) Representative measurement of particles in EV preparation. (B) Transmission electron microcopy of EV preparation. Scale bar: 500 nm. (C) Protein amount per particle count in EV preparations. (D) Western blot analysis of EV marker TSG101 and lipoprotein contaminants ApoA1 and ApoB in whole infrantant (IN) and purified EV samples (EV). 10 µg protein loaded per lane.

Selected proteins are enriched in lipedema EVs compared to control

To identify proteins in significantly different abundance in lipedema EVs compared to control, we used a statistical method previously reported by Dr. Lev Becker and colleagues combining the use of *t*-test with G-test [22]. We found 10 proteins significantly upregulated and 6 proteins significantly downregulated in lipedema thigh EVs compared to control thigh EVs (**Figure 5.7** A-B). Upregulated proteins included Plectin, Fas cell surface death receptor and Transglutaminase-2. Downregulated proteins included Aminopeptidase N and Protein disulfide isomerase family A member 4 (**Figure 5.7** C). Principal component analysis (PCA)

of the 16 differentially regulated proteins tended to cluster lipedema and control patients separately (**Figure 5.7** D).

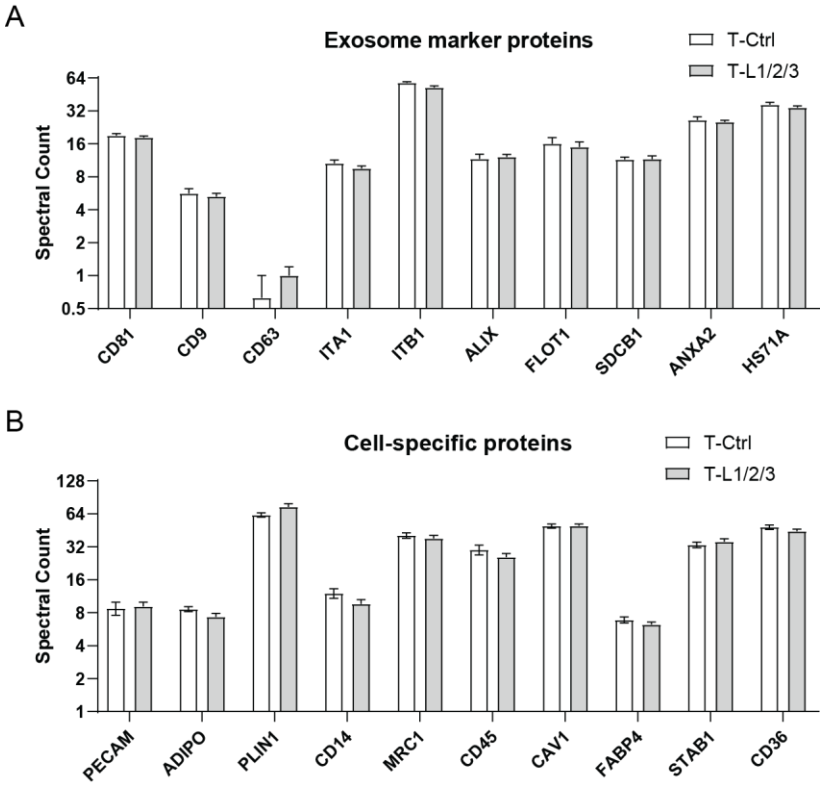

Figure 5.6. Infranatant EVs carry proteins typical of exosomes and EVs derived from cells of the adipose tissue. Spectral counts of proteins identified by mass spectrometry in thigh EVs of control (T-Ctrl) and lipedema (T-L1/2/3) patients. (A) Typical exosome-associated proteins: CD81, CD9, CD63, ITA1, ITB1, ALIX, FLOT1, SDCB1, ANXA2, HS71A. (B) Proteins specific to cells present in the adipose microenvironment: PECAM, ADIPO, PLIN1, CD14, MRC1, CD45, CAV1, FABP4, STAB1, CD36.

A

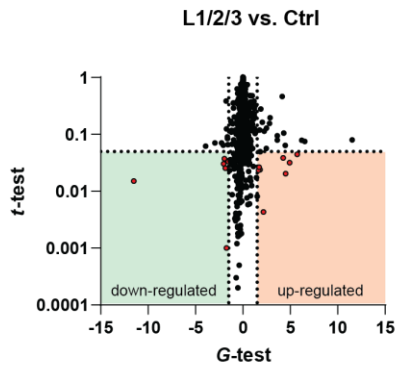

B

Protein	Control	Lipedema	*G*-test	*t*-test
Plectin (PLEC)	2.1	10.2	5.721	0.044
Fas cell surface death receptor (FAS)	46.0	69.8	4.918	0.032
Alpha fibrinogen (FIBA)	16.0	30.3	4.508	0.020
Fibrinogen beta chain (FIBB)	10.9	22.7	4.235	0.038
NIMA related kinase 9 (NEK9)	0.0	1.6	2.156	0.004
Dynactin subunit 1 (DCTN1)	4.5	9.5	1.826	0.050
Tubulin gamma-1 chain (TBG1)	0.5	2.8	1.803	0.024
Transglutaminase 2 (TGM2)	1.0	3.8	1.721	0.026
Fibrinogen gamma chain (FIBG)	9.3	15.6	1.646	0.023
Intersectin 1 (ITSN1)	0.1	1.6	1.508	0.008
HLA class I histocompatibility antigen, A-68 alpha chain (1A68)	30.0	21.1	-1.554	0.033
Aminopeptidase N (AMPN)	49.3	37.1	-1.729	0.001
Protein disulfide isomerase family A member 4(PDIA4)	50.1	37.4	-1.860	0.026
Reticulocalbin-1 (RCN1)	23.8	15.1	-1.965	0.037
Endoplasmic reticulum aminopeptidase 1 (ERAP1)	32.3	21.8	-2.043	0.030
Telomere elongation protein EST1 (EST1)	222.4	156.5	-11.512	0.015

C

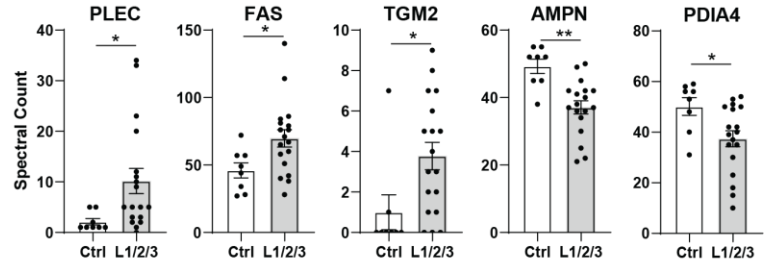

D

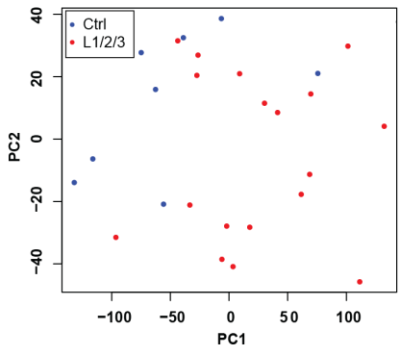

Figure 5.7. Selected proteins are different in abundance in lipedema EVs. (A-D) Thigh extracellular vesicle (EV) proteins differing in relative abundance between lipedema (L1,2,3) and control (Ctrl) patients identified with a significant difference in the total number of peptides by both t-test ($p < 0.05$) and G-test (G-test >1.5). (A) G-test and t-test values of all proteins detected in EVs. Proteins significantly up- or down-regulated in L1,2,3 vs. Ctrl EVs are shown in red. (B) Proteins significantly differing in abundance between L1,2,3 and Ctrl, average abundance in Ctrl and L1,2,3 EVs, G-test and t-test values. (C) Spectral counts of selected proteins differing in abundance between L1,2,3 and Ctrl. (D) Principal component analysis of Thigh EVs based on proteins listed in (B).

Lipedema affects mostly buttocks, hips and legs while abdomen is not as affected by the disease. However, we found that abdomen had selected adipokines that were upregulated in lipedema abdomen as well, suggesting that microenvironment factors in abdomen – although to a different extent from thigh – may be differentially regulated, too. In order to determine whether differences were observed between lipedema and control abdomen EVs,

and/or between thigh and abdomen lipedema EVs, and whether such proteins were also differentially regulated in lipedema versus control thighs EVs, we selected all proteins that were found at significantly different levels in 7 selected group comparisons in t-test and G-tests. We then compared the G-test values of those genes across those 7 group comparisons, to determine whether proteins that were up- or downregulated in lipedema thighs compared to lipedema controls were also differentially regulated in the abdomen (**Figure 5.8** A). A few proteins showed similar modulation pattern in thigh and abdomen lipedema EVs compared to control, or in thigh vs. abdomen lipedema. However, the majority of proteins identified in lipedema thigh compared to control thigh EVs were not found to be dysregulated in other group comparisons. Lastly, we performed a principal component analysis on the 75 proteins identified in **Figure 5.8** A , and found that both thigh and abdomen lipdema EVs tended to associate within a cluster distinct from control EVs (**Figure 5.8** B). Together, this data suggests that both thigh and abdomen EVs are different in lipedema, but that the two compartments produce EVs enriched in different cargos.

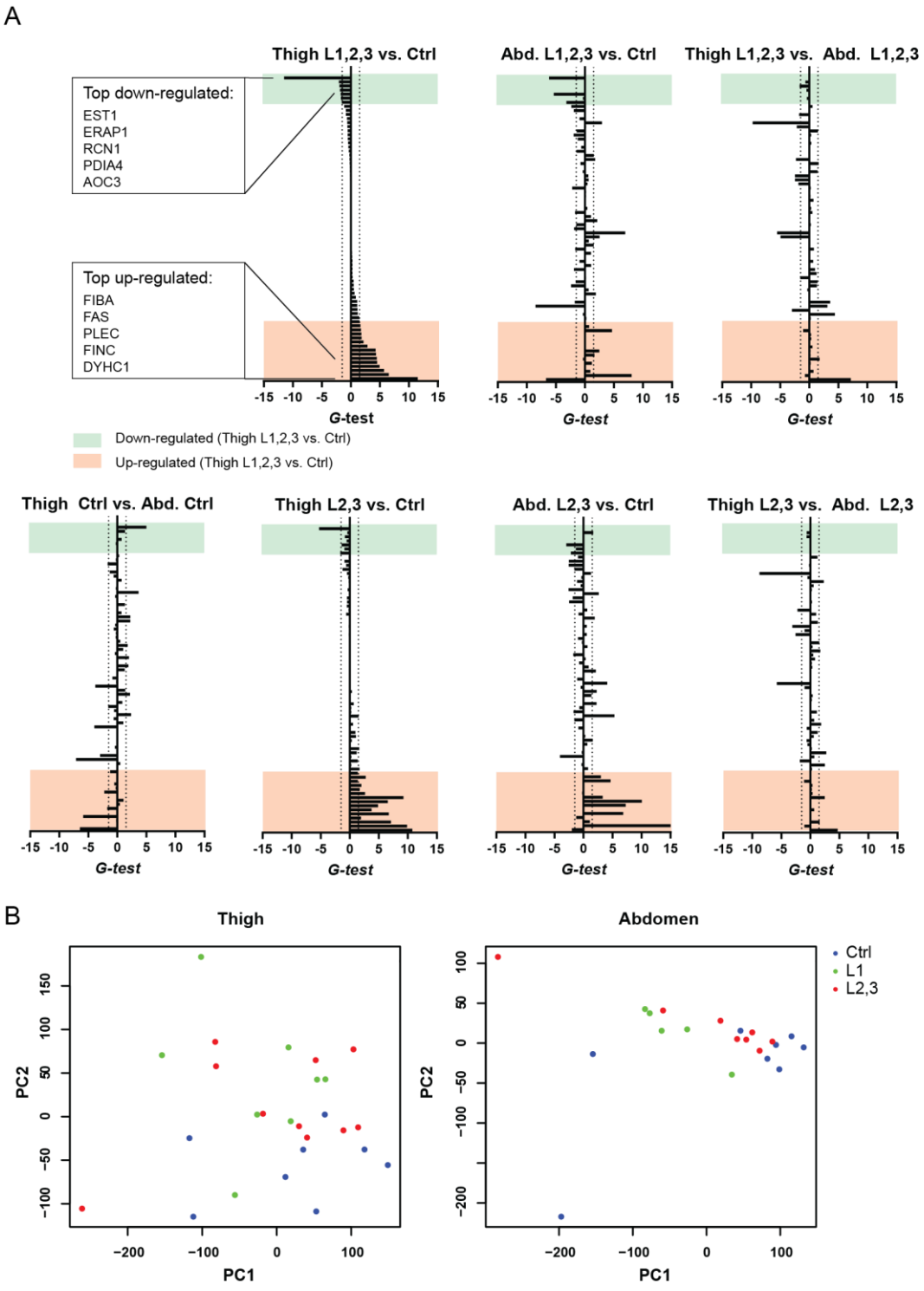

Figure 5.8. Protein enrichment profiles in control and lipedema EVs. (A) G-test values of proteins that were significantly up- or downregulated based on G-test and t-test in at least one of the 7 comparisons: Thigh Lipedema stage (L) 1,2,3 vs. Thigh Control (Ctrl); Abdomen (Abd.) L1,2,3 vs. Abd. Ctrl; Thigh L1,2,3 vs. Abd. L1,2,3; Thigh Ctrl vs. Abd. Ctrl; Thigh L2,3 vs. Thigh Ctrl; Abd. L2,3 vs. Abd. Ctrl; Thigh L2,3 vs. Abd. L2,3.

Figure 5.8, continued. Proteins in all graphs are in the same order and sorted based on G-test values of Thigh L1,2,3 vs. Thigh Control. (B) Principal component analysis (PCA) of 75 proteins identified in (A).

5.4. Discussion

We found that infranatant contains high concentrations of proteins including adipokines and extracellular vesicles. Because the infranatant is composed of interstitial fluid and solutes, as opposed to cellular or extracellular matrix compartments, the identified factors are likely transported to the lymphatic system via interstitial flow and delivered into the blood. As such, infranatant may enable the identification of tissue-derived factors which could then be found, albeit likely at lower levels, in the blood. Additionally, as liposuction represents a widely indicated surgical procedure to treat both diet-induced obese and lipedema patients, infranatant could be used as an easily accessible source of adipose tissue-derived EVs. This type of analysis, while fitting into a patient's treatment journey, may be relevant to identify microenvironmental cues involved in intercellular communication and potential biomarkers of metabolic disorders.

The underlying cause of lipedema and mechanisms of disease progression are poorly understood. The microenvironmental cues that we have identified in this work including adipokines and EV-associated proteins may pinpoint to inflammatory and metabolic pathways which could be involved. For example, pro-inflammatory cytokines TNFα and IL-1β were highly upregulated in lipedema compared to control patients, while adipokines important for maintenance of homeostasis Adipsin was downregulated. Additionally, selected proteins upregulated in lipedema EVs included extracellular matrix proteins as well

as proteins involved in cellular dynamics. Such pathways could be investigated in cells of the adipose microenvironment to determine their possible functions in driving lipedema.

This study has several limitations. First, the low number of patients does not allow powerful statistical analyses. Second, a new workflow of EV purification has been used. While we have validated it using various quality controls as recommended by the society for extracellular vesicles [23], it is possible that other techniques of EV purification may not yield the same results. Finally, factors which have been identified in this study cohort have not been validated in another independent cohort, which is a common practice in the process of identification of disease biomarkers.

To date, diagnosis of lipedema has remained challenging, and as such there is a crucial need to identify disease biomarkers that would accurately define disease status. We identified a number of adipose tissue-derived factors that were differentially regulated in lipedema tissue infranatant compared to control. Therefore, future studies may investigate the presence and possible differential abundance of those factors in the blood, and their potential use as liquid biopsy biomarker. Finally, this study highlights the relevance of the use of infranatant for future studies on the adipose tissue microenvironment.

5.5. Acknowledgements

I would like to thank Dr. Karen Herbst, Dr. Sara Al-Ghadban, Marisol Allen and Dr. Karol Gutkowski for providing liposuction samples. I am thankful to Dr. Lev Becker and Dr. Tomas Vaisar for the proteomic analysis and helpful discussions. I would like to thank Rachel Weathered for technical assistance. I would like to thank the Lipedema Foundation for funding this research.

5.6. References

[1] S. Al-Ghadban, K. L. Herbst, B. A. Bunnell, Lipedema: A Painful Adipose Tissue Disorder, Adipose Tissue - An Updat. (2019). https://doi.org/10.5772/intechopen.88632.

[2] S. Al-Ghadban, Z.T. Diaz, H.J. Singer, K.B. Mert, B.A. Bunnell, Increase in Leptin and PPAR-γ Gene Expression in Lipedema Adipocytes Differentiated in vitro from Adipose-Derived Stem Cells, Cells. 9 (2020) 430. https://doi.org/10.3390/cells9020430.

[3] E. Priglinger, K. Strohmeier, M. Weigl, C. Lindner, D. Auer, M. Gimona, M. Barsch, J. Jacak, H. Redl, J. Grillari, M. Sandhofer, M. Hackl, S. Wolbank, SVF-derived extracellular vesicles carry characteristic miRNAs in lipedema, Sci. Rep. 10 (2020) 1–12. https://doi.org/10.1038/s41598-020-64215-w.

[4] P. Arner, A. Kulyté, MicroRNA regulatory networks in human adipose tissue and obesity, Nat. Rev. Endocrinol. 11 (2015) 276–288. https://doi.org/10.1038/nrendo.2015.25.

[5] S. Kita, N. Maeda, I. Shimomura, Interorgan communication by exosomes, adipose tissue, and adiponectin in metabolic syndrome, J. Clin. Invest. 129 (2019) 4041–4049. https://doi.org/10.1172/JCI129193.

[6] J.H. Stern, J.M. Rutkowski, P.E. Scherer, Review Adiponectin , Leptin , and Fatty Acids in the Maintenance of Metabolic Homeostasis through Adipose Tissue Crosstalk, Cell Metab. 23 (2016) 770–784. https://doi.org/10.1016/j.cmet.2016.04.011.

[7] C. Crewe, Y.A. An, P.E. Scherer, The ominous triad of adipose tissue dysfunction: Inflammation, fibrosis, and impaired angiogenesis, J. Clin. Invest. 127 (2017) 74–82. https://doi.org/10.1172/JCI88883.

[8] C. Crewe, N. Joffin, J.M. Rutkowski, D.A. Towler, R. Gordillo, P.E. Scherer, C. Crewe, N. Joffin, J.M. Rutkowski, M. Kim, F. Zhang, D.A. Towler, R. Gordillo, An Endothelial-to-Adipocyte Extracellular Vesicle Article An Endothelial-to-Adipocyte Extracellular, Cell. (2018) 1–14. https://doi.org/10.1016/j.cell.2018.09.005.

[9] I. Huang-doran, C. Zhang, A. Vidal-puig, Extracellular Vesicles : Novel Mediators of Cell Communication In Metabolic Disease, Trends Endocrinol. Metab. 28 (2017) 3–18. https://doi.org/10.1016/j.tem.2016.10.003.

[10] T. Thomou, M.A. Mori, J.M. Dreyfuss, M. Konishi, M. Sakaguchi, C. Wolfrum, T.N. Rao, J.N. Winnay, R. Garcia-martin, S.K. Grinspoon, P. Gorden, C.R. Kahn, Adipose-derived circulating miRNAs regulate gene expression in other tissues, Nature. 542 (2017) 450–455. https://doi.org/10.1038/nature21365.

[11] C. Castaño, S. Kalko, A. Novials, M. Párrizas, Obesity-associated exosomal miRNAs modulate glucose and lipid metabolism in mice, Proc. Natl. Acad. Sci. U. S. A. 115 (2018) 12158–12163. https://doi.org/10.1073/pnas.1808855115.

[12] Y. Pan, X. Hui, R.L. Chong Hoo, D. Ye, C.Y. Cheung Chan, T. Feng, Y. Wang, K.S. Ling Lam,

A. Xu, Adipocyte-secreted exosomal microRNA-34a inhibits M2 macrophage polarization to promote obesity-induced adipose inflammation, J. Clin. Invest. 129 (2019) 834–849. https://doi.org/10.1172/JCI123069.

[13] M.E.G. Kranendonk, F.L.J.J. Visseren, B.W.M. Van Balkom, E.N.M. Nolte-'T Hoen, J.A. Van Herwaarden, W. De Jager, H.S. Schipper, A.B. Brenkman, M.C. Verhaar, M.H.M. Wauben, E. Kalkhoven, E.G. Kranendonk, F.L.J.J. Visseren, B.W.M. Van Balkom, E.N.M.N.- Hoen, J.A. Van Herwaarden, W. De Jager, H.S. Schipper, A.B. Brenkman, M.C. Verhaar, Human Adipocyte Extracellular Vesicles in Reciprocal Signaling Between Adipocytes and Macrophages, Obesity. 22 (2014) 1296–1308. https://doi.org/10.1002/oby.20679.

[14] A. Khalifeh-Soltani, W. McKleroy, S. Sakuma, Y.Y. Cheung, K. Tharp, Y. Qiu, S.M. Turner, A. Chawla, A. Stahl, K. Atabai, Mfge8 promotes obesity by mediating the uptake of dietary fats and serum fatty acids, Nat. Med. 20 (2014) 175–183. https://doi.org/10.1038/nm.3450.

[15] S. AL-Ghadban, W. Cromer, M. Allen, C. Ussery, M. Badowski, D. Harris, K.L. Herbst, Dilated Blood and Lymphatic Microvessels, Angiogenesis, Increased Macrophages, and Adipocyte Hypertrophy in Lipedema Thigh Skin and Fat Tissue, J. Obes. (2019). https://doi.org/10.1155/2019/8747461.

[16] G. Felmerer, A. Stylianaki, M. Hollmén, P. Ströbel, A. Stepniewski, A. Wang, F.S. Frueh, B.S. Kim, P. Giovanoli, N. Lindenblatt, E. Gousopoulos, Increased levels of VEGF-C and macrophage infiltration in lipedema patients without changes in lymphatic vascular morphology, Sci. Rep. 10 (2020) 10947. https://doi.org/10.1038/s41598-020-67987-3.

[17] S. Bilancini, M. Lucchi, S. Tucci, P. Eleuteri, Functional lymphatic alterations in patients suffering from lipedema., Angiology. 46 (1995) 333–9. https://doi.org/10.1177/000331979504600408.

[18] N. Escobedo, G. Oliver, The Lymphatic Vasculature: Its Role in Adipose Metabolism and Obesity, Cell Metab. 26 (2017) 598–609. https://doi.org/10.1016/j.cmet.2017.07.020.

[19] S. Al-Ghadban, I.A. Pursell, Z.T. Diaz, K.L. Herbst, B.A. Bunnell, 3D Spheroids Derived from Human Lipedema ASCs Demonstrated Similar Adipogenic Differentiation Potential and ECM Remodeling to Non-Lipedema ASCs In Vitro, Int. J. Mol. Sci. 21 (2020) 8350. https://doi.org/10.3390/ijms21218350.

[20] G. Brock, E. Castellanos-Rizaldos, L. Hu, C. Coticchia, J. Skog, Liquid biopsy for cancer screening, patient stratification and monitoring, Transl. Cancer Res. 4 (2015) 280–290. https://doi.org/10.3978/j.issn.2218-676X.2015.06.05.

[21] N. Karimi, A. Cvjetkovic, S.C. Jang, R. Crescitelli, M.A. Hosseinpour Feizi, R. Nieuwland, J. Lötvall, C. Lässer, Detailed analysis of the plasma extracellular vesicle proteome after separation from lipoproteins, Cell. Mol. Life Sci. (2018) 1–14. https://doi.org/10.1007/s00018-018-2773-4.

[22] L. Becker, S.A. Gharib, A.D. Irwin, E. Wijsman, T. Vaisar, J.F. Oram, J.W. Heinecke, A Macrophage Sterol-Responsive Network Linked to Atherogenesis, Cell Metab. 11 (2010) 125–135. https://doi.org/10.1016/j.cmet.2010.01.003.

[23] C. Théry, K.W. Witwer, E. Aikawa, M.J. Alcaraz, J.D. Anderson, e t Al., Minimal information for studies of extracellular vesicles 2018 (MISEV2018): a position statement of the International Society for Extracellular Vesicles and update of the MISEV2014 guidelines, J. Extracell. Vesicles. 7 (2018). https://doi.org/10.1080/20013078.2018.1535750.

CHAPTER 6

DISCUSSION

6.1. Mechanisms governing EV transport and distribution

Although EVs have received extraordinary attention from the biomedical research community over the past decade, the physical mechanisms governing EV transport and availability for uptake by cells, both at the tissue and system level, have remained poorly understood. In this thesis, I have made inroads into defining tissue biomechanical properties that may affect such mechanisms. Specifically, I suggest that because EVs are too large to diffuse, interstitial flow plays crucial roles in the distribution of EVs upon release by cells in the interstitial space. This concept has multiple consequences on the mechanisms by which EVs may contribute to tissue homeostasis and disease development. First, prior to cellular uptake, EVs are mainly transported unidirectionally with flow within the interstitium. Consequently, the localization of cells with respect to flow directionality will impact their likelihood to receive EVs from another cell. For example, within a tissue, blood endothelial cells are less likely to receive EVs from cells of the interstitium than lymphatic endothelial cells due to flow directed toward lymphatic vessels. Second, a directional gradient of EVs is likely generated by interstitial flow around a given cell and may serve it as its own chemoattractant, a process which our laboratory has previously described as "autologous chemotaxis" [1–3]. Lastly, I have shown in this work that lymphatic vessels represent the main route of EV distribution. This is attributed to the fact that interstitial flow drives EVs towards lymphatic vessels rather than blood vessels. In addition to their physiological relevance, these findings may be useful in the design of EV-based diagnostics and therapies.

6.2. Consequences of EV transport properties for diagnostics and therapies

Liquid biopsies have received increasing interest as an easily accessible patient diagnostic and monitoring tool. As EVs encapsulate specific biomolecules from their tissue of origin, they represent an attractive source of biomarkers in liquid biopsies [4–6]. To date, blood has been the most investigated source of EV biomarkers. However, considering that EVs travel to lymphatic vessels before getting diluted in the blood, we and others have suggested that lymph or lymphatic exudate should be investigated further as a liquid biopsy enriched in tissue-specific exosomes [7–9]. In cancer patients, lymph can be collected at time of sentinel lymph node biopsy [9]. Alternatively, the extracellular fluid leaking after surgery, called lymphatic exudate, can be collected from surgical drains and is enriched in tumor-relevant factors including EVs compared to blood [7,8]. In these settings, as well as in other tumor removal surgical procedures, lymph biopsies may represent an additional valuable source of information without further medical intervention on the patient. Additionally, lymph biopsies may also be a relevant source of biomarkers not only in cancer but also in other pathologies. For example, lymph in atherosclerotic mice was shown to carry more EVs than in healthy controls [10]. In patients as well as in experimental animals, lymph can also be collected by cannulation of collecting lymphatic vessels [11,12].

Another rich source of EVs is interstitial fluid as it represents the milieu into which EVs are released from cells in a tissue. However, interstitial fluid may be challenging to collect in sufficient quantity from a given tissue biopsy. In this work, we demonstrated that liposuction materials, which can be obtained in high amounts from patients with disorders

associated with elevated body mass index such as obesity and lipedema, represent an efficient method to sample interstitial fluid for downstream analysis of solutes and EVs.

EVs present promising therapeutic targets and drug delivery vehicles. Many EV types have been suggested to provide therapeutic benefit in their native form, and approaches have been developed to engineer exosomes via direct surface conjugation or loading of biomolecules [13–15], transgene insertion in exosome-producing cells, or development of EV mimics. Detailed information on the availability and transient distribution of EVs will be crucial to optimize treatment routes, doses and timing.

6.3. Functions of the lymphatic vasculature in tumor development

Tumor-derived factors, including EVs, prime tumor-draining LNs as well other distant organs for subsequent seeding and growth of metastatic tumors cells. While the role of lymphatic vessels as routes for tumor cell trafficking has been known for decades, in this work I demonstrated that tumor lymphangiogenesis also increased the dissemination of tumor-derived factors, in particular EVs, to promote the formation of the pre-metastatic niche. This new mechanism linking tumor lymphangiogenesis with pre-metastatic niche formation further deepens our understanding of how lymphatic vessels and tumor lymphangiogenesis contribute to tumor development and supports the concept that high tumor VEGFC signaling may negatively affect patient outcomes.

It is important to underline that tumor-associated lymphatic vessels may also play beneficial roles during tumor development, most notably in the promotion of a potent antitumor adaptive immune response. Our group has shown that while tumor VEGFC signaling is associated with immune suppression [16], it is also importantly linked with

higher overall T cell infiltration in melanoma, and thus renders tumors more responsive to immunotherapy [17,18]. We and others have now developed therapeutic strategies to favor antitumor immune priming by leveraging those findings (Potin, Maillat et al., in revision, Sasso et al., in revision, [19]).

LECs in pre-metastatic niches have been reported to substantially alter their gene expression profile to support preliminary metastatic colonization, referring to the concept of "lymphovascular niche" [20]. Such changes include increased lymphatic vessel permeability to solutes and cells and expression of adhesion molecules and chemokines, all of which are susceptible to support tumor cell invasion [2,21,22]. LECs have unique immunomodulatory properties as well, as they interact with the innate and adaptive immune system through cytokines, co-stimulatory and co-inhibitory molecules and antigen presentation [23–25]. The uptake of tumor-derived EVs by LECs may play important roles in modulating these functions, particularly since some of these have been shown to be modulated by tumor-derived EVs in other cell types including blood endothelial cells [26–28].

6.4. Future directions

In this thesis, we have provided theoretical and experimental evidence of interstitial flow-driven EV transport. Many additional biophysical factors are likely to influence EV distribution. In particular, the extracellular matrix (ECM) constitutes a barrier to EV transport and might partially entrap EVs locally via physical and biochemical interactions [29]. Importantly, different tissues develop unique ECMs with distinct pore sizes, electrochemical charge and EV ligand availability. Additionally, the ECM is a feature of the microenvironment that is often critically remodeled upon disease development. In cancer,

ECM remodeling in primary tumors and in the pre-metastatic niche is thought to be a crucial driver of tumor development [30–32]. Future work may investigate the impact of the extracellular matrix on EV distribution. For this, a bottom-up approach may be used in which specific ECM components may be utilized *in vitro* to create 3-dimensional environments in which to analyze EV transport. Additionally, biodistribution experiments may be performed *in vivo* in different tissues and tumor types.

A consequence of interstitial flow-governed transport is the generation of directional gradients of EVs around a cell [3]. As EVs have been shown to have chemoattractant properties, it would be important to determine whether cells could migrate toward their own EVs. This could potentially represent a mechanism favoring tumor cell invasion. For this, a modified transwell assay previously optimized in the lab where flow is applied by means of a pressure head could be used [2], and tumor cell migration could be assessed in presence of selective EV inhibitors such as GW4869.

This work identified the lymphatic system as a crucial route of transport of EVs. We found that lymphatic endothelial cells can take up EVs into endosomal compartments as well. Knowing that LECs are able to transport solutes via transcellular routes [33], we speculate that LECs could shuttle EVs via such pathways from the tissue interstitium into the lymph. Such mechanisms are likely to play important roles due to the large size of EVs which makes paracellular transport difficult due to small size pores between intercellular junctions. The relevance of such pathways could be investigated *in vivo* using mouse models which lack crucial genes involved in transcytosis, such as lymphatic-specific Caveolin-1-deficient mice,

similarly to prior work demonstrating the ability of blood endothelial cells to transcytose solutes [34].

LECs of the lymph nodes have unique capacities to archive antigens for prolonged periods of time, which enable extended immune responses [35]. It would be interesting to speculate that LECs could use similar mechanisms to archive EVs. In order to determine this, one could use combined EV labeling approaches and confocal microscopy to assess the localization of EVs within LECs over time.

Lymphatic vessels are exposed to large amounts of EVs that they transport. As EVs are partially internalized by LECs, they likely affect their function via delivery of biomolecular cargos. EVs may remodel LEC gene expression via miRNAs and induce various signaling pathways via protein interactions. Tumor-derived EVs may induce a tumor-promoting phenotype in LECs by modulating their proliferation and their transport and immune-modulatory functions. It has been suggested that tumor-derived EVs may induce LEC proliferation and tube formation in oral squamous cell carcinoma [36], and it is thus likely that other types of tumor cells may have similar effects on LECs. Additionally, it is possibly that EVs increase lymphatic permeability. It was shown that cancer EVs can increase blood vessel junction permeability by modulating the expression of junctional proteins through miRNAs [27,28]. Additionally, tumor-derived EVs display high levels of proteases such as ADAM10 and ADAM17 which can cleave junctional proteins of endothelial cells and likely enhance permeability [37]. Increased LEC permeability may lead to enhanced transport of tumor-derived factors and may affect immune and tumor cell migration into lymphatic vessels as well. Lastly, EVs are known to induce expression of adhesion molecules,

chemokines and cytokines in target cells, many of which can be expressed by LECs [38,39]. It would thus be interesting to determine whether tumor-derived EVs could have such effects on LECs, which could further contribute to cancer progression via immune and tumor cell modulation.

6.5. Conclusion

In conclusion, this doctoral work analyzed an important yet overlooked aspect of EV biology, namely the mechanisms of EV transport to local and distant sites. We highlight the importance of interstitial flow in EV transport within the extracellular space and showed for the first time the importance of lymphatic vessels in the transport of EVs to distant sites. We suggest that these mechanisms have important consequences in cancer metastasis, where the transport of EVs from primary tumors to distant organs plays crucial roles in the establishment of pre-metastatic niches.

6.6. References

[1] M.E. Fleury, K.C. Boardman, M.A. Swartz, Autologous morphogen gradients by subtle interstitial flow and matrix interactions., Biophys. J. 91 (2006) 113–21. https://doi.org/10.1529/biophysj.105.080192.

[2] J.D. Shields, M.E. Fleury, C. Yong, A.A. Tomei, G.J. Randolph, M.A. Swartz, Autologous chemotaxis as a mechanism of tumor cell homing to lymphatics via interstitial flow and autocrine CCR7 signaling., Cancer Cell. 11 (2007) 526–38. https://doi.org/10.1016/j.ccr.2007.04.020.

[3] J.M. Rutkowski, M.A. Swartz, A driving force for change: interstitial flow as a morphoregulator, Trends Cell Biol. 17 (2007) 44–50. https://doi.org/10.1016/j.tcb.2006.11.007.

[4] A. Hoshino, H.S. Kim, L. Bojmar, K.E. Gyan, M. Cioffi, J. Hernandez, C.P. Zambirinis, G. Rodrigues, H. Molina, S. Heissel, M.T. Mark, L. Steiner, A. Benito-Martin, S. Lucotti, A. Di Giannatale, K. Offer, M. Nakajima, C. Williams, L. Nogués, F.A. Pelissier Vatter, A. Hashimoto, A.E. Davies, D. Freitas, C.M. Kenific, Y. Ararso, W. Buehring, P. Lauritzen, Y. Ogitani, K. Sugiura, N. Takahashi, M. Alečković, K.A. Bailey, J.S. Jolissant, H. Wang, A. Harris, L.M. Schaeffer, G. García-Santos, Z. Posner, V.P. Balachandran, Y. Khakoo, G.P.

Raju, A. Scherz, I. Sagi, R. Scherz-Shouval, Y. Yarden, M. Oren, M. Malladi, M. Petriccione, K.C. De Braganca, M. Donzelli, C. Fischer, S. Vitolano, G.P. Wright, L. Ganshaw, M. Marrano, A. Ahmed, J. DeStefano, E. Danzer, M.H.A. Roehrl, N.J. Lacayo, T.C. Vincent, M.R. Weiser, M.S. Brady, P.A. Meyers, L.H. Wexler, S.R. Ambati, A.J. Chou, E.K. Slotkin, S. Modak, S.S. Roberts, E.M. Basu, D. Diolaiti, B.A. Krantz, F. Cardoso, A.L. Simpson, M. Berger, C.M. Rudin, D.M. Simeone, M. Jain, C.M. Ghajar, S.K. Batra, B.Z. Stanger, J. Bui, K.A. Brown, V.K. Rajasekhar, J.H. Healey, M. de Sousa, K. Kramer, S. Sheth, J. Baisch, V. Pascual, T.E. Heaton, M.P. La Quaglia, D.J. Pisapia, R. Schwartz, H. Zhang, Y. Liu, A. Shukla, L. Blavier, Y.A. DeClerck, M. LaBarge, M.J. Bissell, T.C. Caffrey, P.M. Grandgenett, M.A. Hollingsworth, J. Bromberg, B. Costa-Silva, H. Peinado, Y. Kang, B.A. Garcia, E.M. O'Reilly, D. Kelsen, T.M. Trippett, D.R. Jones, I.R. Matei, W.R. Jarnagin, D. Lyden, Extracellular Vesicle and Particle Biomarkers Define Multiple Human Cancers., Cell. (2020). https://doi.org/10.1016/j.cell.2020.07.009.

[5] P. Vallabhajosyula, L. Korutla, A. Habertheuer, M. Yu, S. Rostami, C.X. Yuan, S. Reddy, C. Liu, V. Korutla, B. Koeberlein, J. Trofe-Clark, M.R. Rickels, A. Naji, Tissue-specific exosome biomarkers for noninvasively monitoring immunologic rejection of transplanted tissue, J. Clin. Invest. 127 (2017) 1375–1391. https://doi.org/10.1172/JCI87993.

[6] L.M. Doyle, M.Z. Wang, Overview of Extracellular Vesicles, Their Origin, Composition, Purpose, and Methods for Exosome Isolation and Analysis, Cells. 8 (2019) 727. https://doi.org/10.3390/cells8070727.

[7] M.A.S. Broggi, L. Maillat, C.C.C. Clement, N. Bordry, P. Corth, A. Auger, M. Matter, R. Hamelin, P. Corthésy, A. Auger, M. Matter, R. Hamelin, L. Potin, D. Demurtas, E. Romano, A. Harari, D.E. Speiser, L. Santambrogio, M.A. Swartz, Tumor-associated factors are enriched in lymphatic exudate compared to plasma in metastatic melanoma patients, J. Exp. Med. 216 (2019) 1–17. https://doi.org/10.1084/jem.20181618.

[8] S. García-Silva, A. Benito-Martín, S. Sánchez-Redondo, A. Hernández-Barranco, P. Ximénez-Embún, L. Nogués, M.S. Mazariegos, K. Brinkmann, A.A. López, L. Meyer, C. Rodríguez, C. García-Martín, J. Boskovic, R. Letón, C. Montero, M. Robledo, L. Santambrogio, M.S. Brady, A. Szumera-Ciećkiewicz, I. Kalinowska, J. Skog, M. Noerholm, J. Muñoz, P.L. Ortiz-Romero, Y. Ruano, J.L. Rodríguez-Peralto, P. Rutkowski, H. Peinado, Use of extracellular vesicles from lymphatic drainage as surrogate markers of melanoma progression and BRAFV600E mutation, J. Exp. Med. 216 (2019) 1061–1070. https://doi.org/10.1084/jem.20181522.

[9] R.L.G. Maus, J.W. Jakub, T.J. Hieken, W.K. Nevala, T.A. Christensen, S.L. Sutor, T.J. Flotte, S.N. Markovic, Identification of novel, immune-mediating extracellular vesicles in human lymphatic effluent draining primary cutaneous melanoma, Oncoimmunology. (2019) 1667742. https://doi.org/10.1080/2162402X.2019.1667742.

[10] A. Milasan, N. Tessandier, S. Tan, A. Brisson, E. Boilard, C. Martel, Extracellular vesicles are present in mouse lymph and their level differs in atherosclerosis, J.

Extracell. Vesicles. 5 (2016) 1–9. https://doi.org/10.3402/jev.v5.31427.

[11] C.C. Clement, E.S. Cannizzo, M.D. Nastke, R. Sahu, W. Olszewski, N.E. Miller, L.J. Stern, L. Santambrogio, An expanded self-antigen peptidome is carried by the human lymph as compared to the plasma, PLoS One. 5 (2010). https://doi.org/10.1371/journal.pone.0009863.

[12] D.C. Zawieja, S. Thangaswamy, W. Wang, R. Furtado, C.C. Clement, Z. Papadopoulos, M. Vigano, E.A. Bridenbaugh, L. Zolla, A.A. Gashev, J. Kipnis, G. Lauvau, L. Santambrogio, Lymphatic Cannulation for Lymph Sampling and Molecular Delivery, J. Immunol. 203 (2019) 2339–2350. https://doi.org/10.4049/jimmunol.1900375.

[13] L. Zitvogel, A. Regnault, A. Lozier, J. Wolfers, C. Flament, D. Tenza, P. Ricciardi-Castagnoli, G. Raposo, S. Amigorena, Eradication of established murine tumors using a novel cell-free vaccine: Dendritic cell-derived exosomes, Nat. Med. 4 (1998) 594–600. https://doi.org/10.1038/nm0598-594.

[14] S. Kamerkar, V.S. Lebleu, H. Sugimoto, S. Yang, C.F. Ruivo, S.A. Melo, J.J. Lee, R. Kalluri, Exosomes Facilitate Therapeutic Targeting of Oncogenic KRAS in Pancreatic Cancer, Nature. 546 (2017) 498–503. https://doi.org/10.1038/nature22341.

[15] B. Zuo, H. Qi, Z. Lu, L. Chen, B. Sun, R. Yang, Y. Zhang, Z. Liu, X. Gao, A. You, L. Wu, R. Jing, Q. Zhou, H. Yin, Alarmin-painted exosomes elicit persistent antitumor immunity in large established tumors in mice, Nat. Commun. 11 (2020) 1790. https://doi.org/10.1038/s41467-020-15569-2.

[16] A.W. Lund, F. V. Duraes, S. Hirosue, V.R. Raghavan, C. Nembrini, S.N. Thomas, A. Issa, S. Hugues, M.A. Swartz, VEGF-C promotes immune tolerance in B16 melanomas and cross-presentation of tumor antigen by lymph node lymphatics., Cell Rep. 1 (2012) 191–199. https://doi.org/10.1016/j.celrep.2012.01.005.

[17] A.W. Lund, M. Wagner, M. Fankhauser, E.S. Steinskog, M.A. Broggi, S. Spranger, T.F. Gajewski, K. Alitalo, H.P. Eikesdal, H. Wiig, M.A. Swartz, Lymphatic vessels regulate immune microenvironments in human and murine melanoma, J. Clin. Invest. 126 (2016) 3389–3402. https://doi.org/10.1172/JCI79434.

[18] M. Fankhauser, M.A.S. Broggi, L. Potin, N. Bordry, L. Jeanbart, A.W. Lund, E. Da Costa, S. Hauert, M. Rincon-Restrepo, C. Tremblay, E. Cabello, K. Homicsko, O. Michielin, D. Hanahan, D.E. Speiser, M.A. Swartz, Tumor lymphangiogenesis promotes T cell infiltration and potentiates immunotherapy in melanoma, Sci. Transl. Med. 9 (2017) 1–13. https://doi.org/10.1126/scitranslmed.aal4712.

[19] E. Song, T. Mao, H. Dong, L.S.B. Boisserand, S. Antila, M. Bosenberg, K. Alitalo, J.L. Thomas, A. Iwasaki, VEGF-C-driven lymphatic drainage enables immunosurveillance of brain tumours, Nature. 577 (2020) 689–694. https://doi.org/10.1038/s41586-019-1912-x.

[20] C.D. Commerford, L.C. Dieterich, Y. He, T. Hell, J.A. Montoya-Zegarra, S.F. Noerrelykke, E. Russo, M. Röcken, M. Detmar, Mechanisms of Tumor-Induced Lymphovascular Niche Formation in Draining Lymph Nodes, Cell Rep. 25 (2018) 3554-3563.e4. https://doi.org/10.1016/j.celrep.2018.12.002.

[21] L.C. Dieterich, K. Kapaklikaya, T. Cetintas, S.T. Proulx, C.D. Commerford, K. Ikenberg, S.B. Bachmann, J. Scholl, M. Detmar, Transcriptional profiling of breast cancer-associated lymphatic vessels reveals VCAM-1 as regulator of lymphatic invasion and permeability, Int. J. Cancer. 145 (2019) 2804–2815. https://doi.org/10.1002/ijc.32594.

[22] M. Pisano, V. Triacca, K.A. Barbee, M.A. Swartz, An in vitro model of the tumor-lymphatic microenvironment with simultaneous transendothelial and luminal flows reveals mechanisms of flow enhanced invasion, Integr. Biol. 7 (2015) 525–533. https://doi.org/10.1039/c5ib00085h.

[23] C.M. Card, S.S. Yu, M.A. Swartz, Emerging roles of lymphatic endothelium in regulating adaptive immunity, J. Clin. Invest. 124 (2014) 943–952. https://doi.org/10.1172/JCI73316.

[24] S. Hirosue, E. Vokali, V.R. Raghavan, M. Rincon-restrepo, A.W. Lund, P. Corthésy-Henrioud, F. Capotosti, C. Halin Winter, S. Hugues, M.A. Swartz, Steady-State Antigen Scavenging, Cross-Presentation, and CD8+ T Cell Priming: A New Role for Lymphatic Endothelial Cells., J. Immunol. 192 (2014) 5002–11. https://doi.org/10.4049/jimmunol.1302492.

[25] J. Dubrot, F. V. Duraes, L. Potin, F. Capotosti, D. Brighouse, T. Suter, S. LeibundGut-Landmann, N. Garbi, W. Reith, M.A. Swartz, S. Hugues, Lymph node stromal cells acquire peptide-MHCII complexes from dendritic cells and induce antigen-specific CD4+ T cell tolerance., J. Exp. Med. 211 (2014) 1153–1166. https://doi.org/10.1084/jem.20132000.

[26] J.L. Hood, H. Pan, G.M. Lanza, S. a Wickline, Paracrine induction of endothelium by tumor exosomes., Lab. Invest. 89 (2009) 1317–28. https://doi.org/10.1038/labinvest.2009.94.

[27] W. Zhou, M.Y. Fong, Y. Min, G. Somlo, L. Liu, M.R. Palomares, Y. Yu, A. Chow, S.T.F. O'Connor, A.R. Chin, Y. Yen, Y. Wang, E.G. Marcusson, P. Chu, J. Wu, X. Wu, A.X. Li, Z. Li, H. Gao, X. Ren, M.P. Boldin, P.C. Lin, S.E. Wang, Cancer-Secreted miR-105 destroys vascular endothelial barriers to promote metastasis, Cancer Cell. 25 (2014) 501–515. https://doi.org/10.1016/j.ccr.2014.03.007.

[28] Z. Zeng, Y. Li, Y. Pan, X. Lan, F. Song, J. Sun, K. Zhou, X. Liu, X. Ren, F. Wang, J. Hu, X. Zhu, W. Yang, W. Liao, G. Li, Y. Ding, L. Liang, Cancer-derived exosomal miR-25-3p promotes pre-metastatic niche formation by inducing vascular permeability and angiogenesis, Nat. Commun. 9 (2018) 1–14. https://doi.org/10.1038/s41467-018-07810-w.

[29] H. Wiig, M.A. Swartz, Interstitial fluid and lymph formation and transport: physiological regulation and roles in inflammation and cancer., Physiol. Rev. 92 (2012) 1005–60. https://doi.org/10.1152/physrev.00037.2011.

[30] M.R. Junttila, F.J. de Sauvage, Influence of tumour micro-environment heterogeneity on therapeutic response., Nature. 501 (2013) 346–54. https://doi.org/10.1038/nature12626.

[31] A.C. Shieh, H.A. Rozansky, B. Hinz, M.A. Swartz, Tumor cell invasion is promoted by interstitial flow-induced matrix priming by stromal fibroblasts., Cancer Res. 71 (2011) 790–800. https://doi.org/10.1158/0008-5472.CAN-10-1513.

[32] G. Follain, D. Herrmann, S. Harlepp, V. Hyenne, N. Osmani, S.C. Warren, P. Timpson, J.G. Goetz, Fluids and their mechanics in tumour transit: shaping metastasis, Nat. Rev. Cancer. 20 (2019) 107–124. https://doi.org/10.1038/s41568-019-0221-x.

[33] V. Triacca, E. Güç, W.W. Kilarski, M. Pisano, M.A. Swartz, Transcellular Pathways in Lymphatic Endothelial Cells Regulate Changes in Solute Transport by Fluid Stress, Circ. Res. 120 (2017) 1440–1452. https://doi.org/10.1161/CIRCRESAHA.116.309828.

[34] R.D. Minshall, C. Tiruppathi, S.M. Vogel, W.D. Niles, A. Gilchrist, H.E. Hamm, A.B. Malik, Endothelial Cell-surface gp60 Activates Vesicle Formation and Trafficking via G i -coupled Src Kinase Signaling Pathway, J. Cell Biol. 150 (2000) 1057–1069. https://doi.org/10.1083/jcb.150.5.1057.

[35] B.A. Tamburini, M.A. Burchill, R.M. Kedl, Antigen capture and archiving by lymphatic endothelial cells following vaccination or viral infection, Nat. Commun. 5 (2014) 1–13. https://doi.org/10.1038/ncomms4989.

[36] B. Sun, Y. Zhou, Y. Fang, Z. Li, X. Gu, J. Xiang, Colorectal cancer exosomes induce lymphatic network remodeling in lymph nodes, Int. J. Cancer. (2019). https://doi.org/10.1002/ijc.32196.

[37] E. Groth, J. Pruessmeyer, A. Babendreyer, J. Schumacher, T. Pasqualon, D. Dreymueller, S. Higashiyama, I. Lorenzen, J. Grötzinger, D. Cataldo, A. Ludwig, Stimulated release and functional activity of surface expressed metalloproteinase ADAM17 in exosomes, Biochim. Biophys. Acta - Mol. Cell Res. 1863 (2016) 2795–2808. https://doi.org/10.1016/j.bbamcr.2016.09.002.

[38] J.L. Hood, R.S. San, S.A. Wickline, Exosomes Released by Melanoma Cells Prepare Sentinel Lymph Nodes for Tumor Metastasis, Cancer Res. 71 (2011) 3792–3801. https://doi.org/10.1158/0008-5472.CAN-10-4455.

[39] B. Costa-Silva, N.M. Aiello, A.J. Ocean, S. Singh, H. Zhang, B.K. Thakur, A. Becker, A. Hoshino, M.T. Mark, H. Molina, J. Xiang, T. Zhang, T.-M. Theilen, G. García-Santos, C. Williams, Y. Ararso, Y. Huang, G. Rodrigues, T.-L. Shen, K.J. Labori, I.M.B. Lothe, E.H. Kure, J. Hernandez, A. Doussot, S.H. Ebbesen, P.M. Grandgenett, M.A. Hollingsworth, M. Jain, K. Mallya, S.K. Batra, W.R. Jarnagin, R.E. Schwartz, I. Matei, H. Peinado, B.Z. Stanger, J. Bromberg, D. Lyden, Pancreatic cancer exosomes initiate pre-metastatic niche formation in the liver, Nat. Cell Biol. 17 (2015) 816–826. https://doi.org/10.1038/ncb3169.